Effect of uniaxial magnetic anisotropy on charge transport in a junction with a precessing anisotropic molecular spin

Milena Filipović *

Institute of Physics Belgrade, University of Belgrade, Pregrevica 118, 11080 Belgrade, Serbia

(Received 5 August 2024; revised 26 February 2025; accepted 31 March 2025; published 18 April 2025)

Anisotropic magnetic molecules can be employed to manipulate charge transport in molecular nanojunctions. Charge transport through a molecular orbital connected to two leads and exchange-coupled with a precessing anisotropic molecular spin in a constant magnetic field is studied here. The magnetic field and the uniaxial magnetic anisotropy parameter of the molecular spin modulate the total precession frequency. The precessing molecular magnetization drives inelastic tunneling processes between electronic quasienergy levels. The dc-bias voltages allow to unveil the quasienergy levels, Larmor frequency, and the anisotropy parameter, through characteristics of charge-transport measurements involving features such as steps, peaks, and dips. Quantum interference effects between states connected with spin-flip events are reflected in the shot noise as peak-dip (dip-peak) features, resembling Fano-like resonance profiles, and are controlled by the anisotropy parameter and Larmor frequency. Under zero bias, the increase of the anisotropy parameter enables the decrease of the precession frequency or alters the precession direction, and shot noise is reduced. Furthermore, it is possible to adjust the anisotropy parameter to suppress the precession frequency, leading to the suppression of shot noise. The results show that in the given setup, the charge current and shot noise can be controlled by the magnetic anisotropy parameter of the molecular spin.

DOI: 10.1103/PhysRevB.111.165415

I. INTRODUCTION

Single-molecule magnets have gained much attention since the beginning of the new century due to the possibility to be used as constituent elements in spintronic devices for high-density information storage and quantum information processing [1–6]. The key role in these applications plays the uniaxial magnetic anisotropy, characterized by parameter D, which leads to the bistability of the molecular spin states, with two degenerate ground states $\pm S$, separated by an energy barrier to spin reversal DS^2 (for integer spins) at low temperatures [2,3,7,8]. Depending on the sign of the anisotropy parameter, there are two types of uniaxial anisotropy: easy-axis ($D > 0$) and easy-plane ($D < 0$) anisotropy [2]. For successful applications in magnetic storage, the energy barrier needs to be enhanced [9], but its increase cannot be accomplished by a simultaneous increase of the anisotropy parameter D and the ground state spin S, and the only way to control the barrier height it to modulate the value of D [10–13]. On the other hand, in-plane and small magnetic anisotropy is desirable for applications in quantum information processing [14]. In order to design magnetic molecules with desired characteristics, learning to control and manipulate the magnetic anisotropy parameter D is essential.

Charge transport through magnetic molecules has been studied both theoretically [15–27] and experimentally [28–35]. The studies have addressed various phenomena, such as, e.g., Kondo effect [36–39], Pauli spin blockade [40–42], Coulomb blockade [28,43–45], molecular magnetization dynamics in tunnel junctions [17,46,47] or in contact with a superconducting lead [48], and spin-dependent Seebeck and Peltier effect [49–52]. The possibility to manipulate molecular magnetization by charge current has already been demonstrated experimentally [29–33,53]. It has been theoretically predicted that exchange interactions between molecular magnets can be electrically controlled [21,22]. Magnetic anisotropy can be varied and controlled by various means such as electrical current [18,44,54–57], electric field [44,58–61], molecular mechanical stretching [62], and by ligand substitution [63]. High anisotropy barriers for spin reversal were observed in some isolated metal complexes, but due to their reactivity and instability, they are not suitable candidates to be exploited in magnetic storage [64–67]. Also, new optical techniques of spin readout in single-molecule magnets have been investigated recently [68–70].

The nonequilibrium Green's functions technique [71–73] has been used to derive various characteristics of quantum transport through single molecules and molecular magnets, such as charge current, current-current correlations, spin current, inelastic transport, heat current, etc. [19,21–23,52,74–78]. Charge-current noise in transport junctions arising from the discreteness of charge of conducting electrons is an exciting topic in nanophysics, since it can give us additional information about charge transport which is hidden from the current measurements [79]. Within the framework of nonequilibrium Green's functions technique, the effect of inelastic transport on shot noise has been studied [74,80–83], as well as current fluctuations in the transient regime [84]. It has been shown previously that a spin flip

*Contact author: milena.filipovic@ipb.ac.rs

can lead to suppression [80,85] or enhancement [86,87] of the shot noise. The shot noise has been employed to give information on, e.g., energy of transmission channels [79], fractional charges [88], and Cooper pairs [89]. Recently, the nonequilibrium noise due to temperature gradient at zero-bias voltage has become an active research topic [90–94].

The goal of this paper is to theoretically study charge transport through a single electronic level that may be an orbital of a molecular magnet or belong to a nearby quantum dot, in the presence of a precessing anisotropic molecular spin in a constant external magnetic field, connected to electric contacts. The precession frequency is contributed by the Larmor precession frequency and a term with uniaxial magnetic anisotropy parameter of the molecular spin, and kept undamped by external means. The spin of the itinerant electron in the electronic level and the molecular spin are coupled via exchange interaction. The charge current and current noise are calculated by means of the Keldysh nonequilibrium Green's functions technique [71–73]. The shot noise of charge current is a result of the competition between correlations of currents with the same spins and correlations of currents with the opposite spins. Both elastic tunneling, driven by the dc-bias voltage, and inelastic tunneling involving a spin flip of the itinerant electrons, driven by the precessional motion of the anisotropic molecular spin, contribute to the charge transport. It is shown that by proper tuning of the uniaxial magnetic anisotropy parameter, the charge current and shot noise can be manipulated. The energies of the channels available for electron transport are Floquet quasienergies, which are obtained by the Floquet theorem [95–98]. They are dependent on the magnetic anisotropy of the molecular spin and can be varied accordingly. Both charge current and shot noise are saturated for sufficiently large magnetic anisotropy parameter at nonzero bias-voltage conditions. Similarly to our previous work where the precessing molecular spin was isotropic [83], the peak-dip (dip-peak) features in the shot noise are manifestations of the quantum interference [99,100] between the states connected with inelastic tunneling, accompanied with a spin flip, here involving absorption (emission) of an energy which is linearly dependent on the uniaxial magnetic anisotropy parameter. Finally, the results show that the shot noise at zero-bias voltage conditions and zero temperature is reduced for chemical potentials of the metallic leads that enable inelastic tunneling processes, if the magnetic anisotropy parameter increases, leading to the decrease of the total precession frequency or reversed direction of the molecular spin precession with respect to the external magnetic field. Moreover, the magnetic anisotropy parameter can suppress the precession frequency of the molecular magnetization, leading to zero shot noise.

The rest of the paper is arranged in the following way. The model setup of the system is described in Sec. II. Theoretical formalism used to derive the results is given in Sec. III. The expressions for the charge current and the current noise are calculated by means of the Keldysh nonequilibrium Green's functions technique [71–73]. The results are shown and discussed in Sec. IV, where the effects of the uniaxial magnetic anisotropy of the molecular spin on the charge-transport properties at zero temperture are analysed. This section is followed by Sec. V in which the conclusions are presented.

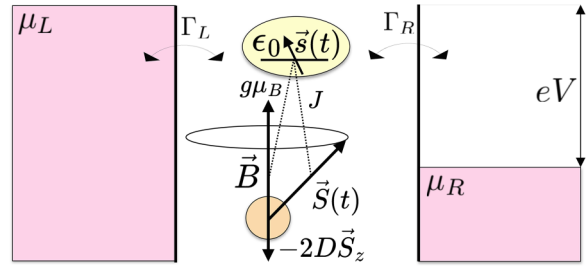

FIG. 1. Tunneling through a single molecular orbital with energy ϵ_0 coupled to the anisotropic spin $\vec{S}(t)$ of a molecular magnet via exchange interaction with the coupling constant J, in the presence of a magnetic field $\vec{B}$, connected to two metallic leads with chemical potentials μ_L and μ_R. The applied bias voltage $eV = \mu_L - \mu_R$, with tunnel rates Γ_L and Γ_R, and the uniaxial anisotropy constant of the molecular magnet D. The spin of the molecule precesses around the magnetic field axis with modified frequency $\omega = \omega_L - 2DS_z$.

II. MODEL SETUP

The junction under consideration consists of a single molecular orbital of a molecular magnet, in the presence of a precessing anisotropic molecular spin in a constant external magnetic field along z axis, $\vec{B} = B\vec{e}_z$, coupled to two noninteracting metallic leads (see Fig. 1). The leads with chemical potentials μ_L (left) and μ_R (right) are unaffected by the magnetic field. The Hamiltonian describing the junction is given by $\hat{H}(t) = \hat{H}_L + \hat{H}_R + \hat{H}_T + \hat{H}_{\rm MO}(t) + \hat{H}_S$. Here, the Hamiltonian of lead $\xi = L, R$ can be written as $\hat{H}_\xi = \sum_{k,\sigma} \epsilon_{k\xi} \hat{c}^\dagger_{k\sigma\xi} \hat{c}_{k\sigma\xi}$. The subscript $\sigma = \uparrow, \downarrow = 1, 2 = \pm 1$ denotes the spin-up or spin-down state of the electrons. The tunnel coupling between the molecular orbital and the leads is introduced by $\hat{H}_T = \sum_{k,\sigma,\xi} [V_{k\xi} \hat{c}^\dagger_{k\sigma\xi} \hat{d}_\sigma + V^*_{k\xi} \hat{d}^\dagger_\sigma \hat{c}_{k\sigma\xi}]$, with matrix element $V_{k\xi}$. Here, $\hat{c}^\dagger_{k\sigma\xi}(\hat{c}_{k\sigma\xi})$ and $\hat{d}^\dagger_\sigma(\hat{d}_\sigma)$ denote the creation (annihilation) operators of the electrons in the leads and the molecular orbital. The Hamiltonian of the molecular orbital is given by $\hat{H}_{\rm MO}(t) = \sum_\sigma \epsilon_0 \hat{d}^\dagger_\sigma \hat{d}_\sigma + (g\mu_B/\hbar)\hat{\vec{s}}\vec{B} + J\hat{\vec{s}}\vec{S}(t)$, where the first term is the Hamiltonian of the noninteracting molecular orbital with energy ϵ_0. The second term describes the electronic spin in the molecular orbital, $\hat{\vec{s}} = (\hbar/2) \sum_{\sigma\sigma'} (\hat{\vec{\sigma}})_{\sigma\sigma'} \hat{d}^\dagger_\sigma \hat{d}_{\sigma'}$, in the presence of the magnetic field $\vec{B}$. The vector of the Pauli matrices is given by $\hat{\vec{\sigma}} = (\hat{\sigma}_x, \hat{\sigma}_y, \hat{\sigma}_z)^T$, while g and μ_B are the g factor of the electron and the Bohr magneton. The third term in the Hamiltonian of the orbital represents the exchange interaction between the electronic spin and spin of the molecule, where J is the exchange coupling constant. The term $\hat{H}_S = (g\mu_B/\hbar)\hat{\vec{S}}\vec{B} - D\hat{S}^2_z$ represents the Hamiltonian of the anisotropic molecular spin $\hat{\vec{S}} = \hat{S}_x\vec{e}_x + \hat{S}_y\vec{e}_y + \hat{S}_z\vec{e}_z$, where D is the uniaxial magnetic anisotropy parameter. It is presumed that g factor of the molecular spin equals that of a free electron.

Assuming that the spin of the molecular magnet is large and that it can be considered as a classical variable $\vec{S}$, with constant length $S = |\vec{S}| \gg \hbar$, where $\vec{S} = \langle \hat{\vec{S}} \rangle$ is the expectation value of the molecular spin operator, its

dynamics is given by the Heisenberg equation of motion $\dot{\vec{S}} = \langle\dot{\hat{\vec{S}}}\rangle = (i/\hbar)\langle[\hat{H}, \hat{\vec{S}}]\rangle$. Neglecting the quantum fluctuations and using external means, such as radio-frequency fields [101], to compensate for the loss of the molecular magnetic energy due to its interaction with the itinerant electrons, so that the molecular spin dynamics remains unaffected by the exchange interaction, the equation $\dot{\vec{S}} = (g\mu_B/\hbar)\vec{B} \times \vec{S} - 2D\vec{S}_z \times \vec{S}$ is obtained [17]. The molecular spin precesses around z axis, with frequency $\omega = \omega_L - 2DS_z$, where $\omega_L = g\mu_B B/\hbar$ is the Larmor precession frequency in the external magnetic field $\vec{B}$, while $-2DS_z$ is the contribution of the uniaxial anisotropy to the precession frequency ω. The motion of the molecular spin is then given by $\vec{S}(t) = S_\perp \cos(\omega t)\vec{e}_x + S_\perp \sin(\omega t)\vec{e}_y + S_z\vec{e}_z$, where θ is the tilt angle between z axis and $\vec{S}$, $S_\perp = S\sin(\theta)$ and $S_z = S\cos(\theta)$. Although the motion of the molecular spin is kept precessional externally [101], the molecular magnet itself pumps charge current into the leads, thus affecting the transport properties of the junction. In the rotating reference frame attached to the end point of the molecular spin, the Hamiltonian of the molecular orbital $\hat{\hat{H}}_{\rm MO}$ is time-independent and can be written as $\hat{\hat{H}}_{\rm MO} = \hat{U}\hat{H}_{\rm MO}\hat{U}^\dagger + i\hbar(\partial_t\hat{U})\hat{U}^\dagger$, where $\hat{U}$ is the unitary operator $\hat{U}(t) = e^{i\omega t\hat{s}_z/\hbar}$. The orbital Hamiltonian $\hat{\hat{H}}_{\rm MO}$ can be further expressed as $\hat{\hat{H}}_{\rm MO} = \sum_\sigma \epsilon_0\hat{d}^\dagger_\sigma\hat{d}_\sigma + (2D+J)S_z\hat{s}_z + JS_\perp\hat{s}_x$.

Separation between a molecular level and a localized molecular spin can be obtained in, e.g., molecular magnets containing atoms of transition metals or rare earth elements [23,55,102], since the molecular spin here is composed of localized d or f orbitals belonging to transition metal or rare earth element. The s and p orbitals in the molecular ligands form the localized molecular level, i.e., the highest occupied or lowest unoccupied molecular orbital. If we take into account that the Coulomb interaction in the s and p orbitals in the ligands can be considered negligible, then the on-site Coulomb repulsion can be neglected.

III. THEORETICAL FORMALISM

A. Charge current

The charge-current operator of the contact ξ is given by the Heisenberg equation [72,73]

$$\hat{I}_\xi(t) = -e\frac{d\hat{N}_\xi}{dt} = -e\frac{i}{\hbar}[\hat{H}, \hat{N}_\xi], \tag{1}$$

where $\hat{N}_\xi = \sum_{k,\sigma}\hat{c}^\dagger_{k\sigma\xi}\hat{c}_{k\sigma\xi}$ represents the charge occupation number operator of the contact ξ, while $[\ ,\ ]$ denotes the commutator. The average charge current from the lead ξ to the molecular orbital is then given by

$$I_\xi(t) = -e\left\langle\frac{d}{dt}\hat{N}_\xi\right\rangle = -e\frac{i}{\hbar}\langle[\hat{H}, \hat{N}_\xi]\rangle. \tag{2}$$

Using the Keldysh nonequilibrium Green's functions technique, the charge current can be calculated as [72,73]

$$I_\xi(t) = 2e\,\mathrm{Re}\int dt'\mathrm{Tr}\big\{\hat{G}^r(t,t')\hat{\Sigma}^<_\xi(t',t) + \hat{G}^<(t,t')\hat{\Sigma}^a_\xi(t',t)\big\}, \tag{3}$$

in units in which $\hbar = e = 1$. The retarded, advanced, lesser and greater self-energies from the tunnel coupling between the molecular orbital and contact ξ are denoted by $\hat{\Sigma}^{r,a,<,>}_\xi(t,t')$. Their matrix elements are diagonal in the electron spin space with respect to the basis of the eigenstates of $\hat{s}_z$, with nonzero matrix elements given by $\Sigma^{r,a,<}_\xi(t,t') = \sum_k V_{k\xi}g^{r,a,<,>}_{k\xi}(t,t')V^*_{k\xi}$, where $g^{r,a,<,>}_{k\xi}(t,t')$ represent the retarded, advanced, lesser and greater Green's functions of the electrons in the lead ξ. The Green's functions of the electrons in the molecular orbital are given by $\hat{G}^{r,a,<,>}(t,t')$, with matrix elements $G^{r,a}_{\sigma\sigma'}(t,t') = \mp i\theta(\pm t \mp t')\langle\{\hat{d}_\sigma(t), \hat{d}^\dagger_{\sigma'}(t')\}\rangle$, while $G^<_{\sigma\sigma'}(t,t') = i\langle\hat{d}^\dagger_{\sigma'}(t')\hat{d}_\sigma(t)\rangle$ and $G^>_{\sigma\sigma'}(t,t') = -i\langle\hat{d}_\sigma(t)\hat{d}^\dagger_{\sigma'}(t')\rangle$, with the anticommutator denoted as $\{\cdot,\cdot\}$. Applying the double Fourier transformations in Eq. (3), one obtains

$$I_\xi(t) = -2e\Gamma_\xi\mathrm{Im}\int\frac{d\epsilon}{2\pi}\int\frac{d\epsilon'}{2\pi}e^{-i(\epsilon-\epsilon')t} \times \mathrm{Tr}\left\{f_\xi(\epsilon')\hat{G}^r(\epsilon,\epsilon') + \frac{1}{2}\hat{G}^<(\epsilon,\epsilon')\right\}, \tag{4}$$

where the tunnel coupling between the molecular orbital and contact ξ, $\Gamma_\xi(\epsilon) = 2\pi\sum_k|V_{k\xi}|^2\delta(\epsilon-\epsilon_{k\xi})$, is energy independent in the wide-band limit and considered constant. The Fermi-Dirac distribution of the electrons in the lead ξ is given by $f_\xi(\epsilon) = [e^{(\epsilon-\mu_\xi)/k_BT}+1]^{-1}$, with k_B the Boltzmann constant and T the temperature.

The matrix elements of the retarded Green's function $\hat{G}^r(t,t')$ of the electrons in the molecular orbital, can be obtained by applying Dyson's expansion and analytic continuation rules [73],

$$\hat{G}^r(t,t') = \hat{G}^{0r}(t-t') + \int dt_1\hat{G}^{0r}(t-t_1)\hat{H}'(t_1)\hat{G}^r(t_1,t'). \tag{5}$$

Here, $\hat{G}^{0r}(t-t')$ is the retarded Green's function of the electrons in the orbital in the presence of only the static component of the molecular spin S_z along the axis of the external magnetic field. It can be found using the equation of motion technique [103], and after applying the Fourier transformations, one obtains $\hat{G}^{0r}(\epsilon) = [\epsilon - \epsilon_0 - \Sigma^r - \hat{\sigma}_z(g\mu_B B + JS_z)/2]^{-1}$ [17,104], where $\Sigma^{r,a} = \mp i\Gamma/2$ and $\Gamma = \sum_\xi\Gamma_\xi$. In the second term of Eq. (5), $\hat{H}'(t) = \gamma(e^{-i\omega t}\hat{d}^\dagger_\uparrow\hat{d}_\downarrow + e^{i\omega t}\hat{d}^\dagger_\downarrow\hat{d}_\uparrow)$ is the off diagonal part of the Hamiltonian, representing the exchange interaction between the electronic spin in the orbital and the rotational component of the molecular spin, with $\gamma = JS_\perp/2$. The double Fourier transforms of the matrix elements of $\hat{G}^r(t,t')$ read [104,105]

$$G^r_{\sigma\sigma}(\epsilon,\epsilon') = \frac{2\pi\delta(\epsilon-\epsilon')G^{0r}_{\sigma\sigma}(\epsilon)}{1-\gamma^2G^{0r}_{\sigma\sigma}(\epsilon)G^{0r}_{-\sigma-\sigma}(\epsilon_\sigma)}, \tag{6}$$

$$G^r_{\sigma-\sigma}(\epsilon,\epsilon') = \frac{2\pi\gamma\delta(\epsilon_\sigma-\epsilon')G^{0r}_{\sigma\sigma}(\epsilon)G^{0r}_{-\sigma-\sigma}(\epsilon_\sigma)}{1-\gamma^2G^{0r}_{\sigma\sigma}(\epsilon)G^{0r}_{-\sigma-\sigma}(\epsilon_\sigma)}, \tag{7}$$

where the abbreviation $\epsilon_\sigma = \epsilon - \sigma\omega = \epsilon - \sigma(\omega_L - 2DS_z)$ is used. Applying the double Fourier transformations to the Keldysh equation [73]

$$\hat{G}^{<,>}(t,t') = \int dt_1dt_2\hat{G}^r(t,t_1)\hat{\Sigma}^{<,>}(t_1-t_2)\hat{G}^a(t_2,t'), \tag{8}$$

the lesser and greater Green's functions can be calculated as $\hat{G}^{<,>}(\epsilon,\epsilon') = \int d\epsilon'' \hat{G}^r(\epsilon,\epsilon'')\hat{\Sigma}^{<,>}(\epsilon'')\hat{G}^a(\epsilon'',\epsilon')/2\pi$, where $\Sigma^<(\epsilon) = i\sum_\xi \Gamma_\xi f_\xi(\epsilon)$, $\Sigma^>(\epsilon) = i\sum_\xi \Gamma_\xi (f_\xi(\epsilon)-1)$ and $\hat{G}^a(\epsilon,\epsilon') = [\hat{G}^r(\epsilon',\epsilon)]^\dagger$.

Finally, using Eqs. (4)–(8), the average charge current from the contact ξ can be written as

$$I_\xi = \frac{e\Gamma_\xi\Gamma_\zeta}{\hbar}\int \frac{d\epsilon}{2\pi}[f_\xi(\epsilon)-f_\zeta(\epsilon)] \times \sum_{\substack{\sigma\sigma'\\ \sigma\neq\sigma'}} \frac{\left|G^{0r}_{\sigma\sigma}(\epsilon)\right|^2\left[1+\gamma^2\left|G^{0r}_{\sigma'\sigma'}(\epsilon+\sigma'\omega_L-2\sigma' DS_z)\right|^2\right]}{\left|1-\gamma^2 G^{0r}_{\sigma\sigma}(\epsilon)G^{0r}_{\sigma'\sigma'}(\epsilon+\sigma'\omega_L-2\sigma' DS_z)\right|^2}, \tag{9}$$

with $\xi \neq \zeta$. Using the spin-resolved charge currents I^σ_ξ, the charge current can be written as $I_\xi = I^\uparrow_\xi + I^\downarrow_\xi$. In the limit $DS_z \ll \omega_L$, Eq. (9) reduces to the previously calculated expression for the charge current [83].

B. Density of states in the molecular orbital

The positions of the resonant transmission channels available for electron transport in the molecular orbital can be obtained from the density of states in the orbital

$$\rho(\epsilon) = -\frac{1}{\pi}\sum_{\sigma=\pm1}\mathrm{Im}\left\{\frac{G^{0r}_{\sigma\sigma}(\epsilon)}{1-\gamma^2 G^{0r}_{\sigma\sigma}(\epsilon)G^{0r}_{-\sigma-\sigma}(\epsilon_\sigma)}\right\}. \tag{10}$$

Taking into account that the Hamiltonian of the molecular orbital is a periodic function of time $\hat{H}_{\mathrm{MO}}(t) = \hat{H}_{\mathrm{MO}}(t+\mathcal{T})$, with $\mathcal{T} = 2\pi/\omega$, the energies of the molecular levels at which the resonant transmission channels are located, can be calculated as Floquet quasienergies ϵ_i, $i \in \{1,2,3,4\}$, using the Floquet theorem [95–98]. They are given by

$$\epsilon_{1,3} = \epsilon_0 - \frac{\omega_L}{2} + DS_z \pm \sqrt{D(D+J)S_z^2 + \left(\frac{JS}{2}\right)^2}, \tag{11}$$

$$\epsilon_{2,4} = \epsilon_0 + \frac{\omega_L}{2} - DS_z \pm \sqrt{D(D+J)S_z^2 + \left(\frac{JS}{2}\right)^2}. \tag{12}$$

The derivation of the Floquet quasienergies is presented in the Appendix. Note that $\epsilon_2 = \epsilon_1 + \omega$ and $\epsilon_4 = \epsilon_3 + \omega$. Some of the spin-flip absorption and emission processes are shown in Fig. 2, for $\omega > 0$. In the molecular orbital, an electron with energy $\epsilon_1(\epsilon_2)$ or $\epsilon_3(\epsilon_4)$ can absorb (emit) an energy equal to one energy quantum ω and flip its spin, due to the exchange interaction with the precessing component of the anisotropic molecular spin, ending up in the quasienergy level with energy $\epsilon_2(\epsilon_1)$ or $\epsilon_4(\epsilon_3)$, and then tunneling into either lead, so that the $\downarrow$ state with quasienergy $\epsilon_1(\epsilon_3)$ is coupled with the $\uparrow$ state with quasienergy $\epsilon_2(\epsilon_4)$. An inelastic spin-flip process is presented in Fig. 2(a). Here, an electron tunnels from the left lead into the $\downarrow$ level ϵ_1 (or ϵ_3) of the molecular orbital, flips its spin and absorbs an energy quantum ω. Then it tunnels into either lead.

C. Noise of charge current

Additional properties of the charge transport in the junction can be obtained by analyzing the charge-current noise. In view

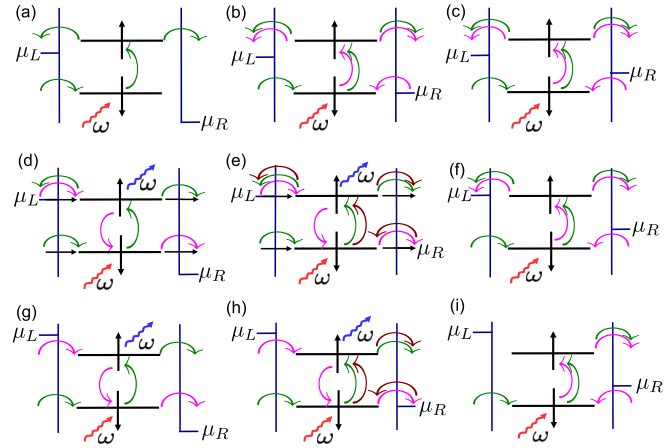

FIG. 2. Inelastic spin-flip processes between quasienergy levels of the molecular orbital in the presence of the precessing anisotropic molecular spin with frequency $\omega = \omega_L - 2DS_z$, for different positions of the levels with respect to chemical potentials μ_L and μ_R. Different processes are represented with different colors. In (d) and (e), the elastic tunneling processes are represented with horizontal black arrows. For $\omega > 0$, a spin $\downarrow$ ($\uparrow$) electron absorbs (emits) an energy quantum ω and flips its spin due to the exchange interaction with the precessing component of the molecular spin.

of the fact that the nonzero commutator in Eq. (1) is generated by the tunneling Hamiltonian $\hat{H}_T$, the charge current operator $\hat{I}_\xi(t)$ can be written as

$$\hat{I}_\xi(t) = e\frac{i}{\hbar}\sum_\sigma \hat{I}_{\xi\sigma}(t), \tag{13}$$

with the operator component $\hat{I}_{\xi\sigma}(t)$ given by

$$\hat{I}_{\xi\sigma}(t) = \sum_k [V_{k\xi}\hat{c}^\dagger_{k\sigma\xi}(t)\hat{d}_\sigma(t) - V^*_{k\xi}\hat{d}^\dagger_\sigma(t)\hat{c}_{k\sigma\xi}(t)]. \tag{14}$$

The fluctuation operator of the charge current in contact ξ is given by

$$\delta\hat{I}_\xi(t) = \hat{I}_\xi(t) - \langle\hat{I}_\xi(t)\rangle. \tag{15}$$

The correlation between fluctuations of currents in leads ξ and ζ, known as nonsymmetrized charge-current noise is written as [73,79]

$$S_{\xi\zeta}(t,t') = \langle\delta\hat{I}_\xi(t)\delta\hat{I}_\zeta(t')\rangle, \tag{16}$$

while the symmetrized noise is defined as [73,79]

$$S_{\xi\zeta S}(t,t') = \tfrac{1}{2}\langle\{\delta\hat{I}_\xi(t),\delta\hat{I}_\zeta(t')\}\rangle. \tag{17}$$

With the help of Eqs. (13)–(15), one obtains the nonsymmetrized noise as

$$S_{\xi\zeta}(t,t') = \sum_{\sigma\sigma'} S^{\sigma\sigma'}_{\xi\zeta}(t,t'), \tag{18}$$

with $S^{\sigma\sigma'}_{\xi\zeta}(t,t') = (-e^2/\hbar^2)\langle\delta\hat{I}_{\xi\sigma}(t)\delta\hat{I}_{\zeta\sigma'}(t')\rangle$ representing the correlation between fluctuations of spin-resolved charge currents $I_{\xi\sigma}$ and $I_{\zeta\sigma'}$. Applying Wick's theorem [106] and Langreth analytical continuation rules [107], the correlation functions $S^{\sigma\sigma'}_{\xi\zeta}(t,t')$ introduced in Eq. (18) can be calculated [73,84]. Using the Fourier transforms of Green's functions

$G^{r,a,<,>}_{\sigma\sigma'}(\epsilon,\epsilon')$ and self-energies $\Sigma^{r,a,<,>}_{\xi}(\epsilon)$, the formal expression for the nonsymmetrized noise of charge current in standard coordinates t and t', obtained previously [73,83,84], becomes

$$
\begin{aligned}
S_{\xi\zeta}(t,t') = -\frac{e^2}{\hbar^2}\sum_{\sigma\sigma'}\Bigg\{\int\frac{d\epsilon_1}{2\pi}\int\frac{d\epsilon_2}{2\pi}\int\frac{d\epsilon_3}{2\pi}\int\frac{d\epsilon_4}{2\pi}e^{-i(\epsilon_1-\epsilon_2)t}e^{i(\epsilon_3-\epsilon_4)t'}\\
\times\Big\{\big[G^r_{\sigma\sigma'}(\epsilon_1,\epsilon_3)\Sigma^>_\zeta(\epsilon_3)+2G^>_{\sigma\sigma'}(\epsilon_1,\epsilon_3)\Sigma^a_\zeta\big]\big[G^r_{\sigma'\sigma}(\epsilon_4,\epsilon_2)\Sigma^<_\xi(\epsilon_2)+2G^<_{\sigma'\sigma}(\epsilon_4,\epsilon_2)\Sigma^a_\xi\big]\\
+\big[\Sigma^>_\xi(\epsilon_1)G^a_{\sigma\sigma'}(\epsilon_1,\epsilon_3)+2G^>_{\sigma\sigma'}(\epsilon_1,\epsilon_3)\Sigma^r_\xi\big]\big[\Sigma^<_\zeta(\epsilon_4)G^a_{\sigma'\sigma}(\epsilon_4,\epsilon_2)+2G^<_{\sigma'\sigma}(\epsilon_4,\epsilon_2)\Sigma^r_\zeta\big]\\
+4\Sigma^r_\xi\Sigma^a_\zeta G^>_{\sigma\sigma'}(\epsilon_1,\epsilon_3)G^<_{\sigma'\sigma}(\epsilon_4,\epsilon_2)\Big\}-\delta_{\xi\zeta}\delta_{\sigma\sigma'}\int\frac{d\epsilon_1}{2\pi}\int\frac{d\epsilon_2}{2\pi}\int\frac{d\epsilon_3}{2\pi}\\
\times\{e^{-i(\epsilon_1-\epsilon_3)t}e^{i(\epsilon_2-\epsilon_3)t'}G^>_{\sigma\sigma'}(\epsilon_1,\epsilon_2)\Sigma^<_\xi(\epsilon_3)+e^{-i(\epsilon_1-\epsilon_3)t}e^{i(\epsilon_1-\epsilon_2)t'}\Sigma^>_\xi(\epsilon_1)G^<_{\sigma'\sigma}(\epsilon_2,\epsilon_3)\}\Bigg\}. \qquad (19)
\end{aligned}
$$

The resulting nonsymmetrized noise depends only on the time difference $\tau = t - t'$, and its power spectrum is given by

$$S_{\xi\zeta}(\Omega) = \int d\tau e^{i\Omega\tau}S_{\xi\zeta}(\tau), \qquad (20)$$

while the symmetrized noise spectrum reads

$$S_{\xi\zeta S}(\Omega) = \tfrac{1}{2}[S_{\xi\zeta}(\Omega) + S_{\zeta\xi}(-\Omega)]. \qquad (21)$$

The individual noise components, $S^{\sigma\sigma'}_{\xi\zeta}(\Omega)$ and symmetrized $S^{\sigma\sigma'}_{\xi\zeta S}(\Omega) = \frac{1}{2}[S^{\sigma\sigma'}_{\xi\zeta}(\Omega) + S^{\sigma'\sigma}_{\zeta\xi}(-\Omega)]$ can be calculated using Eqs. (18)–(21), and represent correlations between fluctuations of charge currents with the same spins for $\sigma = \sigma'$, or different spins for $\sigma \neq \sigma'$. The charge current given by Eq. (9) is conserved, implying that the zero-frequency ($\Omega = 0$) noise power satisfies the relations $S_{LL}(0) = S_{RR}(0) = -S_{LR}(0) = -S_{RL}(0)$. In experimental configurations zero-frequency noise power is standardly measured. In the remainder of this paper, the noise power $S_{LL} = S_{LL}(0) = S_{LLS}(0)$ at zero temperature will be discussed, as in this particular case it is contributed only by the shot noise, while thermal noise vanishes. The elastic tunneling events are induced by the bias voltage. The inelastic tunneling events, each involving a spin flip and absorption (emission) of an energy quantum ω, are induced by the exchange interaction between the spins of the conduction electrons and the precessing component of the anisotropic molecular spin. The second term in Eq. (19) involving $\delta_{\sigma\sigma'}$ vanishes for $\sigma \neq \sigma'$. Hence, the shot noise S_{LL} is the result of the competition between positive correlations of currents with the same spins $S^{\uparrow\uparrow}_{LL} = S^{\uparrow\uparrow}_{LLS}$ and $S^{\downarrow\downarrow}_{LL} = S^{\downarrow\downarrow}_{LLS}$, and negative correlations of currents with opposite spins, induced by spin-flip events, $S^{\uparrow\downarrow}_{LL}$ and $S^{\downarrow\uparrow}_{LL}$, which are a complex conjugate pair $S^{\downarrow\uparrow}_{LL} = (S^{\uparrow\downarrow}_{LL})^*$, with $S^{\uparrow\downarrow}_{LLS} = S^{\downarrow\uparrow}_{LLS}$.

IV. RESULTS

Now we analyze the behavior of the charge current I_L, zero-frequency noise power S_{LL}, and Fano factor $F = S_{LL}/e|I_L|$ as functions of the uniaxial magnetic anisotropy parameter D, bias voltage $eV = \mu_L - \mu_R$, and Larmor frequency ω_L (magnetic field B), focusing on the influence of tuning the anisotropy parameter D on charge transport properties of the system. In particular, it will be shown that the anisotropy parameter D can contribute to controlling and reducing the noise power, especially via quantum interference effects, that occur at resonant conditions $\mu_\xi = \epsilon_i$, and manifest themselves as Fano-like peak-dip (dip-peak) features in the noise S_{LL}.

In Fig. 3, the average charge current from the left lead I_L and autocorrelation shot noise S_{LL} are presented as functions of the magnetic anisotropy parameter D, for five different tilt angles θ, while the Fano factor F is shown in Fig. 4. The current and noise in Fig. 3 show the molecular quasienergy spectrum, with each dip, dip-peak, peak-dip, or step-like feature denoting the anisotropy parameter D corresponding to the matching between level ϵ_i and chemical potential μ_ξ. The fano factor $F < 1$, so the noise is sub-Poissonian. Both elastic tunneling, and inelastic processes involving absorption (emission) of an energy ω with longer electron dwell time on the molecular orbital, contribute to sub-Poissonian noise. We see that the current, shot noise and consequently the Fano factor are constant for $\theta = 0$ (orange, dotted lines) and $\theta = \pi/2$ (pink, dashed lines). If we look at the expression for the current, given by Eq. (9), we notice that for $\theta = 0$, $\gamma = 0$ as well, and the charge current dependence on D vanishes. On the other hand, $S_z = 0$ for $\theta = \pi/2$, hence the current does not depend on the anisotropy parameter D either. For the tilt angle $\theta = \pi/3$ (green line in Figs. 3 and 4) and $D = -0.01312\,\epsilon_0$ (grid line), corresponding to $\mu_L = \epsilon_2 = 2.5\,\epsilon_0$ and $\epsilon_1 = 0.69\,\epsilon_0$, there is a dip-peak feature in the current, and a peak-dip feature in the shot noise and Fano factor. The position of the quasienergy levels ϵ_i with respect to μ_ξ for this set of parameters corresponds to Fig. 2(d), where we see the available tunneling processes between levels with energies ϵ_1 and ϵ_2, and 2(i) where the tunneling processes between levels with energies $\epsilon_3 = -0.5\,\epsilon_0$ and $\epsilon_4 = 1.31\,\epsilon_0$ are shown. There are two available spin-flip processes for electrons tunneling into $\downarrow$ level $\epsilon_1(\epsilon_3)$ from the left lead [green curved arrows in Figs. 2(d) and 2(i)], and one elastic tunneling process [black horizontal arrow in Fig. 2(d)]. For an electron from the left lead entering $\uparrow$ level with energy ϵ_2, one spin-flip process is available in Fig. 2(d) (magenta curved line), while one electron can jump into the left lead from $\uparrow$ level ϵ_2, and elastic tunneling to $\uparrow$ level ϵ_2 (ϵ_4) is available [black horizontal arrow in Fig. 2(d)]. As a result $I^\uparrow_L < I^\downarrow_L > 0$.

Similarly as in the Fano effect [99,100], the peak-dip (dip-peak) features are manifestations of the quantum interference between the states connected with spin-flip events, accompa-

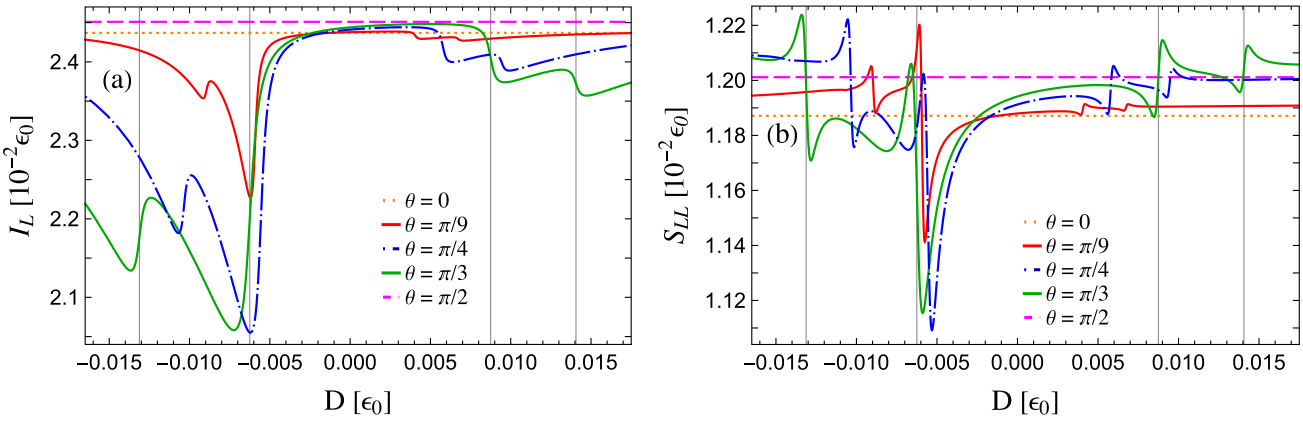

FIG. 3. (a) Charge current I_L and (b) autocorrelation shot noise S_{LL} as functions of the uniaxial magnetic anisotropy parameter D for different tilt angles θ, at zero temperature, with $\vec{B} = B\vec{e}_z$. The chemical potentials of the leads are equal to $\mu_L = 2.5\,\epsilon_0$ and $\mu_R = 0$. The other parameters are set to $\Gamma = 0.05\,\epsilon 0$, $\Gamma_L = \Gamma_R = \Gamma/2$, $\omega_L = 0.5\,\epsilon_0$, $J = 0.01\,\epsilon_0$, and $S = 100$. Grid lines for $\theta = \pi/3$ (green line) are positioned at $D = -0.01312\,\epsilon_0$ ($\mu_L = \epsilon_2$), $-0.00625\,\epsilon_0$ ($\mu_R = \epsilon_3$), $0.00875\,\epsilon_0$ ($\mu_R = \epsilon_4$), and $0.01406\,\epsilon_0$ ($\mu_L = \epsilon_1$).

nied by an energy change ω. Namely, e.g., in Fig. 2(d) an electron from the left lead can tunnel through a $\uparrow$ state via an elastic tunneling process (black horizontal arrow), or via inelastic spin-flip process from $\downarrow$ to $\uparrow$ state, with absorption of an energy ω, before it tunnels out of the orbital (green curved lines). The electron can alternatively tunnel through a $\downarrow$ state elastically (black horizontal line), or via spin flip from $\uparrow$ to $\downarrow$ state, with emission of an energy ω (pink curved lines). The superposition of two electron wave functions along the two tunneling pathways, one elastic and the other inelastic, ending in the same final $\uparrow$ or $\downarrow$ state leads to constructive (peaks) or destructive (dips) quantum interference, manifested in the shot noise. The asymmetric line shape in S_{LL} resembles the shape of the asymmetric Fano resonance profile, described by the Fano formula [99,100]. Around a resonant anisotropy parameter $D_{\rm res}$, for $\mu_\xi = \epsilon_i$, with destructive interference corresponding to a minimum (dip) at $D_{\rm min}$, and constructive interference corresponding to a maximum (peak) at $D_{\rm max}$, the

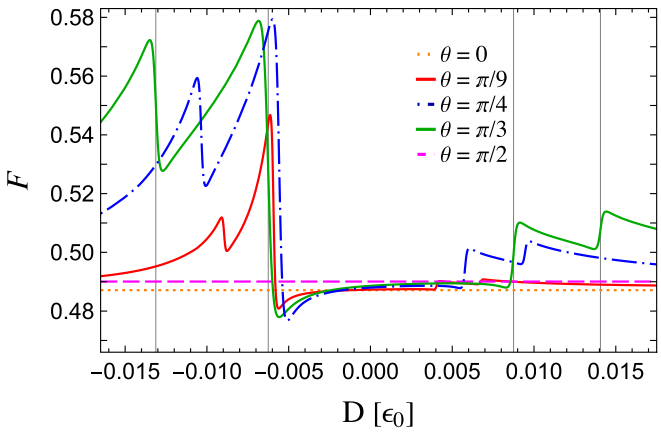

FIG. 4. Fano factor F as a function of the uniaxial anisotropy parameter D. The plots are obtained for different tilt angles θ at zero temperature, with $\vec{B} = B\vec{e}_z$. The chemical potentials of the leads are equal to $\mu_L = 2.5\,\epsilon_0$ and $\mu_R = 0$. The other parameters are set to $\Gamma = 0.05\,\epsilon 0$, $\Gamma_L = \Gamma_R = \Gamma/2$, $\omega_L = 0.5\,\epsilon_0$, $J = 0.01\,\epsilon_0$, and $S = 100$.

shot noise S_{LL} matches the Fano-like shape given by

$$\sigma_S(D) = C + A\frac{(D - D_{\rm res} + q\Gamma_{\rm res}/2)^2}{(D - D_{\rm res})^2 + (\Gamma_{\rm res}/2))^2}, \qquad (22)$$

where $q = \pm 1$ is the asymmetry parameter. For $\omega > 0$, $q = -1$, whereas for $\omega < 0$, $q = 1$. The width of the resonance is $\Gamma_{\rm res} = |D_{\rm max} - D_{\rm min}|$, C represents the shot noise at $D_{\rm min}$, $C = S_{LL}(D_{\rm min})$, while A is half of the amplitude of the Fano-like shape, $A = [S_{LL}(D_{\rm max}) - S_{LL}(D_{\rm min})]/2$. The asymmetry parameter q, represents the ratio of the probabilities of elastic and inelastic tunneling interfering pathways. Since $|q| = 1$, both elastic and inelastic processes are equally probable, and $D_{\rm res}$ is located at equal distance from $D_{\rm min}$ and $D_{\rm max}$.

As the anisotropy parameter D increases, the quasienergy level ϵ_3 moves up the energy scale and enters the bias-voltage window around $D = -0.00625\,\epsilon_0$ for $\theta = \pi/3$ (another grid line in Figs. 3 and 4), with $\mu_R = \epsilon_3 = 0$, leading to the increase of the Fano factor since new quasienergy level becomes available for elastic or inelastic processes [see Figs. 2(g) and 2(h)]. Now, all levels satisfy $\mu_R < \epsilon_i < \mu_L$, leading to the enhancement of the current after its minimum value, with $I_L^{\uparrow} \approx I_L^{\downarrow} > 0$, and the most prominent peak-dip feature in S_{LL} and F, where the dips represent their minimum values. The Fano-like shape of the resonance profile, $\sigma_S(D)$, given by Eq. (22), corresponding to S_{LL} with $\theta = \pi/3$ [green line in Fig. 3(b)] for $D_{\rm res} = -0.00625\,\epsilon_0$ and $D_{\rm res} = 0.00875\,\epsilon_0$ is presented in Fig. 5. The noise S_{LL} resembles the Fano-like resonance profile σ_S, around resonant anisotropy parameters $D_{\rm res}$, $S_{LL} \approx \sigma_S$ (blue line around $D_{\rm res} = -0.00625\,\epsilon_0$ and red line around $D_{\rm res} = 0.00875\,\epsilon_0$ in Fig. 5). For $D_{\rm res} = -0.00625\,\epsilon_0$, the parameters of the Fano-like profile σ_S are the following: $q = -1$, $D_{\rm min} \approx -0.0059\,\epsilon_0$, $D_{\rm max} \approx -0.0066\,\epsilon_0$, $\Gamma_{\rm res} \approx 0.0007\,\epsilon_0$, $C \approx 1.1154 \times 10^{-2}\,\epsilon_0$, and $A \approx 4.5312 \times 10^{-4}\,\epsilon_0$. The inset shows individual contributions of two interference profiles to Fano-like shapes in S_{LL}. The interference of electron waves propagating, one elastically through $\uparrow$ level (ϵ_4) and the other inelastically with absorption of an energy ω, and a spin flip from $\downarrow$ level (ϵ_3) to $\uparrow$ level (ϵ_4) [see Fig. 2(h)], is presented in the contribution $S_{LLS}^{\uparrow\uparrow} + S_{LLS}^{\uparrow\downarrow}$ (pink line, inset in Fig. 5). The interference of pathways involving $\downarrow$ state (ϵ_3)

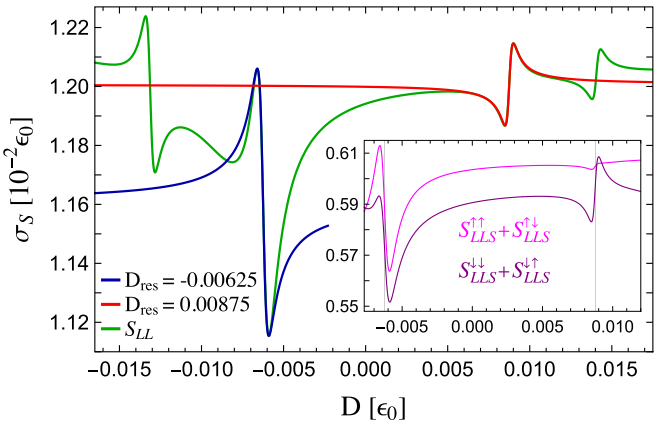

FIG. 5. Fano-like shape of the resonance profile σ_S as a function of the uniaxial anisotropy parameter D, corresponding to noise S_{LL} for $\theta = \pi/3$ in Fig. 3(b) (green line), for two resonant anisotropy parameters $D_{\rm res} = -0.00625\,\epsilon_0$ (blue line), and $D_{\rm res} = 0.00875\,\epsilon_0$ (red line). Around $D_{\rm res}$ the shot noise S_{LL} matches σ_S. The inset shows contributions of $S^{\uparrow\uparrow}_{LLS} + S^{\uparrow\downarrow}_{LLS}$ (pink line) and $S^{\downarrow\downarrow}_{LLS} + S^{\downarrow\uparrow}_{LLS}$ (purple line) to the resulting shapes of the resonance profiles in S_{LL}. The other parameters are the same as in Fig. 3.

and a spin flip from ↑ state (ϵ_4) to ↓ state (ϵ_3) accompanied by the emission of an energy ω is presented in $S^{\downarrow\downarrow}_{LLS} + S^{\downarrow\uparrow}_{LLS}$ (purple line, inset in Fig. 5). In both lines $q = -1$, showing equal probabilities of elastic and inelastic spin-flip processes involving absorption (pink line) or emission (purple line), with the ratio of amplitudes of their resonance profiles around 1.186.

With further increase of the parameter D, I_L and S_{LL} approach constant values, and $F \approx 0.49$ [108], in the region between second and third grid lines, until $D = 0.00875\,\epsilon_0$ [green line in Fig. 3(b)], since all levels ϵ_i lie within the bias-voltage window. The quasienergy level ϵ_4 moves down the energy scale with the increase od D, and for $D = 0.00875\,\epsilon_0$ (grid line in Figs. 3 and 4), $\mu_R = \epsilon_4 = 0$, leading to a decrease of I_L, with $I_L^{\uparrow} > I_L^{\downarrow} > 0$ [tunneling processes in Figs. 2(g) and 2(h)] and a dip peak in S_{LL}. Around $D_{\rm res} = 0.00875\,\epsilon_0$, S_{LL} resembles the Fano-like resonance shape given by Eq. (22) (red line in Fig. 5). The asymmetry parameter is now $q = 1$ as a consequence of the reversed direction of the effective magnetic field $\vec{B}_{\rm eff} = (\omega/g\mu_B)\vec{e}_z$ ($\omega < 0$). The ↓ level with energy ϵ_3 lies above ↑ level with energy ϵ_4 for $\omega < 0$, $\epsilon_3 > \epsilon_4$. The contribution of the interference between elastic tunneling pathway through ↑ level (ϵ_4) and inelastic emission pathway with a spin flip from ↓ level (ϵ_3) to ↑ level (ϵ_4), against the direction of the effective magnetic field $\vec{B}_{\rm eff}$ ($B_{\rm eff} < 0, B > 0$) is negligible (pink line, inset in Fig. 5), while the interference between elastic process through ↓ level (ϵ_3) and inelastic absorption process accompanied with spin flip from ↑ level (ϵ_4) to ↓ level (ϵ_3) almost entirely participates in the formation of the Fano-like resonance profile (purple line, inset in Fig. 5).

As the parameter D increases, the level ϵ_4 leaves the bias-voltage window. At $D = 0.01406\,\epsilon_0$, for $\theta = \pi/3$ (grid line in Figs. 3 and 4), $\mu_L = \epsilon_1$, before the level ϵ_1 leaves the bias-voltage window with further increase of D, resulting in the final decrease in I_L, with $I_L^{\uparrow} > I_L^{\downarrow} > 0$, [tunneling processes in Figs. 2(d) and 2(i)] and a dip-peak in S_{LL}. All the plots in Fig. 3, except for $\theta = 0$ and $\theta = \pi/2$, show that both I_L and S_{LL} have minimum values around the value of D that corresponds to the entrance of all ϵ_i into the bias-voltage window. Both I_L and S_{LL} are saturated at high anisotropy $|D| \gg \omega_L/2S_z$, and $F \approx 0.49$. In this case only two levels, ϵ_1 and ϵ_4 (for $D < 0$, $\omega > 0$), or ϵ_2 and ϵ_3 (for $D > 0$, $\omega < 0$), lie between μ_L and μ_R, and more energy is needed to flip an electron spin to the direction of the effective magnetic field, so that its spin flip is energetically unfavourable. Besides, an electron dwell time on the molecular orbital during a spin-flip process also increases. Therefore, at a high anisotropy, $|D| \gg \omega_L/2S_z$, the dominant tunneling processes are elastic, with spin-resolved charge currents $I_L^{\uparrow} \approx I_L^{\downarrow}$ and correlations of currents with the same spins, $S_{LL}^{\uparrow\uparrow} \approx S_{LL}^{\downarrow\downarrow}$, while the probability of electron spin flip decreases, so that the contribution of the correlations of currents with opposite spins to noise $S_{LL}^{\uparrow\downarrow} + S_{LL}^{\downarrow\uparrow} \to 0$.

The average charge current I_L as a function of the applied bias voltage eV at zero temperature is plotted for six different values of anisotropy parameter D in Fig. 6(a), where the bias voltage is varied such that $\mu_{L,R} = \pm eV/2$. As the bias voltage increases, a new channel available for electron transport, with an energy ϵ_i enters the bias-voltage window, resulting in a step increase in the current. Since the positions of the quasienergy levels ϵ_i depend on molecular spin anisotropy, for different values of D, the staircase current function will show steps at different values of eV. The shot noise of charge current S_{LL} and Fano factor F as functions of eV are shown in Figs. 6(b) and 7. The peak-dip (dip-peak) features, which occur due to the quantum interference, and steplike features in S_{LL} and F, correspond to resonances $\mu_\xi = \pm eV/2 = \epsilon_i$. Hence, they change their positions with the change of the magnetic anisotropy parameter D. For the set of parameters: $\omega_L = 0.5\epsilon_0$, $\theta = \pi/3$, and $D = 0.005\epsilon_0$ in Fig. 6 (blue, dot-dashed line), one obtains $\omega = \omega_L - 2DS_z = 0$, with only two transport channels, with energies $\epsilon = 0.34\epsilon_0$ and $\epsilon\prime = 1.66\epsilon_0$, available for the elastic tunneling, denoted by the steps at $\pm eV/2 = \epsilon$ and $\pm eV/2 = \epsilon\prime$. In this case, the Fano factor is Poissonian, $F = 1$, for $|eV| < 2\epsilon$ (blue dot-dashed line in Fig. 7), since the transmission probability is very low, depending on the level broadening Γ, and the currents remain uncorrelated until the first channel available for electron transport appears. For $\omega \neq 0$, the average current I_L is equal to zero at $eV = 0$, but the noise S_{LL} is contributed by the inelastic processes in which an electron flips its spin and absorbs an energy ω, leading to the divergence of the Fano factor (see Fig. 7). The noise becomes sub-Poissonian ($F < 1$) as soon as one of the levels ϵ_i enters the bias-voltage window, since the transmission probability increases. After all the levels ϵ_i enter the bias-voltage window [tunneling processes in Fig. 2(g)], the Fano factor becomes constant $F = 1/2$ [108].

The average charge current I_L and noise S_{LL} as functions of the Larmor frequency ω_L at zero temperature, for several different values of the magnetic anisotropy parameter D, are shown in Figs. 8(a) and 8(b). The corresponding Fano factor F is presented in Fig. 9. Here, the bias voltage is varied as $eV = \mu_L - \mu_R$, with $\mu_R = 0$, while $\mu_L = 2.5\,\epsilon_0$, except for the blue dot-dashed lines where $\mu_L = 1.125\,\epsilon_0$. All steps in the current I_L, as well as steps and dip-peak features in the noise S_{LL}, correspond to a resonance $\mu_\xi = \epsilon_i$. At $\omega_L = 0$, for

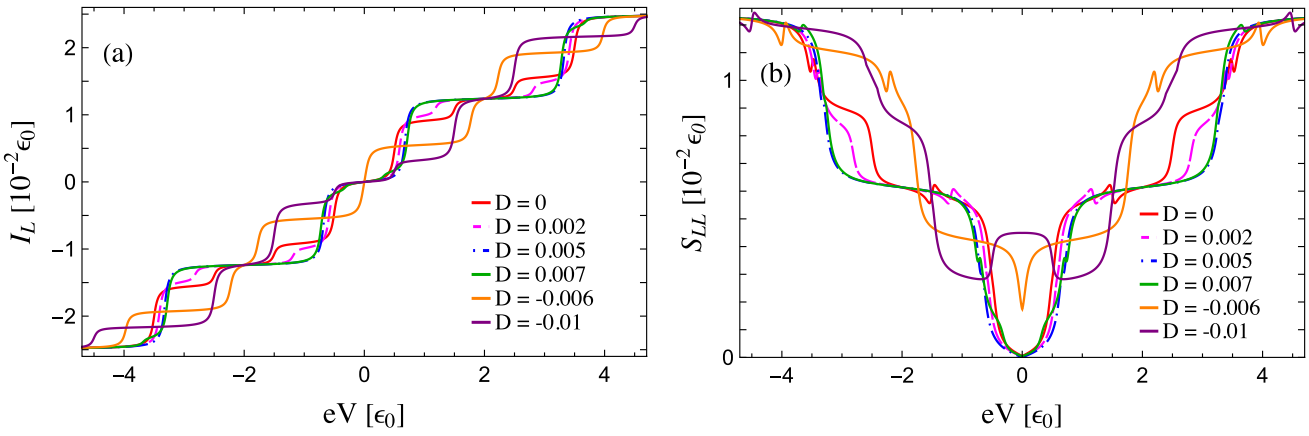

FIG. 6. (a) Charge current I_L and (b) autocorrelation shot noise S_{LL} as functions of the applied bias voltage $eV = \mu_L - \mu_R$ with $\mu_{L,R} = \pm eV/2$ and $\vec{B} = B\vec{e}_z$, for different uniaxial magnetic anisotropy parameters D at zero temperature. The other parameters are set to $\Gamma = 0.05\,\epsilon 0$, $\Gamma_L = \Gamma_R = \Gamma/2$, $\omega_L = 0.5\,\epsilon_0$, $J = 0.01\,\epsilon_0$, $S = 100$, and $\theta = \pi/3$. All energies are given in the units of ϵ_0. The peak-dip (dip-peak) features in the shot noise S_{LL} as manifestations of the quantum interference effect, and steps in the charge current function I_L and shot noise S_{LL} correspond to resonances $\mu_\xi = \epsilon_i$, with $\xi = L, R$ and $i = 1, 2, 3, 4$.

$D = -0.00625\,\epsilon_0$ and $\mu_L = 1.125\,\epsilon_0$ (blue dot-dashed lines in Fig. 8), both I_L and S_{LL} increase, since $\mu_L = \epsilon_1$, while $\epsilon_2 = 1.75\,\epsilon_0$, $\epsilon_3 = 0.25\,\epsilon_0$ and $\epsilon_4 = 0.875\,\epsilon_0$. The spin-resolved charge currents $I_L^{\uparrow} > 0$ and $I_L^{\downarrow} > 0$. In Fig. 8(b), around $\omega_L = 0.5\epsilon_0$ (grid line), one observes a small peak-dip for $D = 0.00875\,\epsilon_0$ (pink line), as $\epsilon_4 = \mu_R$ and quantum interference occurs between channels with energies ϵ_3 and ϵ_4, with $\epsilon_3 > \epsilon_4$ ($\omega < 0$), while for the anisotropy parameter $D = -0.01312\,\epsilon_0$ [green line in Fig. 8(b)] there is a dip-peak feature, as $\mu_L = \epsilon_2$, showing the impact of the quantum interference effect between channels with energies ϵ_1 and ϵ_2 [tunneling processes for all levels in Figs. 2(d) and 2(i)]. In both cases, the Fano factor is sub-Poissonian, $F < 1$. Again, one can see that $F \to 1/2$ if all the quasienergy levels lie within the bias voltage window [108], e.g., for $D = 0.005\,\epsilon_0$ and $\omega_L \leqslant 1.18\,\epsilon_0$, where $\omega_L = 1.18\,\epsilon_0$ corresponds to $\epsilon_3 = \mu_R$ (orange line in Fig. 9).

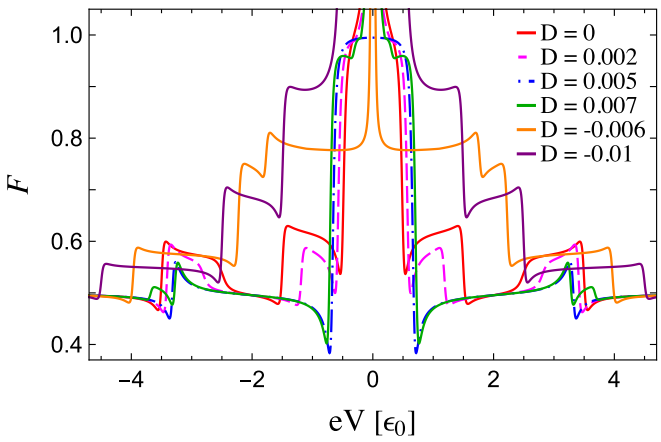

FIG. 7. Fano factor F as a function of the applied bias voltage $eV = \mu_L - \mu_R$ with $\mu_{L,R} = \pm eV/2$ and $\vec{B} = B\vec{e}_z$, for different uniaxial magnetic anisotropy parameters D at zero temperature. The other parameters are set to $\Gamma = 0.05\,\epsilon 0$, $\Gamma_L = \Gamma_R = \Gamma/2$, $\omega_L = 0.5\,\epsilon_0$, $J = 0.01\,\epsilon_0$, $S = 100$, and $\theta = \pi/3$. All energies are given in the units of ϵ_0.

For $D = -0.00625\,\epsilon_0$, around $\omega_L = 0.5\,\epsilon_0$, the double resonance occurs: $\mu_R = \epsilon_3$ and $\mu_L = \epsilon_4$, with $\epsilon_1 = 0.875\,\epsilon_0$ and $\epsilon_2 = 2\,\epsilon_0$ [see tunneling processes for all levels in Figs. 2(a) and 2(e)], resulting in a dip with higher magnitude in the noise S_{LL} as a sign of destructive quantum interference between channels with energies ϵ_3 and ϵ_4, connected with spin-flip events [blue dot-dashed line in Fig. 8(b)]. The charge current I_L shows a steplike decrease with $I_L^{\uparrow} < 0$ and $I_L^{\downarrow} > 0$, whereas in the Fano factor F a step increase occurs around $\omega_L = 0.5\,\epsilon_0$, leading to super-Poissonian noise, with $F > 1$ (blue dot-dashed line in Fig. 9). For $D = -0.0625\,\epsilon_0$, and $\omega_L > 0.5\,\epsilon_0$, the spin-resolved currents $I_L^{\uparrow} < 0$ and $I_L^{\downarrow} > 0$.

In Fig. 8(b), note that around ω_L corresponding to $\mu_\xi = \epsilon_i$, S_{LL} either increases, or if the quantum interference occurs, decreases around Fano-like line shapes (except around $\omega_L = 0.5$ for $D = -0.00625$). Accordingly, for each value of D, around ω_L such that one remaining quasienergy level ϵ_i within the bias-voltage window is in resonance with the chemical potential of one of the leads, one notices the final step decrease in the current I_L, and the final step increase or a dip-peak feature in S_{LL} (see Fig. 8). For instance, at $\omega_L = 2.25\,\epsilon_0$ and $D = -0.00625\,\epsilon_0$ (blue dot-dashed line), the remaining level within the bias-voltage window, $\epsilon_1 = \mu_R$ [see tunneling processes for all levels in Figs. 2(b) and 2(c)], whereas, for $D = -0.01312\,\epsilon_0$ and $\omega_L = 2.87\epsilon_0$ (green line in Fig. 8), the energy of the only level within the bias-voltage window equals $\epsilon_4 = \mu_L$ [tunneling processes in Figs. 2(c) and 2(f)]. With further increase of ω_L, all four levels ϵ_i lie out of the bias-voltage window, two below μ_R: $\epsilon_1 < \mu_R$ and $\epsilon_3 < \mu_R$, and two above μ_L: $\epsilon_2 > \mu_L$ and $\epsilon_4 > \mu_L$. Hence, the average current I_L drops to zero, with nonzero spin-resolved currents $I_L^{\uparrow} = -I_L^{\downarrow} < 0$, while S_{LL} becomes a constant, due to the spin-flip absorption processes, and $F > 1$, indicating the super-Poissonian noise.

In Fig. 10, the dependence of the autocorrelation noise S_{LL} on frequency ω_L is plotted for several values of the anisotropy parameter D and equal chemical potentials of the leads, $\mu_L = \mu_R = \mu = 0.25\epsilon_0$, at zero temperature. Here, only absorp-

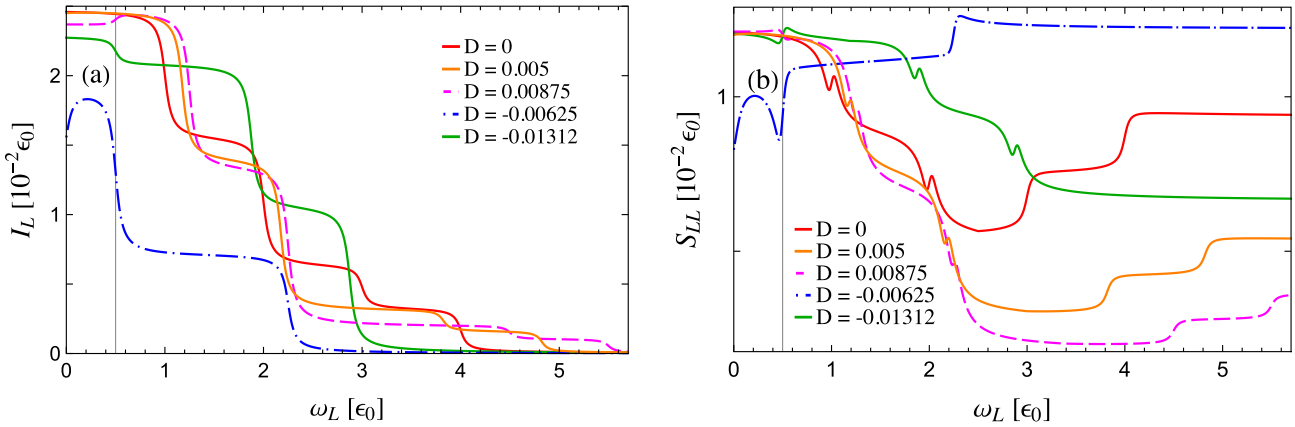

FIG. 8. (a) Charge current I_L and (b) autocorrelation shot noise S_{LL} as functions of the Larmor frequency ω_L for different uniaxial magnetic anisotropy parameters D. All plots are obtained at zero temperature with $\vec{B} = B\vec{e}_z$. The chemical potentials of the leads are equal to $\mu_R = 0$ and $\mu_L = 2.5\,\epsilon_0$, except for $D = -0.00625\,\epsilon_0$, where $\mu_L = 1.125\,\epsilon_0$. The other parameters are set to $\Gamma = 0.05\,\epsilon 0$, $\Gamma_L = \Gamma_R = \Gamma/2$, $J = 0.01\,\epsilon_0$, $S = 100$, and $\theta = \pi/3$. All energies are given in the units of ϵ_0. All steps in the current I_L, and the corresponding steps and dip-peak features in the noise S_{LL}, denote a resonance $\mu_\xi = \epsilon_i$, with $\xi = L, R$. A distinct dip in the noise S_{LL} and a significant drop of the corresponding current appear for $D = -0.00625\,\epsilon_0$ (blue dot-dashed line) around $\omega_L = 0.5\,\epsilon_0$ (grid line), due to the double resonance: $\mu_R = \epsilon_3$ and $\mu_L = \epsilon_4$.

tion processes between levels connected with spin-flip events occur. For isotropic molecular spin with $D = 0$ (red line in Fig. 10), the shot noise S_{LL} is an even function of ω_L at zero-bias conditions $eV = 0$, $S_{LL}(\omega_L) = S_{LL}(-\omega_L)$ [83], whereas if the molecular spin is anisotropic ($D \neq 0$), the shot noise is an even function of the frequency ω, $S_{LL}(\omega) = S_{LL}(-\omega)$. In all the plots each steplike increase or decrease corresponds to $\mu = \epsilon_i$ (not all are shown). For instance, if we take Larmor frequency $\omega_L = 0.5\,\epsilon_0$ (marked by a vertical grid line), there is a step-like increase for the magnetic anisotropy parameter $D = 0$ (red line) since the chemical potential μ is in resonance with quasienergy level ϵ_3, $\mu = \epsilon_3$. Similar step for $D = 0.002\,\epsilon_0$ occurs around $\omega_L = 0.586\,\epsilon_0$, where $\mu = \epsilon_3$ (purple line in Fig. 10). For $\omega_L = 0.5\,\epsilon_0$ and $D = 0.005\,\epsilon_0$, the resulting $\omega = 0$, with only two molecular levels, positioned above μ, at $\epsilon = 0.34\,\epsilon_0$ and $\epsilon' = 1.66\,\epsilon_0$, and neither elastic nor spin-flip processes occur. The shot noise S_{LL} monotonically decreases around $\omega_L = 0.5\,\epsilon_0$, drops to zero at $\omega_L = 0.5\,\epsilon_0$ (intersection between grid line and black line), since spin-resolved correlations $S_{LL}^{\sigma\sigma'} = 0$, and then monotonically increases. Similarly, the charge current noise S_{LL} is equal to zero at $\omega_L = 0.6\,\epsilon_0$, for $D = 0.006\epsilon_0$ (green line), at $\omega_L = 0.8\,\epsilon_0$, for $D = 0.008\,\epsilon_0$ (orange line), and at $\omega_L = \epsilon_0$, for $D = 0.01\,\epsilon_0$ (blue dot-dashed line). For $D = 0.006\,\epsilon_0$, $\mu = \epsilon_4$ at $\omega_L = 0.5\epsilon_0$ and one observes a step-like decrease (intersection between grid line and green line in Fig. 10). With further

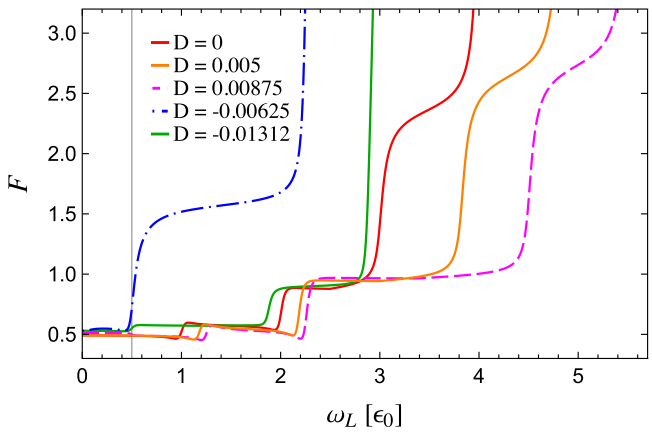

FIG. 9. Fano factor F as a function of the Larmor frequency ω_L for different uniaxial magnetic anisotropy parameters D. All plots are obtained at zero temperature with $\vec{B} = B\vec{e}_z$. The chemical potentials of the leads are equal to $\mu_R = 0$ and $\mu_L = 2.5\,\epsilon_0$, except for $D = -0.00625$ (blue dot-dashed line), where $\mu_L = 1.125\,\epsilon_0$. The other parameters are set to $\Gamma = 0.05\,\epsilon 0$, $\Gamma_L = \Gamma_R = \Gamma/2$, $J = 0.01\,\epsilon_0$, $S = 100$, and $\theta = \pi/3$. All energies are given in the units of ϵ_0.

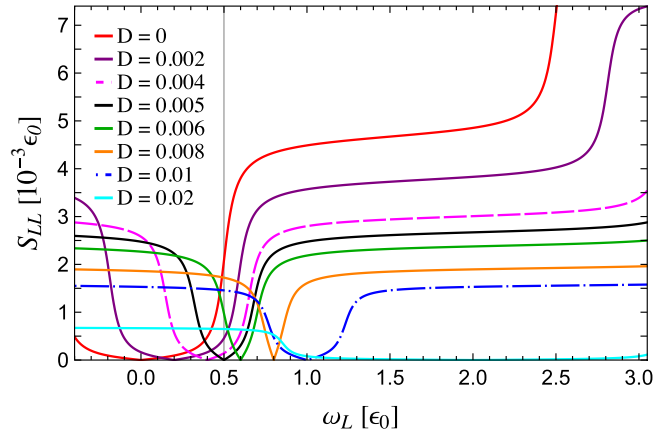

FIG. 10. Shot noise of charge current S_{LL} as a function of the Larmor frequency ω_L for different uniaxial magnetic anisotropy parameters D at zero-bias voltage. All plots are obtained at zero temperature with $\vec{B} = B\vec{e}_z$. The chemical potentials of the leads are equal: $\mu_L = \mu_R = 0.25\,\epsilon_0$. The other parameters are set to $\Gamma = 0.05\,\epsilon 0$, $\Gamma_L = \Gamma_R = \Gamma/2$, $J = 0.01\,\epsilon_0$, $S = 100$, and $\theta = \pi/3$. All energies are given in the units of ϵ_0. The noise S_{LL} is suppressed for $\omega = 0$, i.e., $D = \omega_L/2S_z$.

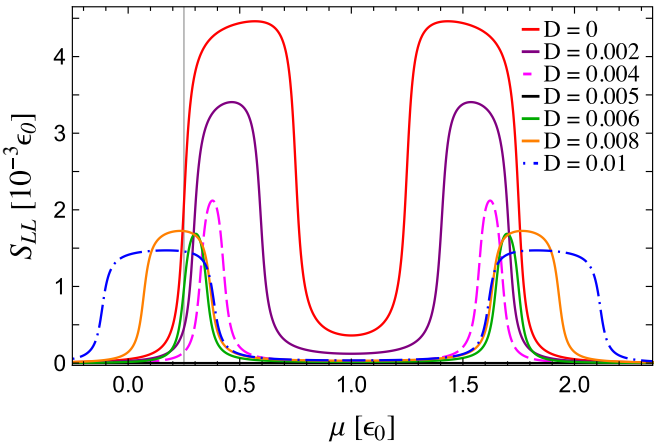

FIG. 11. Shot noise of charge current S_{LL} at zero bias-voltage conditions, as a function of the chemical potential of the leads $\mu = \mu_L = \mu_R$, for different uniaxial magnetic anisotropy parameters D. All plots are obtained at zero temperature with $\vec{B} = B\vec{e}_z$. The other parameters are set to $\Gamma = 0.05\,\epsilon 0$, $\Gamma_L = \Gamma_R = \Gamma/2$, $J = 0.01\,\epsilon_0$, $S = 100$, $\omega_L = 0.5\,\epsilon_0$, and $\theta = \pi/3$. All energies are given in the units of ϵ_0. The shot noise S_{LL} is positive between levels connected with spin-flip absorption events for $\omega \neq 0$, i.e., $D \neq \omega_L/2S_z$.

increase of the magnetic anisotropy parameter D, the noise S_{LL} decreases (cyan line in Fig. 10), and for a sufficiently large D, drops to zero, as $S_{LL}^{\uparrow\downarrow} + S_{LL}^{\downarrow\uparrow} \to 0$ and $S_{LL}^{\uparrow\uparrow} = S_{LL}^{\downarrow\downarrow} \to 0$.

The autocorrelation shot noise S_{LL} as a function of chemical potential of the leads at zero-bias voltage conditions $\mu = \mu_L = \mu_R$, when the average charge current is equal to zero, for several values of the magnetic anisotropy parameter D, at zero temperature, is shown in Fig. 11. The Larmor frequency $\omega_L = 0.5\,\epsilon_0$ and the tilt angle $\theta = \pi/3$. Since the contribution of the correlations between currents with the same spin $S_{LL}^{\sigma\sigma}$ is dominant, the noise S_{LL} takes positive values for $\omega \neq 0$, i.e., for $D \neq \omega_L/2S_z$ in the regions between quasienergy levels connected with spin-flip absorption processes, taking into account the level broadening Γ. The grid line in Fig. 11 at $\mu = 0.25\,\epsilon_0$, corresponding to the grid line in Fig. 10 at $\omega_L = 0.5\,\epsilon_0$, intersects with all the plots showing that the autocorrelation noise S_{LL} is reduced with the increase of the magnetic anisotropy parameter D. The noise can vanish at zero-bias voltage conditions for $\omega = 0$, and that is satisfied for $D = \omega_L/2S_z = 0.005\,\epsilon_0$ (black line in Fig. 11). In that case the spin-resolved correlations $S_{LL}^{\sigma\sigma'} = 0$. With further increase of the magnetic anisotropy parameter D, the frequency $\omega < 0$, i.e., the direction of the precession is altered, the anisotropy parameter $D > \omega_L/2S_z$, and the shot noise S_{LL} takes positive low values between quasienergy levels connected with spin-flip events (green, orange, and blue dot-dashed lines in Fig. 11), compared to the one at the highest positive frequency $\omega = \omega_L$, for the isotropic molecular spin (red line in in Fig. 11). In order to reduce the shot noise S_{LL} at zero-bias voltage conditions, one needs to increase the magnetic anisotropy parameter D and either slow down the precession of the molecular spin, or reverse the direction of the spin precession with respect to the Larmor precession. With further increase of the magnetic anisotropy parameter, for a sufficiently large anisotropy parameter D, the shot noise S_{LL} becomes entirely suppressed and drops to zero.

V. CONCLUSIONS

In this paper, the characteristics of charge transport through a single molecular orbital in the presence of a precessing anisotropic molecular spin in a magnetic field, connected to two noninteracting metallic leads, was theoretically studied. The Larmor frequency is modified by a term with the uniaxial magnetic anisotropy parameter of the molecular spin, and the resulting precession is externally kept undamped. The expressions for charge current and current noise were obtained using the Keldysh nonequilibrium Green's functions technique.

The results show rich transport characteristics at zero temperature. The quantum interference effects between the states connected with precession-assisted inelastic tunneling processes, involving absorption (emission) of an energy ω and a spin flip, manifest themselves as peaks (constructive interference) and dips (destructive interference) in the shot noise, matching the Fano-like line shapes, controlled by the anisotropy parameter and Larmor frequency. Each resonance between a chemical potential and an anisotropy dependent quasienergy level is visible in a transport measurement through characteristics such as steps, peaks and dips, and can be varied by tuning the anisotropy. The correlations between the same-spin (opposite-spin) currents are positive (negative), and are particularly interesting at zero-bias conditions since the resulting shot noise is positive for chemical potentials between quasienergy levels, which are connected by the inelastic absorption processes accompanied with a spin flip. Here, with the increase of the anisotropy parameter, the precession frequency decreases or the precession direction becomes altered, and the noise is reduced. Additionally, the anisotropy parameter can be adjusted to suppress the precession frequency, so that the resulting shot noise vanishes. It was shown that the charge current and shot noise can be controlled by a proper adjustment of the anisotropy parameter of the molecular magnet and reach their saturation if the anisotropy is large at nonzero bias voltage.

Taking into account that the charge transport in the given setup with the anisotropic magnetic molecule can be manipulated by the uniaxial magnetic anisotropy parameter of the molecular spin, and other parameters, the results of this study may be useful in the field of single-molecule electronics and spintronics. It might be useful for magnetic storage applications to study the charge- and spin-transport properties using a setup with a molecular spin modelled as a quantum object in the future.

ACKNOWLEDGMENTS

The author acknowledges funding provided by the Institute of Physics Belgrade, through the Grant No: 451-03-68/2022-14/200024 of the Ministry of Education, Science, and Technological Development of the Republic of Serbia.

APPENDIX: DERIVATION OF FLOQUET QUASIENERGIES

Here, the derivation of the Floquet quasienergies given by Eqs. (11) and (12) is presented. A periodic Hamiltonian $\hat{H}(t) = \hat{H}(t + \mathcal{T})$, with a period $\mathcal{T} = 2\pi/\omega$ can be written as

a Fourier series

$$\hat{H}(t) = \sum_{n=-\infty}^{\infty} \hat{H}^{(n)} e^{in\omega t}. \tag{A1}$$

According to the Floquet theorem [95–98], the so called quasienergy states

$$|\psi_\alpha(t)\rangle = e^{-i\epsilon_\alpha t}|\phi_\alpha(t)\rangle, \tag{A2}$$

with quasienergies ϵ_α and time-periodic functions $|\phi_\alpha(t)\rangle = |\phi_\alpha(t+\mathcal{T})\rangle$, represent solutions of the Schrödinger equation

$$\hat{H}(t)|\psi(t)\rangle = i\hbar\frac{\partial}{\partial t}|\psi(t)\rangle. \tag{A3}$$

Substituting Eq. (A2) into Eq. (A3), one obtains [95–98]

$$\hat{\mathcal{H}}(t)|\phi_\alpha(t)\rangle = \epsilon_\alpha|\phi_\alpha(t)\rangle, \tag{A4}$$

where $\hat{\mathcal{H}}(t) = \hat{H}(t) - i\partial/\partial t$. Using an orthonormal basis $\{|\alpha\rangle\}$ for the Hilbert space in which the Hamiltonian $\hat{H}(t)$ can be represented, the quasienergy state $|\psi_\alpha(t)\rangle$ can be expanded as a Fourier series, while the quasienergies ϵ_α can be calculated as the eigenvalues of the Floquet Hamiltonian $\hat{H}^{\mathrm{F}}$,

$$\det|\hat{H}^{\mathrm{F}} - \epsilon\hat{I}| = 0. \tag{A5}$$

The matrix elements of $\hat{H}^{\mathrm{F}}$ in the orthonormal basis $\{|\alpha n\rangle\}$, with $|\alpha n\rangle = |\alpha\rangle \otimes |n\rangle$ representing products $|\alpha\rangle e^{in\omega t}$, with $n \in \mathbb{Z}$, are given by [96]

$$\langle\alpha n|\hat{H}^{\mathrm{F}}|\beta m\rangle = \langle\alpha|\hat{H}^{(n-m)}|\beta\rangle + n\omega\delta_{\alpha\beta}\delta_{nm}, \tag{A6}$$

which can be further expressed as

$$H^{\mathrm{F}}_{\alpha n,\beta m} = H^{(n-m)}_{\alpha\beta} + n\omega\delta_{\alpha\beta}\delta_{nm}. \tag{A7}$$

The infinite number of quasienergies, $\epsilon_\alpha + n\hbar\omega$ can be obtained for each quasienergy state $|\psi_\alpha(t)\rangle$, so that one only needs to calculate quasienergies within one interval, e.g., $[0, \omega)$.

In the Hilbert space spanned by the eigenvectors of operator $\hat{s}_z$, $|\uparrow\rangle = |1\rangle$ and $|\downarrow\rangle = |2\rangle$, the time-periodic Hamiltonian of the molecular orbital $\hat{H}_{\mathrm{MO}}(t) = \hat{H}_{\mathrm{MO}}(t + 2\pi/\omega)$ reads

$$\hat{H}_{\mathrm{MO}}(t) = \lambda_1|1\rangle\langle 1| + \lambda_2|2\rangle\langle 2| + \frac{JS_\perp}{2}e^{-i\omega t}|1\rangle\langle 2| + \frac{JS_\perp}{2}e^{i\omega t}|2\rangle\langle 1|, \tag{A8}$$

with $\lambda_1 = \epsilon_0 + (\omega_L + JS_z)/2$, $\lambda_2 = \epsilon_0 - (\omega_L + JS_z)/2$ and $\omega = \omega_L - 2DS_z$. The Hamiltonian of the molecular orbital expressed as a Fourier series

$$\hat{H}_{\mathrm{MO}}(t) = \sum_{n=-\infty}^{\infty} \hat{H}^{(n)}_{\mathrm{MO}} e^{in(\omega_L - 2DS_z)t}, \tag{A9}$$

has the following nonzero components, calculated using Eq. (A7):

$$\hat{H}^{(0)}_{\mathrm{MO}} = \lambda_1|1\rangle\langle 1| + \lambda_2|2\rangle\langle 2|, \tag{A10}$$

$$\hat{H}^{(-1)}_{\mathrm{MO}} = \frac{JS_\perp}{2}e^{-i(\omega_L - 2DS_z)t}|1\rangle\langle 2|, \tag{A11}$$

$$\hat{H}^{(1)}_{\mathrm{MO}} = \frac{JS_\perp}{2}e^{i(\omega_L - 2DS_z)t}|2\rangle\langle 1|. \tag{A12}$$

According to Eq. (A7) the matrix elements of the Floquet Hamiltonian can be calculated as

$$H^{\mathrm{F}}_{1n,1m} = [\lambda_1 + n(\omega_L - 2DS_z)]\delta_{nm}, \tag{A13}$$

$$H^{\mathrm{F}}_{1n,2m} = \frac{JS_\perp}{2}\delta_{n,m-1}, \tag{A14}$$

$$H^{\mathrm{F}}_{2n,1m} = \frac{JS_\perp}{2}\delta_{n,m+1}, \tag{A15}$$

$$H^{\mathrm{F}}_{2n,2m} = [\lambda_2 + n(\omega_L - 2DS_z)]\delta_{nm}. \tag{A16}$$

Since the Floquet Hamiltonian is block diagonal, it is enough to write one block,

$$\begin{pmatrix} \lambda_1 + (n-1)(\omega_L - 2DS_z) & JS_\perp/2 \\ JS_\perp/2 & \lambda_2 + n(\omega_L - 2DS_z) \end{pmatrix}. \tag{A17}$$

The Floquet quasienergies ϵ_1 and ϵ_3 are the eigenvalues of the block for $n = 0$, given by

$$\epsilon_{1,3} = \epsilon_0 - \frac{\omega_L}{2} + DS_z \pm \sqrt{D(D+J)S_z^2 + \left(\frac{JS}{2}\right)^2}, \tag{A18}$$

while the quasienergies $\epsilon_2 = \epsilon_1 + \omega$ and $\epsilon_4 = \epsilon_3 + \omega$ are the eigenvalues of the neighboring block with diagonal matrix elements shifted by ω.

[1] L. Thomas, F. Lionti, R. Ballou, D. Gatteschi, R. Sessoli, and B. Barbara, Macroscopic quantum tunnelling of magnetization in a single crystal of nanomagnets, Nature (London) **383**, 145 (1996).

[2] D. Gatteschi, R. Sessoli, and J. Villain, *Molecular Nanomagnets*, (Oxford University Press, New York, 2006).

[3] L. Bogani and W. Wernsdorfer, Molecular spintronics using single-molecule magnets, Nat. Mater. **7**, 179 (2008).

[4] C. Timm and M. Di Ventra, Memristive properties of single-molecule magnets, Phys. Rev. B **86**, 104427 (2012).

[5] M. N. Leuenberger and D. Loss, Quantum computing in molecular magnets, Nature (London) **410**, 789 (2001).

[6] R. E. P. Winpenny, Quantum information processing using molecular nanomagnets As qubits, Angew. Chem. Int. Ed. **47**, 7992 (2008).

[7] R. Sessoli, D. Gatteschi, A. Caneschi, and M. A. Novak, Magnetic bistability in a metal-ion cluster, Nature (London) **365**, 141 (1993).

[8] M. Misiorny and J. Barnaś, Effects of intrinsic spin-relaxation in molecular magnets on current-induced magnetic switching, Phys. Rev. B **77**, 172414 (2008).

[9] M. Mannini, F. Pineider, P. Sainctavit, C. Danieli, E. Otero, C. Sciancalepore, A. M. Talarico, M-A. Arrio, A. Cornia, D. Gatteschi, and R. Sessoli, Magnetic memory of a single-molecule quantum magnet wired to a gold surface, Nat. Mater. **8**, 194 (2009)

[10] O. Waldmann, A criterion for the anisotropy barrier in single-molecule magnets, Inorg. Chem. **46**, 10035 (2007).

[11] C. J. Milios, R. Inglis, R. Bogai, W. Wernsdorfer, A. Collins, S. Moggach, S. Parsons, S. P. Perlepes, G. Christou, and E. K. Brechin, Enhancing SMM properties in a family of [Mn_6] clusters, Chem. Commun., 3476 (2007).

[12] F. Neese and D. A. Pantazis, What is not required to make a single molecule magnet, Faraday Discuss. **148**, 229 (2011).

[13] Y.-S. Meng, S.-D. Jiang, B.-W. Wang, and S. Gao, Understanding the magnetic anisotropy toward single-ion magnets, Acc. Chem. Res. **49**, 2381 (2016).

[14] A. Chiesa, P. Santini, E. Garlatti, F. Luis, and S. Carreta, Molecular nanomagnets: A viable path toward quantum information processing? Rep. Prog. Phys. **87**, 034501 (2024).

[15] J.-X. Zhu and A. V. Balatsky, Quantum electronic transport through a precessing spin, Phys. Rev. Lett. **89**, 286802 (2002).

[16] J.-X. Zhu and A. V. Balatsky, Josephson current in the presence of a precessing spin, Phys. Rev. B **67**, 174505 (2003).

[17] N. Bode, L. Arrachea, G. S. Lozano, T. S. Nunner, and F. von Oppen, Current-induced switching in transport through anisotropic magnetic molecules, Phys. Rev. B **85**, 115440 (2012).

[18] M. Misiorny, M. Hell, and M. R. Wegewijs, Spintronic magnetic anisotropy, Nat. Phys. **9**, 801 (2013).

[19] P. Stadler, C. Holmqvist, and W. Belzig, Josephson current through a quantum dot coupled to a molecular magnet, Phys. Rev. B **88**, 104512 (2013).

[20] M. Filipović, C. Holmqvist, F. Haupt, and W. Belzig, Spin transport and tunable Gilbert damping in a single-molecule magnet junction, Phys. Rev. B **87**, 045426 (2013); Erratum: Spin transport and tunable Gilbert damping in a single-molecule magnet junction [Phys. Rev. B 87, 045426 (2013)], **88**, 119901 (2013).

[21] J. Fransson, J. Ren, and J.-X. Zhu, Electrical and thermal control of magnetic exchange interactions, Phys. Rev. Lett. **113**, 257201 (2014).

[22] T. Saygun, J. Bylin, H. Hammar, and J. Fransson, Voltage-induced switching dynamics of a coupled spin pair in a molecular junction, Nano Lett. **16**, 2824 (2016).

[23] H. Hammar and J. Fransson, Time-dependent spin and transport properties of a single-molecule magnet in a tunnel junction, Phys. Rev. B **94**, 054311 (2016).

[24] A. Płomińska, M. Misiorny, and I. Weymann, Manipulating spins of magnetic molecules: Hysteretic behavior with respect to bias voltage, Europhys. Lett. **121**, 38006 (2018).

[25] U. Bajpai and B. Nikolić, Time-retarded damping and magnetic inertia in the Landau-Lifshitz-Gilbert equation self-consistently coupled to electronic time-dependent nonequilibrium Green functions, Phys. Rev. B **99**, 134409 (2019).

[26] Z. Zhang, Y. Wang, H. Wang, H. Liu, and L. Dong, Controllable Spin Switching in a Single-Molecule Magnetic Tunneling Junction, Nanoscale. Res. Lett. **16**, 77 (2021).

[27] R. Smorka, M. Thoss, and M. Žonda, Dynamics of spin relaxation in nonequilibrium magnetic nanojunctions, New J. Phys. **26**, 013056 (2024).

[28] H. B. Heersche, Z. de Groot, J. A. Folk, H. S. J. van der Zant, C. Romeike, M. R. Wegewijs, L. Zobbi, D. Barreca, E. Tondello, and A. Cornia, Electron transport through single Mn_{12} molecular magnets, Phys. Rev. Lett. **96**, 206801 (2006).

[29] J. R. Hauptmann, J. Paaske, and P. E. Lindelof, Electric-field-controlled spin reversal in a quantum dot with ferromagnetic contacts, Nat. Phys. **4**, 373 (2008).

[30] S. Loth, K. von Bergmann, M. Ternes, A. F. Otte, C. P. Lutz, and A. J. Heinrich, Controlling the state of quantum spins with electric currents, Nat. Phys. **6**, 340 (2010).

[31] T. Komeda, H. Isshiki, J. Liu, Y.-F. Zhang, N. Lorente, K. Katoh, B. K. Breedlove, and M. Yamashita, Observation and electric current control of a local spin in a single-molecule magnet, Nat. Commun. **2**, 217 (2011).

[32] R. Vincent, S. Klyatskaya, M. Ruben, W. Wernsdorfer, and F. Balestro, Electronic read-out of a single nuclear spin using a molecular spin transistor, Nature (London) **488**, 357 (2012).

[33] F. D. Natterer, K. Yang, W. Paul, P. Willke, T. Choi, T. Greber, A. J. Heinrich, and C. P. Lutz, Reading and writing single-atom magnets, Nature (London) **543**, 226 (2017).

[34] G. Czap, P. J. Wagner, F. Xue, L. Gu, J. Li, J. Yao, R. Q. Wu, and W. Ho, Probing and imaging spin interactions with a magnetic single-molecule sensor, Science **364**, 670 (2019).

[35] T. Pei, J. O. Thomas, S. Sopp, M.-Y. Tsang, N. Dotti, J. Baugh, N. F. Chilton, S. Cardona-Serra, A. Gaita-Ariño, H. L. Anderson, and L. Bogani, Exchange-induced spin polarization in a single magnetic molecule junction, Nat. Commun. **13**, 4506 (2022).

[36] C. Romeike, M. R. Wegewijs, W. Hofstetter, and H. Schoeller, Quantum-tunneling-induced Kondo effect in single molecular magnets, Phys. Rev. Lett. **96**, 196601 (2006).

[37] F. Elste and C. Timm, Resonant and Kondo tunneling through molecular magnets, Phys. Rev. B **81**, 024421 (2010).

[38] M. Misiorny, I. Weymann, and J. Barnaś, Temperature dependence of electronic transport through molecular magnets in the Kondo regime, Phys. Rev. B **86**, 035417 (2012).

[39] Y. Li, H. Kan, Y. Miao, S. Qiu, G. Zhang, J. Ren, C. Wang, and G. Hu, Magnetic manipulation of orbital hybridization and magnetoresistance in organic ferromagnetic co-oligomers, Physica E **124**, 114327 (2020).

[40] C. Timm and F. Elste, Spin amplification, reading, and writing in transport through anisotropic magnetic molecules, Phys. Rev. B **73**, 235304 (2006).

[41] A. Płomińska and I. Weymann, Pauli spin blockade in double molecular magnets, Phys. Rev. B **94**, 035422 (2016).

[42] A. Płomińska and I. Weymann, Magnetoresistive properties of a double magnetic molecule spin valve in different geometrical arrangements, J. Magn. Magn. Mater. **480**, 11 (2019).

[43] M.-H. Jo, J. E. Grose, K. Baheti, M. M. Deshumukh, J. J. Sokol, E. M. Rumberger, D. N. Hendrickson, J. R. Long, H. Park, and D. C. Ralph, Signatures of molecular magnetism in single-molecule transport spectroscopy, Nano Lett. **6**, 2014 (2006).

[44] A. S. Zyazin, J. W. G. van den Berg, E. A. Osorio, H. S. J. van der Zant, N. P. Konstantinidis, M. Leijnse, M. R. Wegewijs, F. May, W. Hofstetter, C. Danieli, and A. Cornia, Electric field controlled magnetic anisotropy in a single molecule, Nano Lett. **10**, 3307 (2010).

[45] N. Roch, R. Vincent, F. Elste, W. Harneit, W. Wernsdorfer, C. Timm, and F. Balestro, Cotunneling through a magnetic

single-molecule transistor based on N@C_{60}, Phys. Rev. B **83**, 081407(R) (2011).

[46] Z. Nussinov, A. Shnirman, D. P. Arovas, A. V. Balatsky, and J.-X. Zhu, Spin and spin-wave dynamics in Josephson junctions, Phys. Rev. B **71**, 214520 (2005).

[47] J. Fransson and J.-X. Zhu, Spin dynamics in a tunnel junction between ferromagnets, New J. Phys. **10**, 013017 (2008).

[48] G. Serrano, L. Poggini, M. Briganti, A. L. Sorentino, G. Cucinotta, L. Malavolti, B. Cortigiani, E. Otero, P. Sainctavit, S. Loth, F. Parenti, A.-L. Barra, A. Vindigni, A. Cornia, F. Totti, M. Mannini, and R. Sessoli, Quantum dynamics of a single molecule magnet on superconducting Pb(111), Nat. Mater. **19**, 546 (2020).

[49] R.-Q. Wang, L. Sheng, R. Shen, B. Wang, and D. Y. Xing, Thermoelectric effect in single-molecule-magnet junctions, Phys. Rev. Lett. **105**, 057202 (2010).

[50] M. Misiorny and J. Barnaś, Spin-dependent thermoelectric effects in transport through a nanoscopic junction involving a spin impurity, Phys. Rev. B **89**, 235438 (2014).

[51] M. Misiorny and J. Barnaś, Effect of magnetic anisotropy on spin-dependent thermoelectric effects in nanoscopic systems, Phys. Rev. B **91**, 155426 (2015).

[52] H. Hammar, J. D. V. Jaramillo, and J. Fransson, Spin-dependent heat signatures of single-molecule spin dynamics, Phys. Rev. B **99**, 115416 (2019).

[53] F. Wang, W. Shen, Y. Shui, J. Chen, H. Wang, R. Wang, Y. Qin, X. Wang, J. Wan, M. Zhang, X. Liu, T. Yang, and F. Song, Electrically controlled nonvolatile switching of single-atom magnetism in a Dy@C_{84} single-molecule transistor, Nat. Commun. **15**, 2450 (2024).

[54] Y. Shiota, T. Nozaki, F. Bonell, S. Murakami, T. Shinjo, and Y. Suzuki, Induction of coherent magnetization switching in a few atomic layers of FeCo using voltage pulses, Nat. Mater. **11**, 39 (2012).

[55] B. W. Heinrich, L. Braun, J. I. Pascual, and K. J. Franke, Tuning the magnetic anisotropy of single molecules, Nano Lett. **15**, 4024 (2015).

[56] J. D. V. Jaramillo, H. Hammar, and J. Fransson, Electronically mediated magnetic anisotropy in vibrating magnetic molecules, ACS Omega **3**, 6546 (2018).

[57] B. Rana and Y. Otani, Towards magnonic devices based on voltage-controlled magnetic anisotropy, Commun. Phys. **2**, 90 (2019).

[58] E. Burzurí, A. S. Zyazin, A. Cornia, and H. S. J. van der Zant, Direct observation of magnetic anisotropy in an individual Fe_4 single-molecule magnet, Phys. Rev. Lett. **109**, 147203 (2012).

[59] R. E. George, J. P. Edwards, and A. Ardavan, Coherent spin control by electrical manipulation of the magnetic anisotropy, Phys. Rev. Lett. **110**, 027601 (2013).

[60] A. Sarkar and G. Rajaraman, Modulating magnetic anisotropy in Ln(III) single-ion magnets using an external electric field, Chem. Sci. **11**, 10324 (2020).

[61] Y. Lu, Y. Wang, L. Zhu, L. Yang, and L. Wang, Electric field tuning of magnetic states in single magnetic molecules, Phys. Rev. B **106**, 064405 (2022).

[62] J. J. Parks, A. R. Champagne, T. A. Costi, W. W. Shum, A. N. Pasupathy, E. Neuscamman, S. Flores-Torres, P. S. Cornaglia, A. A. Aligia, C. A. Balseiro, G. K.-L. Chan, H. D. Abruña, and D. C. Ralph, Mechanical control of spin states in spin-1 molecules and the underscreened Kondo effect, Science **328**, 1370-1373 (2010).

[63] T. Goswami and A. Misra, Ligand effects toward the modulation of magnetic anisotropy and design of magnetic systems with desired anisotropy characteristics, J. Phys. Chem. A **116**, 5207-5215 (2012).

[64] J. M. Zadrozny, D. J. Xiao, M. Atanasov, G. J. Long, F. Grandjean, F. Neese, and J. R. Long, Magnetic blocking in a linear iron(I) complex, Nature Chem. **5**, 577 (2013).

[65] X.-N. Yao, J.-Z. Du, Y.-Q. Zhang, X.-B. Leng, M.-W. Yang, S.-D. Jiang, Z.-X. Wang, Z.-W. Ouyang, L. Deng, B.-W. Wang, and S. Gao, Two-coordinate Co(II) Imido complexes as outstanding single-molecule magnets, J. Am. Chem. Soc. **139**, 373 (2017).

[66] P. C. Bunting, M. Atanasov, E. Damgaard-Møller, M. Perfetti, I. Crassee, M. Orlita, J. Overgaard, J. van Slageren, F. Neese, and J. R. Long, A linear cobalt(II) complex with maximal orbital angular momentum from a non-Aufbau ground state, Science **362**, eaat7319 (2018).

[67] S. Tripathi, S. Vaidya, N. Ahmed, E. A. Klahn, H. Cao, L. Spillecke, C. Koo, S. Spachmann, R. Klingeler, R. Rajaraman, J. Overgaard, and M. Shanmugam, Structure-property correlation in stabilizing axial magnetic anisotropy in octahedral Co(II) complexes, Cell Reports Physical Science **2**, 100404 (2021).

[68] M. M. Paquette, D. Plaul, A. Kurimoto, B. O. Patrick, and N. L. Frank, Opto-spintronics: Photoisomerization-induced spin state switching at 300 K in photochrome cobalt-dioxolene thin films, J. Am. Chem. Soc. **140**, 14990-15000 (2018).

[69] S. L. Bayliss, D. W. Laorenza, P. J. Mintun, B. D. Kovos, D. E. Freedman, and D. D. Awschalom, Optically addressable molecular spins for quantum information processing, Science **370**, 1309-1312 (2020).

[70] K. S. Kumar, D. Serrano, A. M. Nonat, B. Heinrich, L. Karmazin, L. J. Charbonnière, P. Goldner, and M. Ruben, Optical spin-state polarization in a binuclear europium complex towards molecule-based coherent light-spin interfaces, Nat. Commun. **12**, 2152 (2021).

[71] N. S. Wingreen, A.-P. Jauho, and Y. Meir, Time-dependent transport through a mesoscopic structure, Phys. Rev. B **48**, 8487 (1993).

[72] A.-P. Jauho, N. S. Wingreen, and Y. Meir, Time-dependent transport in interacting and noninteracting resonant-tunneling systems, Phys. Rev. B **50**, 5528 (1994).

[73] A.-P. Jauho and H. Haug, *Quantum Kinetics in Transport and Optics of Semiconductors* (Springer, Berlin, 2008).

[74] M. Galperin, A. Nitzan, and M. A. Ratner, Inelastic tunneling effects on noise properties of molecular junctions, Phys. Rev. B **74**, 075326 (2006).

[75] M. Galperin, A. Nitzan, and M. A. Ratner, Molecular transport junctions: Vibrational effects, J. Phys.: Condens. Matter **19**, 103201 (2007).

[76] R. Härtle, M. Butzin, O. Rubio-Pons, M. Thoss, Quantum interference and decoherence in single-molecule junctions: How vibrations induce electrical current, Phys. Rev. Lett. **107**, 046802 (2011).

[77] H. Hammar and J. Fransson, Dynamical exchange and phase induced switching of a localized molecular spin, Phys. Rev. B **98**, 174438 (2018).

[78] G. Cohen and M. Galperin, Green's function methods for single molecule junctions, J. Chem. Phys. **152**, 090901 (2020).
[79] Y. M. Blanter and M. Büttiker, Shot noise in mesoscopic conductors, Phys. Rep. **336**, 1 (2000).
[80] F. M. Souza, A.-P. Jauho, and J. C. Egues, Spin-polarized current and shot noise in the presence of spin flip in a quantum dot via nonequilibrium Green's functions, Phys. Rev. B **78**, 155303 (2008).
[81] F. Haupt, T. Novotný, and W. Belzig, Phonon-assisted current noise in molecular junctions, Phys. Rev. Lett. **103**, 136601 (2009).
[82] H.-K. Zhao, W.-K. Zou, and Q. Chen, Shot noise of charge current in a quantum dot responded by rotating and oscillating magnetic fields, J. Appl. Phys **116**, 093702 (2014).
[83] M. Filipović and W. Belzig, Shot noise of charge and spin transport in a junction with a precessing molecular spin, Phys. Rev. B **97**, 115441 (2018).
[84] Z. Feng, J. Maciejko, J. Wang, and H. Guo, Current fluctuations in the transient regime: An exact formulation for mesoscopic systems, Phys. Rev. B **77**, 075302 (2008).
[85] I. Djuric, B. Dong, and H.-L. Cui, Shot noise in resonant tunneling through an interacting quantum dot with intradot spin-flip scattering, IEEE Trans. Nanotechnol. **4**, 71 (2005).
[86] W. Belzig and M. Zareyan, Spin-flip noise in a multiterminal spin valve, Phys. Rev. B **69**, 140407(R) (2004).
[87] H. K. Zhao, J. Zhang, and J. Wang, Dynamic spin-flip shot noise of mesoscopic transport through a toroidal carbon nanotube, Europhys. Lett. **109**, 18003 (2015).
[88] R. de-Picciotto, M. Reznikov, M. Heiblum, V. Umansky, G. Bunin, and D. Mahalu, Direct observation of a fractional charge, Nature (London) **389**, 162 (1997).
[89] X. Jehl, M. Sanquer, R. Calemczuk, and D. Mailly, Detection of doubled shot noise in short normal-metal/superconductor junctions, Nature (London) **405**, 50 (2000).
[90] E. Sivre, H. Duprez, A. Anthore, A. Assime, F. D. Parmentier, A. Cavanna, A. Ouerghi, U. Gennser, and F. Pierre, Electronic heat flow and thermal shot noise in quantum circuits, Nat. Commun. **10**, 5638 (2019).
[91] S. Larocque, E. Pinsolle, C. Lupien, and B. Reulet, Shot noise of a temperature-biased tunnel junction, Phys. Rev. Lett. **125**, 106801 (2020).
[92] J. Eriksson, M. Acciai, L. Tesser, and J. Splettstoesser, General bounds on electronic shot noise in the absence of currents, Phys. Rev. Lett. **127**, 136801 (2021).
[93] A. Popoff, J. Rech, T. Jonckheere, L. Raymond, B. Grémaud, S. Malherbe, and T. Martin, Scattering theory of nonequilibrium noise and delta T current fluctuations through a quantum dot, J. Phys.: Condens. Matter **34**, 185301 (2022).
[94] M. Hübler and W. Belzig, Light emission in delta-T-driven mesoscopic conductors, Phys. Rev. B **107**, 155405 (2023).
[95] G. Floquet, Sur les équations différentielles linéaires à coefficients périodiques, Annales scientifiques de l'École Normale Supérieure **12**, 47 (1883).
[96] J. H. Shirley, Interaction of a quantum system with a strong oscillating field, Ph.D. thesis, California Institute of Technology, 1963.
[97] M. Grifoni and P. Hänggi, Driven quantum tunneling, Phys. Rep. **304**, 229 (1998).
[98] B. H. Wu and C. Timm, Noise spectra of ac-driven quantum dots: Floquet master-equation approach, Phys. Rev. B **81**, 075309 (2010).
[99] U. Fano, Effects of Configuration Interaction on Intensities and Phase Shifts, Phys. Rev. **124**, 1866 (1961).
[100] A. E. Miroshnichenko, S. Flach, and Y. S. Kivshar, Fano resonances in nanoscale structures, Rev. Mod. Phys. **82**, 2257 (2010).
[101] C. Kittel, On the theory of ferromagnetic resonance absorption, Phys. Rev. **73**, 155 (1948).
[102] C. Godfrin, S. Thiele, A. Ferhat, S. Klyatskaya, M. Ruben, W. Wernsdorfer, and F. Balestro, Electrical read-out of a single spin using an exchange-coupled quantum dot, ASC Nano **11**, 3984 (2017).
[103] H. Bruus and K. Flensberg, *Many-Body Quantum Theory in Condensed Matter Physics* (Oxford University Press, Oxford, UK, 2004).
[104] B. Wang, J. Wang, and H. Guo, Quantum spin field effect transistor, Phys. Rev. B **67**, 092408 (2003).
[105] M. Filipović and W. Belzig, Photon-assisted electronic and spin transport in a junction containing precessing molecular spin, Phys. Rev. B **93**, 075402 (2016).
[106] A. Fetter and J. D. Walecka, *Quantum Theory of Many-Particle Systems* (Dover, Mineola, NY, 2003).
[107] D. C. Langreth, in *Linear and Nonlinear Electron Transport in Solids*, edited by J. T. Devreese and E. Van Doren (Plenum, New York, 1976).
[108] A. Thielmann, M. H. Hettler, J. König, and G. Schön, Shot noise in tunneling transport through molecules and quantum dots, Phys. Rev. B **68**, 115105 (2003).

Spin transport through a nanojunction with a precessing anisotropic molecular spin - quantum interference and spin-transfer torque

Milena Filipović
Institute of Physics Belgrade, University of Belgrade, Pregrevica 118, 11080 Belgrade, Serbia
(Dated: June 12, 2025)

The subject of this study is spin transport through a molecular orbital connected to two leads, and coupled via exchange interaction with a precessing anisotropic molecular spin in a constant magnetic field. The inelastic spin-flip processes between molecular quasienergy levels are driven by the molecular spin precession. By setting the Larmor frequency, the tilt angle of molecular magnetization with respect to the magnetic field, and the magnetic anisotropy parameter, one can modulate the spin current and noise, spin-transfer torque and related torque coefficients. Moreover, the dc-spin current and spin-transfer torque components provide the quasienergy level structure in the orbital. Quantum interference effects between states connected with spin-flip processes manifest themselves as dips (minimums) and peaks (maximums) in spin-current noise, matching Fano-like resonance profiles with equal probabilities of interfering elastic and spin-flip pathways. By proper adjustment of the anisotropy parameter and magnetic field, the precession is suppressed and the torque vanishes, allowing to reveal the anisotropy parameter via a dc-spin current or torque measurement. The results of the study show that spin transport and spin-transfer torque can be manipulated by the anisotropy parameter even in the absence of the magnetic field.

I. INTRODUCTION

Due to small size and uniaxial magnetic anisotropy which leads to magnetic bistability, single-molecule magnets are potential candidates for magnetic storage and information processing.[1–15] Since energy barrier to molecular spin reversal depends on the magnetic anisotropy parameter,[2,3,16,17] it is important to find ways to control it, e.g., via charge current or electric field.[8–10,18–24] For the potential applications in spintronics, various phenomena in magnetic structures have been subject of research, such as spin relaxation,[25–29] spin fluctuations,[30–32] geometrical spin torque,[33,34] self-induced torque[35] and dynamics of magnetization driven by external means.[36–48] The control of magnetization in junctions by spin-polarized current was first theoretically suggested[49,50] and then experimentally confirmed.[51,52] By applying spin torque, the magnetization dynamics can be manipulated,[49] and as a back action the spin pumping occurs.[53,54] It is possible to reverse magnetization via current-induced spin-transfer torque (STT).[36,55–60] For instance, using spin-polarized current through a single-molecule magnet connected with ferromagnetic electrodes, its spin states can be switched.[17,61–64] It has been shown that the anisotropic molecular spin can be reversed even in the absence of a magnetic field by turning on a bias voltage for one ferromagnetic and one paramagnetic lead.[65] Spin-polarized currents exert STTs on the magnetization of magnetic nanostructures in the form of field-like or damping torques.[36,66–72] The effect of superconductivity on the magnetization dynamics has also been studied since the beginning of the new century.[44,73–79]

The nonequilibrium Green's functions (NEGF) formalism[80–82] has been employed in molecular spintronics in investigations of e.g., spin pumps,[83,84] quantum interference,[85] spin-flip inelastic tunneling,[86–89] and magntic skyrmion dynamics.[90–92] NEGF technique has also been used in the theoretical calculations of spin-current shot noise.[93–95] While investigating transport through single-molecule magnets, many effects were analysed such as Kondo effect,[96–100] spin-Seebeck effect,[101–103] STT,[104,105] and spin blockade.[65,106,107] In molecular spintronics experimental studies of spin polarized currents,[108,109] spin interactions,[110,111] spin valves,[112] and spin-flip inelastic electron tunneling spectroscopy[8,113] have been done.

The classical magnetization dynamics is usually described by the Landau-Lifshitz-Gilbert (LLG) equation.[114–116] Even thermal effects on the magnetization dynamics have been studied using LLG equation.[117–119] The contribution of STT due to spin-polarized currents can be included in LLG equation,[36,67] and has been derived for molecular magnets,[41,119–121] and other magnetic systems such as spin-valves or magnetic multilayers,[49] magnetic domain walls,[122] slowly varying magnetization,[123] and magnetic skyrmions.[92,124] In quantum transport calculations, the semiclassical approach is often used, where the local magnetization of a magnetic nanostructure is treated as classical and its dynamics is described by LLG equation, while the spin of the conduction electrons is considered as quantum.[34,121,125–130] It is assumed that the spin-polarized currents are carried by electrons that are fast in comparison to the local magnetization dynamics.

The aim of this article is to theoretically study the spin transport through a single molecular orbital of a molecular magnet with a precessing anisotropic spin in a constant magnetic field. The precession frequency of the molecular spin involves Larmor frequency and a term with the uniaxial magnetic anisotropy parameter. The spin in the orbital and molecular spin are coupled via exchange interaction. The orbital is connected to two normal metal leads, leading to spin tunneling. An STT is then exerted onto the molecular

spin by the inelastic spin currents. As a back action, the molecular spin pumps spin currents into the leads. Using external means to compensate the effect of STT on the molecular spin dynamics, the spin precession remains steady. The spin currents, noise of z-polarized spin current, and STT are calculated using the the Keldysh NEGF technique.[80–82] The initially single molecular orbital results in four quasienergy levels dependent on the magnetic anisotropy parameter,[131] obtained by the Floquet theorem.[132–135] The elastic spin currents are driven by the bias voltage. The inelastic spin currents, driven by the molecular spin precession, contribute to the STT. They involve electron spin-flip events accompanied by an energy change that depends on the anisotropy parameter. The setup can be used to generate and control spin currents and STT by adjusting the anisotropy parameter, the tilt angle of the molecular spin from the magnetic field and the Larmor frequency. Furthermore, if the anisotropy contribution to the precession frequency coincides with the Larmor frequency, the precession is suppressed, and consequently, the STT vanishes. Similarly to charge-current noise,[95,131] the peaks and dips in spin-current noise, resembling Fano-like line shapes,[136,137] occur due to quantum interference between the states connected with spin-flip events. The spin-current and noise, STT, and torque coefficients vanish for large anisotropy parameter, and can be controlled by the anisotropy parameter in the absence of magnetic field as well.

The remainder of the article is organised as follows. The model setup is introduced in Section II. The theoretical framework based on the Keldysh NEGF technique, used to calculate expressions for spin currents, noise of z-polarized spin current and STT is presented in Section III. The results are discussed in Section IV, where the properties of the z-polarized spin current, the corresponding autocorrelation noise, STT and the torque coefficients are analyzed at zero temperature. The conclusions are given in Section V.

II. MODEL SETUP

The junction consists of a single orbital of an anisotropic magnetic molecule in a magnetic field, connected to two noninteracting metallic leads (see Fig. 1). The magnetic field is constant, directed along z-axis, $\vec{B} = B\vec{e}_z$, and does not affect the leads (left and right) with chemical potentials μ_ξ, with $\xi = L, R$. The system Hamiltonian is given by $\hat{H} = \hat{H}_L + \hat{H}_R + \hat{H}_T + \hat{H}_{\rm MO} + \hat{H}_S$. The first two terms represent Hamiltonians of the leads, $\hat{H}_\xi = \sum_{k,\sigma} \epsilon_{k\xi} \hat{c}^\dagger_{k\sigma\xi} \hat{c}_{k\sigma\xi}$, with $\sigma = \uparrow, \downarrow = 1, 2 = \pm 1$ denoting the electron spin state (up or down). The third term in the Hamiltonian, $\hat{H}_T$, represents the tunnel coupling between the orbital of the molecule and the leads, and can be written as $\hat{H}_T = \sum_{k,\sigma,\xi} [V_{k\xi} \hat{c}^\dagger_{k\sigma\xi} \hat{d}_\sigma + V^*_{k\xi} \hat{d}^\dagger_\sigma \hat{c}_{k\sigma\xi}]$, with matrix element $V_{k\xi}$, and creation (annihilation) operators of the electrons in the leads and orbital $\hat{c}^\dagger_{k\sigma\xi}(\hat{c}_{k\sigma\xi})$ and $\hat{d}^\dagger_\sigma(\hat{d}_\sigma)$. The Hamiltonian of the molecular orbital $\hat{H}_{MO}$ consists of three terms, one representing the noninteracting orbital with energy ϵ_0, the second one representing the spin of the electron in the orbital in the presence of the magnetic field, and the third term representing the exchange interaction between the spin of the electron in the orbital and molecular spin, with the exchange coupling constant J, $\hat{H}_{\rm MO} = \sum_\sigma \epsilon_0 \hat{d}^\dagger_\sigma \hat{d}_\sigma + (g\mu_B/\hbar)\hat{\vec{s}}\vec{B} + J\hat{\vec{s}}\vec{S}$. The spin of the electron in the molecular orbital is given by $\hat{\vec{s}} = (\hbar/2)\sum_{\sigma\sigma'} (\hat{\vec{\sigma}})_{\sigma\sigma'} \hat{d}^\dagger_\sigma \hat{d}_{\sigma'}$, with the vector of the Pauli matrices $\hat{\vec{\sigma}} = (\hat{\sigma}_x, \hat{\sigma}_y, \hat{\sigma}_z)^T$. The constants g and μ_B are the gyromagnetic ratio of the electron, which is assumed to be equal to the one of the molecular spin, and the Bohr magneton. The last term in the model Hamiltonian describes the Hamiltonian of the anisotropic spin of the molecule, $\hat{H}_S = (g\mu_B/\hbar)\hat{\vec{S}}\vec{B} - D\hat{S}^2_z$, with molecular spin operator $\hat{\vec{S}} = \hat{S}_x\vec{e}_x + \hat{S}_y\vec{e}_y + \hat{S}_z\vec{e}_z$. Here, the uniaxial magnetic anisotropy parameter is given by D and $\vec{e}_j$ is the unit vector along the axis j, with $j = x, y, z$.

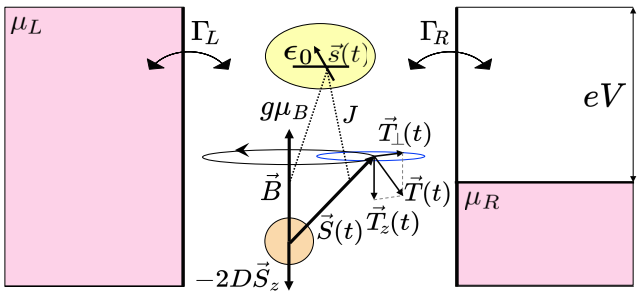

FIG. 1: (Color online) Spin tunneling through a single molecular orbital with energy ϵ_0, coupled to the molecular spin $\vec{S}(t)$ with anisotropy parameter D, via exchange interaction with the coupling constant J, in the presence of a magnetic field $\vec{B}$, connected to two leads with chemical potentials μ_L and μ_R, $eV = \mu_L - \mu_R$, with tunnel rates Γ_L and Γ_R. The molecular spin $\vec{S}(t)$ precesses around the magnetic field axis with frequency $\omega = \omega_L - 2DS_z$. The spin-transfer torque $\vec{T}(t)$ is exerted on the spin $\vec{S}(t)$ by the spin currents from the leads.

The spin of the magnetic molecule is large and regarded as a classical variable $\vec{S}$, with constant length $S = |\vec{S}| \gg \hbar$, neglecting the quantum fluctuations. The vector $\vec{S}$ is the expectation value of the previously mentioned molecular spin operator, $\vec{S} = \langle\hat{\vec{S}}\rangle$, with the dynamics expressed by the Heisenberg equation of motion $\dot{\vec{S}} = \langle\dot{\hat{\vec{S}}}\rangle = (i/\hbar)\langle[\hat{H}, \hat{\vec{S}}]\rangle$. In order to keep the molecular spin dynamics unaffected by the loss of the magnetic energy due to the exchange interaction with the spin of the tunneling electrons, one needs to use external means, e.g., radiofrequency fields.[138] Taking into account the Larmor precession frequency around the magnetic field axis, $\omega_L = (g\mu_B/\hbar)B$, the equation $\dot{\vec{S}} = (g\mu_B/\hbar)\vec{B} \times \vec{S} - 2D\vec{S}_z \times \vec{S}$ is obtained,[121] showing that the molecular spin precesses around z-axis with frequency $\omega = \omega_L - 2DS_z$.

The dynamics of the molecular spin can be expressed as $\vec{S}(t) = S_\perp \cos(\omega t)\vec{e}_x + S_\perp \sin(\omega t)\vec{e}_y + S_z\vec{e}_z$, with $S_\perp = S\sin\theta$ and $S_z = S\cos\theta$, where θ is the tilt angle between the positive direction along z-axis and $\vec{S}$. While the precession of the molecular spin is kept undamped, i.e., the exerted STT by the flow of electron spins from the leads is externally compensated,[138] the precessing spin affects spin of the itinerant electrons during the exchange interaction, as a back action. Thus, the molecular spin pumps spin currents into the leads, having an impact on spin-transport properties of the junction.

In molecular magnets realized by transition metals or rare earth elements, the Coulomb interaction in the s and p orbitals in the molecular ligands can be neglected.[19,43,139] They form the highest occupied or lowest unoccupied molecular orbital, which can be considered as a localized molecular level. The molecular spin is formed of localized d or f orbitals from transition metal or rare earth element, thus allowing separation between the molecular level and localized molecular spin.

III. THEORETICAL FRAMEWORK

A. Spin current

The spin-current operators of the lead ξ are given by the Heisenberg equation

$$\hat{I}_{\xi j}(t) = \frac{\hbar}{2}\frac{d\hat{N}_{\xi j}}{dt} = \frac{i}{2}[\hat{H}, \hat{N}_{\xi j}], \tag{1}$$

where $j = x, y, z$ denotes the component of the spin current with electronic spins oriented along the given spatial direction, [,] symbolizes the commutator, whereas $\hat{N}_{\xi j} = \sum_{k,\sigma,\sigma'} \hat{c}^\dagger_{k\sigma\xi}(\hat{\sigma}_j)_{\sigma\sigma'}\hat{c}_{k\sigma\xi}$ denotes the spin occupation number operator of the lead ξ, with matrix elements of the Pauli oparators $(\hat{\sigma}_j)_{\sigma\sigma'}$. The average spin current, as a flow of spins oriented along j direction from the contact ξ to the molecular orbital, can be written as

$$I_{\xi j}(t) = \frac{1}{2}\left\langle \frac{d}{dt}\hat{N}_{\xi j}\right\rangle = \frac{i}{2}\big\langle[\hat{H}, \hat{N}_{\xi j}]\big\rangle, \tag{2}$$

in units in which $\hbar = e = 1$. Employing the Keldysh NEGF technique,[81,82] the components of the spin current can be calculated as

$$I_{\xi j}(t) = -\,\mathrm{Re}\int dt' \mathrm{Tr}\big\{\hat{\sigma}_j[\hat{G}^r(t,t')\hat{\Sigma}^<_\xi(t',t) + \hat{G}^<(t,t')\hat{\Sigma}^a_\xi(t',t)]\big\}. \tag{3}$$

Here, $\hat{G}^{r,a,<,>}(t,t')$ denote the retarded, advanced, lesser, and greater Green's functions of the spin carriers in the molecular orbital. The matrix elements of the Green's functions are given by $G^{r,a}_{\sigma\sigma'}(t,t') = \mp i\theta(\pm t \mp t')\langle\{\hat{d}_\sigma(t), \hat{d}^\dagger_{\sigma'}(t')\}\rangle$, $G^<_{\sigma\sigma'}(t,t') = i\langle\hat{d}^\dagger_{\sigma'}(t')\hat{d}_\sigma(t)\rangle$ and $G^>_{\sigma\sigma'}(t,t') = -i\langle\hat{d}_\sigma(t)\hat{d}^\dagger_{\sigma'}(t')\rangle$, where $\{\cdot,\cdot\}$ symbolizes the anticommutator. The self-energies from the tunnel coupling between the orbital and lead ξ are represented by $\hat{\Sigma}^{r,a,<,>}_\xi(t,t')$, with diagonal matrix elements in the electron spin space with respect to the basis of the eigenstates of $\hat{s}_z$. Their nonzero matrix elements can be expressed as $\Sigma^{r,a,<}_\xi(t,t') = \sum_k V_{k\xi} g^{r,a,<,>}_{k\xi}(t,t')V^*_{k\xi}$, with $g^{r,a,<,>}_{k\xi}(t,t')$ denoting the Green's functions of the electrons in the lead ξ. Applying the double Fourier transformations in Eq. (3), it can be further simplified as

$$I_{\xi j}(t) = \Gamma_\xi \mathrm{Im}\int\frac{d\epsilon}{2\pi}\int\frac{d\epsilon'}{2\pi}e^{-i(\epsilon-\epsilon')t} \times \mathrm{Tr}\left\{\hat{\sigma}_j\left[f_\xi(\epsilon')\hat{G}^r(\epsilon,\epsilon') + \frac{1}{2}\hat{G}^<(\epsilon,\epsilon')\right]\right\}, \tag{4}$$

with the tunnel coupling between the orbital and lead ξ, $\Gamma_\xi(\epsilon) = 2\pi\sum_k |V_{k\xi}|^2\delta(\epsilon - \epsilon_{k\xi})$, which is energy independent and constant in the wide-band limit. The Fermi-Dirac distribution of the spin carriers in the lead ξ is given by $f_\xi(\epsilon) = [e^{(\epsilon-\mu_\xi)/k_BT}+1]^{-1}$, where T and k_B are the temperature and the Boltzmann constant.

The retarded Green's function of the electrons in the orbital of the molecule can be calculated applying Dyson's expansion and analytic continuation rules.[82] Its double-Fourier transformed matrix elements can be expressed as[89,131,140]

$$G^r_{\sigma\sigma}(\epsilon,\epsilon') = \frac{2\pi\delta(\epsilon-\epsilon')G^{0r}_{\sigma\sigma}(\epsilon)}{1-\gamma^2 G^{0r}_{\sigma\sigma}(\epsilon)G^{0r}_{-\sigma-\sigma}(\epsilon_\sigma)}, \tag{5}$$

$$G^r_{\sigma-\sigma}(\epsilon,\epsilon') = \frac{2\pi\gamma\delta(\epsilon_\sigma-\epsilon')G^{0r}_{\sigma\sigma}(\epsilon)G^{0r}_{-\sigma-\sigma}(\epsilon_\sigma)}{1-\gamma^2 G^{0r}_{\sigma\sigma}(\epsilon)G^{0r}_{-\sigma-\sigma}(\epsilon_\sigma)}, \tag{6}$$

with $\epsilon_\sigma = \epsilon - \sigma\omega = \epsilon - \sigma(\omega_L - 2DS_z)$, $\gamma = JS\sin(\theta)/2$. The Fourier transformed retarded Green's function of the electrons in the molecular orbital in the presence of the static molecular spin, $S = S_z$, calculated using the equation of motion technique,[141] is given by $\hat{G}^{0r}(\epsilon) = [\epsilon - \epsilon_0 - \Sigma^r - \hat{\sigma}_z(g\mu_B B + JS_z)/2]^{-1}$,[121,140] where $\Sigma^{r,a} = \mp i\Gamma/2$ and $\Gamma = \sum_\xi \Gamma_\xi$. The Green's functions $\hat{G}^{<,>}(\epsilon,\epsilon')$ can be obtained using the double-Fourier transformed Keldysh equation, expressed as $\hat{G}^{<,>}(\epsilon,\epsilon') = \int d\epsilon'' \hat{G}^r(\epsilon,\epsilon'')\hat{\Sigma}^{<,>}(\epsilon'')\hat{G}^a(\epsilon'',\epsilon')/2\pi$,[82] with lesser self-energy $\Sigma^<(\epsilon) = i\sum_\xi \Gamma_\xi f_\xi(\epsilon)$, greater self-energy $\Sigma^>(\epsilon) = i\sum_\xi \Gamma_\xi(f_\xi(\epsilon)-1)$ and advanced Green's function $\hat{G}^a(\epsilon,\epsilon') = [\hat{G}^r(\epsilon',\epsilon)]^\dagger$.

The spin current given by Eq. (4) can be calculated using the above expressions for the Green's functions $\hat{G}^r(\epsilon,\epsilon')$ and $\hat{G}^<(\epsilon,\epsilon')$. As a result, the time-dependent spin-current components $I_{\xi x}(t)$ and $I_{\xi y}(t)$ read

$$I_{\xi x}(t) = I_{\xi x}(D)e^{-i(\omega_L - 2DS_z)t} + I^*_{\xi x}(D)e^{i(\omega_L-2DS_z)t}, \tag{7}$$

$$I_{\xi y}(t) = I_{\xi y}(D)e^{-i(\omega_L - 2DS_z)t} + I^*_{\xi y}(D)e^{i(\omega_L-2DS_z)t}, \tag{8}$$

while $I_{\xi z}$ is time-indnpendent. The expressions for $I_{\xi z}$ and the complex functions $I_{\xi x}(D)$ and $I_{\xi y}(D)$, are presented by Eqs. (A1)–(A3) in the Appendix. For the

isotropic molecular spin ($D = 0$), they reduce to the expressions obtained before.[89].

In the presence of the precessing anisotropic molecular spin $\vec{S}(t)$ and the external magnetic field $\vec{B}$, the initial single resonant transmission channel with energy ϵ_0, results in four channels available for spin transport. They are located at Floquet quasienergies[131]

$$\epsilon_{1,3} = \epsilon_0 - \frac{\omega_L}{2} + DS_z \pm \sqrt{D(D+J)S_z^2 + \left(\frac{JS}{2}\right)^2}, \quad (9)$$

$$\epsilon_{2,4} = \epsilon_0 + \frac{\omega_L}{2} - DS_z \pm \sqrt{D(D+J)S_z^2 + \left(\frac{JS}{2}\right)^2}, \quad (10)$$

obtained using the Floquet theorem,[132–135] since the Hamiltonian of the molecular orbital is a periodic function of time $\hat{H}_{\rm MO}(t) = \hat{H}_{\rm MO}(t + 2\pi/\omega)$. As a result of the exchange interaction between the spin of the molecule and the itinerant electron spin, the $\downarrow$ state with quasienergy $\epsilon_1(\epsilon_3)$ is coupled to the $\uparrow$ state with quasienergy $\epsilon_2(\epsilon_4) = \epsilon_1(\epsilon_3) + \omega = \epsilon_1(\epsilon_3) + \omega_L - 2DS_z$. Namely, periodic motion of the molecular spin leads to the absorption (emission) of an energy quantum ω by the spin-carrying electron in the orbital, accompanied by a spin-flip.

B. Noise of z-polarized spin current

In order to obtain further characteristics of spin transport, one can study spin-current noise. The noise of spin current polarized along the z-direction is calculated here, as a complement to previously studied charge-current noise.[131] Since only the tunneling Hamiltonian $\hat{H}_T$ contributes to the commutator in Eq. (1), the resulting spin-current operator $\hat{I}_{\xi z}(t)$ is given by

$$\hat{I}_{\xi z}(t) = \frac{i}{2}\sum_{\sigma}(-1)^{\sigma}\hat{I}_{\xi\sigma}(t), \quad (11)$$

where the operator component $\hat{I}_{\xi\sigma}(t)$ reads

$$\hat{I}_{\xi\sigma}(t) = \sum_k [V_{k\xi}\hat{c}^{\dagger}_{k\sigma\xi}(t)\hat{d}_{\sigma}(t) - V^{*}_{k\xi}\hat{d}^{\dagger}_{\sigma}(t)\hat{c}_{k\sigma\xi}(t)]. \quad (12)$$

The spin-current fluctuation operator $\delta\hat{I}_{\xi z}(t)$ in lead ξ can be written as

$$\delta\hat{I}_{\xi z}(t) = \hat{I}_{\xi z}(t) - \langle\hat{I}_{\xi z}(t)\rangle. \quad (13)$$

The nonsymmetrized noise of z-polarized spin current, defined as correlation between fluctuations of z-polarized spin currents in contacts ξ and ζ, is given by[93,142]

$$S^{zz}_{\xi\zeta}(t,t') = \langle\delta\hat{I}_{\xi z}(t)\delta\hat{I}_{\zeta z}(t')\rangle, \quad (14)$$

whereas, the symmetrized noise can be written as

$$S^{zz}_{\xi\zeta S}(t,t') = \frac{1}{2}\langle\{\delta\hat{I}_{\xi z}(t), \delta\hat{I}_{\zeta z}(t')\}\rangle. \quad (15)$$

According to Eqs. (11) and (13), the nonsymmetrized noise of z-polarized spin current equals[93,142]

$$S^{zz}_{\xi\zeta}(t,t') = -\sum_{\sigma\sigma'}(-1)^{\delta_{\sigma\sigma'}}S^{\sigma\sigma'}_{\xi\zeta}(t,t'), \quad (16)$$

with $S^{\sigma\sigma'}_{\xi\zeta}(t,t') = (-1/4)\langle\delta\hat{I}_{\xi\sigma}(t)\delta\hat{I}_{\zeta\sigma'}(t')\rangle$. Implementing the Wick's theorem[143] and Langreth analytical continuation rules[144] to the correlation function $S^{\sigma\sigma'}_{\xi\zeta}(t,t')$ in Eq. (16), and using the Green's functions of the molecular orbital and the self-energies from the tunnel couplings between the orbital and the leads, one obtains the expression for the noise of z-polarized spin current.[95] Employing the Fourier transforms of the Green's functions $G^{r,a,<,>}_{\sigma\sigma'}(\epsilon,\epsilon')$ and self-energies $\Sigma^{r,a,<,>}_{\xi}(\epsilon)$, this expression can be transformed into

$$\begin{aligned}
S^{zz}_{\xi\zeta}(t,t') = \frac{1}{4}\sum_{\sigma\sigma'}(-1)^{\delta_{\sigma\sigma'}}\Bigg\{ & \int\frac{d\epsilon_1}{2\pi}\int\frac{d\epsilon_2}{2\pi}\int\frac{d\epsilon_3}{2\pi}\int\frac{d\epsilon_4}{2\pi}e^{-i(\epsilon_1-\epsilon_2)t}e^{i(\epsilon_3-\epsilon_4)t'} \\
& \times\Big\{[G^{r}_{\sigma\sigma'}(\epsilon_1,\epsilon_3)\Sigma^{>}_{\zeta}(\epsilon_3) + 2G^{>}_{\sigma\sigma'}(\epsilon_1,\epsilon_3)\Sigma^{a}_{\zeta}][G^{r}_{\sigma'\sigma}(\epsilon_4,\epsilon_2)\Sigma^{<}_{\xi}(\epsilon_2) + 2G^{<}_{\sigma'\sigma}(\epsilon_4,\epsilon_2)\Sigma^{a}_{\xi}] \\
& + [\Sigma^{>}_{\xi}(\epsilon_1)G^{a}_{\sigma\sigma'}(\epsilon_1,\epsilon_3) + 2G^{>}_{\sigma\sigma'}(\epsilon_1,\epsilon_3)\Sigma^{r}_{\xi}][\Sigma^{<}_{\zeta}(\epsilon_4)G^{a}_{\sigma'\sigma}(\epsilon_4,\epsilon_2) + 2G^{<}_{\sigma'\sigma}(\epsilon_4,\epsilon_2)\Sigma^{r}_{\zeta}] \\
& + 4\Sigma^{r}_{\xi}\Sigma^{a}_{\zeta}G^{>}_{\sigma\sigma'}(\epsilon_1,\epsilon_3)G^{<}_{\sigma'\sigma}(\epsilon_4,\epsilon_2)\Big\} \\
& - \delta_{\xi\zeta}\delta_{\sigma\sigma'}\int\frac{d\epsilon_1}{2\pi}\int\frac{d\epsilon_2}{2\pi}\int\frac{d\epsilon_3}{2\pi} \\
& \quad\times\Big\{e^{-i(\epsilon_1-\epsilon_3)t}e^{i(\epsilon_2-\epsilon_3)t'}G^{>}_{\sigma\sigma'}(\epsilon_1,\epsilon_2)\Sigma^{<}_{\xi}(\epsilon_3) \\
& \quad + e^{-i(\epsilon_1-\epsilon_3)t}e^{i(\epsilon_1-\epsilon_2)t'}\Sigma^{>}_{\xi}(\epsilon_1)G^{<}_{\sigma'\sigma}(\epsilon_2,\epsilon_3)\Big\}\Bigg\}. \quad (17)
\end{aligned}$$

Since the noise $S^{zz}_{\xi\zeta}(t,t')$ depends only on the time difference $\tau = t - t'$, its power spectrum equals

$$S^{zz}_{\xi\zeta}(\Omega) = \int d\tau e^{i\Omega\tau}S^{zz}_{\xi\zeta}(\tau). \quad (18)$$

The symmetrized noise spectrum is given by

$$S^{zz}_{\xi\zeta S}(\Omega) = \frac{1}{2}[S^{zz}_{\xi\zeta}(\Omega) + S^{zz}_{\zeta\xi}(-\Omega)], \quad (19)$$

with $S^{\sigma\sigma'}_{\xi\zeta S}(\Omega) = \frac{1}{2}[S^{\sigma\sigma'}_{\xi\zeta}(\Omega) + S^{\sigma'\sigma}_{\zeta\xi}(-\Omega)]$. As it is of experimental interest, the zero-frequency noise power of z-polarized spin-current $S^{zz}_{LL} = S^{zz}_{LL}(0) = S^{zz}_{LLS}(0)$ at zero temperature will be analyzed and discussed.

C. Spin-transfer torque

In the presence of the anisotropic molecular spin $\vec{S}(t)$, interacting with the incoming flow of electron spins from the leads via exchange interactions, the transfer of spin angular momentum to the molecular spin occurs, resulting in the STT $\vec{T}(t)$ exerted on the molecular spin. As already mentioned, the STT is compensated by external means, so that the molecular spin precession remains unaffected. Considering that the total spin angular momentum is conserved, the spin of the molecule generates a torque $-\vec{T}(t)$ acting on the spin currents from the leads,[36,49,50,67]

$$-\vec{T}(t) = \vec{I}_L(t) + \vec{I}_R(t), \tag{20}$$

where $\vec{I}_\xi(t) = \sum_j I_{\xi j}(t)\vec{e}_j$, while $\vec{T}(t) = \sum_j T_j\vec{e}_j$. Employing Eqs. (7), (8), (20) and Eqs. (A1)–(A3) given in the Appendix, the spatial components of the STT, T_j, can be expressed as

$$T_x(t) = -\int \frac{d\epsilon}{2\pi}\sum_{\xi\zeta}\frac{\Gamma_\xi\Gamma_\zeta}{\Gamma}[f_\xi(\epsilon-\omega_L+2DS_z) - f_\zeta(\epsilon)] \times \mathrm{Im}\Big\{\frac{\gamma G^{0r}_{11}(\epsilon)G^{0a}_{22}(\epsilon-\omega_L+2DS_z)}{|1-\gamma^2 G^{0r}_{11}(\epsilon)G^{0r}_{22}(\epsilon-\omega_L+2DS_z)|^2}$$
$$\times[1-\gamma^2 G^{0a}_{11}(\epsilon)G^{0r}_{22}(\epsilon-\omega_L+2DS_z)]e^{-i(\omega_L-2DS_z)t}\Big\}, \tag{21}$$

$$T_y(t) = -\int \frac{d\epsilon}{2\pi}\sum_{\xi\zeta}\frac{\Gamma_\xi\Gamma_\zeta}{\Gamma}[f_\xi(\epsilon-\omega_L+2DS_z) - f_\zeta(\epsilon)] \times \mathrm{Re}\Big\{\frac{\gamma G^{0r}_{11}(\epsilon)G^{0a}_{22}(\epsilon-\omega_L+2DS_z)}{|1-\gamma^2 G^{0r}_{11}(\epsilon)G^{0r}_{22}(\epsilon-\omega_L+2DS_z)|^2}$$
$$\times[1-\gamma^2 G^{0a}_{11}(\epsilon)G^{0r}_{22}(\epsilon-\omega_L+2DS_z)]e^{-i(\omega_L-2DS_z)t}\Big\}, \tag{22}$$

$$T_z = -\int \frac{d\epsilon}{2\pi}\sum_{\xi\zeta}\Gamma_\xi\Gamma_\zeta[f_\xi(\epsilon-\omega_L+2DS_z) - f_\zeta(\epsilon)] \times \frac{\gamma^2|G^{0r}_{11}(\epsilon)G^{0r}_{22}(\epsilon-\omega_L+2DS_z)|^2}{|1-\gamma^2 G^{0r}_{11}(\epsilon)G^{0r}_{22}(\epsilon-\omega_L+2DS_z)|^2}. \tag{23}$$

For the isotropic molecular spin with $D = 0$, Eqs. (21)–(23) reduce to the previously calculated expressions for the spatial components of the STT.[89] If the magnetic field is turned off ($\omega_L = 0$), then $\vec{T}(t) = 0$ for $D = 0$,[89] whereas $\vec{T}(t) \neq 0$ for $D \neq 0$ according to Eqs. (21)–(23).

Both $T_x(t)$ and $T_y(t)$ can be written as $T_x(t) = T_x\cos(\omega t + \phi_x)$ and $T_y(t) = T_y\cos(\omega t + \phi_y)$. The phase difference $\phi_x - \phi_y = \pi/2$, whereas T_x and T_y are the amplitudes. Since the amplitudes are equal, it is convenient to introduce the in-plane torque component, orthogonal to the z-axis, $\vec{T}_\perp(t) = \vec{T}_x(t) + \vec{T}_y(t)$, while

$$\vec{T}(t) = \vec{T}_\perp(t) + \vec{T}_z(t). \tag{24}$$

The in-plane component of the STT, $\vec{T}_\perp(t)$, precesses around the end point of the molecular spin $\vec{S}(t)$ in the xy plane (see Fig. 1), and has a constant magnitude $|\vec{T}_\perp(t)| = T_\perp = T_x = T_y$.

In relation to the molecular spin vector $\vec{S}(t)$, the STT can be reformulated as

$$\vec{T}(t) = \frac{\alpha}{S}\dot{\vec{S}}(t)\times\vec{S}(t) + \beta\dot{\vec{S}}(t) + \eta\vec{S}(t). \tag{25}$$

The Gilbert damping component of the torque is given by the first term in Eq. (25) , with α, the Gilbert damping coefficient. It tends to align the anisotropic molecular spin $\vec{S}(t)$ anti(parallel) to the direction of the effective magnetic field $\vec{B}_{\rm eff} = \vec{B} - (2D/g\mu_B)\vec{S}_z$ and dissipate(add) magnetic energy. The second term with coefficient β tends to change the precession frequency of the molecular spin $\vec{S}(t)$, and the direction of the molecular spin precession for $\beta < 0$. The contribution in the third therm is characterized by the coefficient η. The Cartesian representation of the STT given by Eq. (25) results in spatial components

$$T_x(t) = S_\perp\left(\frac{\alpha}{S}\omega S_z + \eta\right)\cos(\omega t) - \beta\omega S_\perp\sin(\omega t), \tag{26}$$

$$T_y(t) = S_\perp\left(\frac{\alpha}{S}\omega S_z + \eta\right)\sin(\omega t) + \beta\omega S_\perp\cos(\omega t), \tag{27}$$

$$T_z = -\frac{\alpha}{S}\omega S^2_\perp + \eta S_z, \tag{28}$$

where $\dot{\vec{S}}(t) = \omega S_\perp[-\sin(\omega t)\vec{e}_x + \cos(\omega t)\vec{e}_y]$ for the precessing molecular spin. Combining expressions given by Eqs. (21)–(23) and (26)–(28), the resulting torque coefficients α and β can be written as

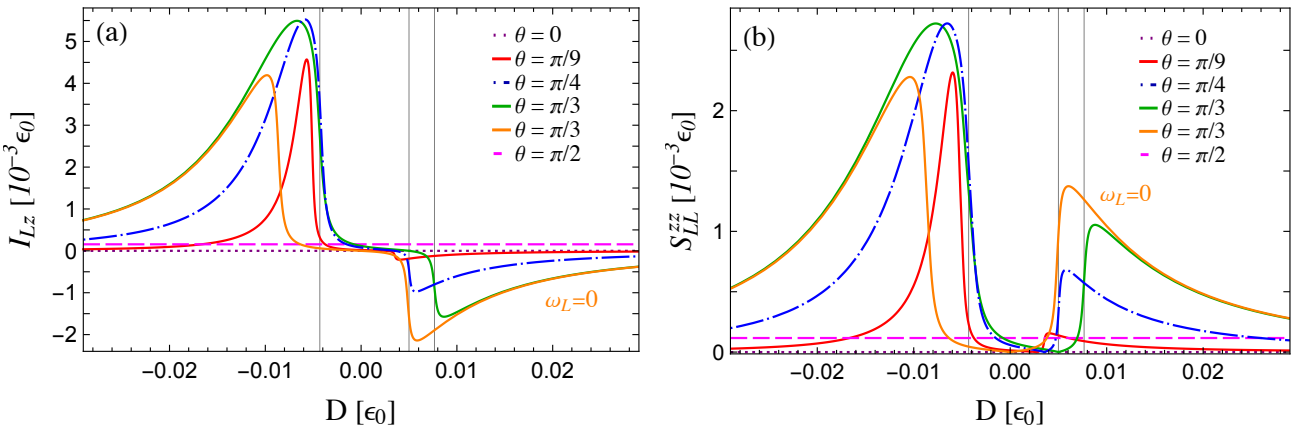

FIG. 2: (Color online) (a) Spin current I_{Lz} and (b) auto-correlation spin-current shot noise S^{zz}_{LL}, as functions of the uniaxial magnetic anisotropy parameter D for different tilt angles θ, at zero temperature. The magnetic field $\vec{B} = B\vec{e}_z$ and Larmor frequency $\omega_L = 0.5\,\epsilon_0$, except for a zero magnetic field where $\omega_L = 0$ (orange line). The chemical potentials of the leads are equal: $\mu_L = \mu_R = 0.1\,\epsilon_0$. The other parameters are set to: $\Gamma = 0.05\,\epsilon 0$, $\Gamma_L = \Gamma_R = \Gamma/2$, $J = 0.01\,\epsilon_0$, and $S = 100$. Grid lines for $\theta = \pi/3$ and $\omega_L = 0.5\,\epsilon_0$ (green line), are positioned at $D = -0.00431\,\epsilon_0$ ($\mu_L = \mu_R = \epsilon_3$), $D = 0.00766\,\epsilon_0$ ($\mu_L = \mu_R = \epsilon_4$), and $D = 0.005\,\epsilon_0$ ($\omega = 0$).

$$\alpha = -\frac{1}{(\omega_L - 2DS_z)S}\int \frac{d\epsilon}{2\pi}\sum_{\xi\zeta}\Gamma_\xi\Gamma_\zeta[f_\xi(\epsilon-\omega_L+2DS_z)-f_\zeta(\epsilon)] \times \frac{(JS_z/2\Gamma)\mathrm{Im}\{G^{0r}_{11}(\epsilon)G^{0a}_{22}(\epsilon-\omega_L+2DS_z)\}-\gamma^2|G^{0r}_{11}(\epsilon)G^{0r}_{22}(\epsilon-\omega_L+2DS_z)|^2}{|1-\gamma^2G^{0r}_{11}(\epsilon)G^{0r}_{22}(\epsilon-\omega_L+2DS_z)|^2}, \tag{29}$$

$$\beta = -\frac{J}{\omega_L - 2DS_z}\int \frac{d\epsilon}{4\pi}\sum_{\xi\zeta}\frac{\Gamma_\xi\Gamma_\zeta}{\Gamma}[f_\xi(\epsilon-\omega_L+2DS_z)-f_\zeta(\epsilon)] \times \frac{\mathrm{Re}\{G^{0r}_{11}(\epsilon)G^{0a}_{22}(\epsilon-\omega_L+2DS_z)\}-\gamma^2|G^{0r}_{11}(\epsilon)G^{0r}_{22}(\epsilon-\omega_L+2DS_z)|^2}{|1-\gamma^2G^{0r}_{11}(\epsilon)G^{0r}_{22}(\epsilon-\omega_L+2DS_z)|^2}, \tag{30}$$

while the coefficient η can be expressed in terms of T_z and Gilbert damping coefficient α as

$$\eta = \frac{T_z}{S_z} + \frac{4\gamma^2(\omega_L - 2DS_z)}{J^2SS_z}\alpha. \tag{31}$$

In the limit $|D| \ll |\omega_L/2S_z|$, the effect of the uniaxial magnetic anisotropy on the STT can be neglected, and Eqs. (29)–(31) are in agreement with the coefficients α, β and η obtained for the isotropic molecular spin.[89] Finally, the magnitude of the in-plane torque component $T_\perp$ can be expressed using α, β and T_z as follows

$$T_\perp = \frac{2|\gamma(\omega_L - 2DS_z)|}{J}\sqrt{\beta^2 + \frac{1}{S_z^2}\left[S\alpha + \frac{T_z}{(\omega_L - 2DS_z)}\right]^2} \tag{32}$$

For a static molecular spin with $\omega = 0$, $\dot{\vec{S}}(t) = 0$, and $D = \omega_L/2S_z$, according to Eqs. (21)–(23) and (31), the STT vanishes, $\vec{T}(t) = \vec{0}$, and $\eta = 0$. This is expected since the exchange of spin angular momentum occurs due to the exchange interaction of electron spins with the rotational component of the molecular spin.[88,89] Using Eqs. (29) and (30) one obtains nonzero coefficients α and β in the limit $\omega \to 0$, given by Eqs. (A4) and (A5) in the Appendix.

IV. RESULTS AND DISCUSSION

In this section, the properties of the z-polarized spin current I_{Lz} and autocorrelation zero-frequency noise power S^{zz}_{LL} at zero temperature are discussed. Then, the characteristics of the STT generated on the anisotropic molecular spin by the spin currents from the leads, and torque coefficients, are analyzed as functions of the uniaxial magnetic anisotropy parameter D, bias voltage $eV = \mu_L - \mu_R$ and Larmor frequency ω_L.

In Fig. 2, the spin current I_{Lz} and auto-correlation noise S^{zz}_{LL} are plotted as functions of the anisotropy parameter D, for different tilt angles θ, at zero temperature and zero-bias conditions, with chemical potentials of the leads $\mu = \mu_L = \mu_R = 0.1\,\epsilon_0$. For a static molec-

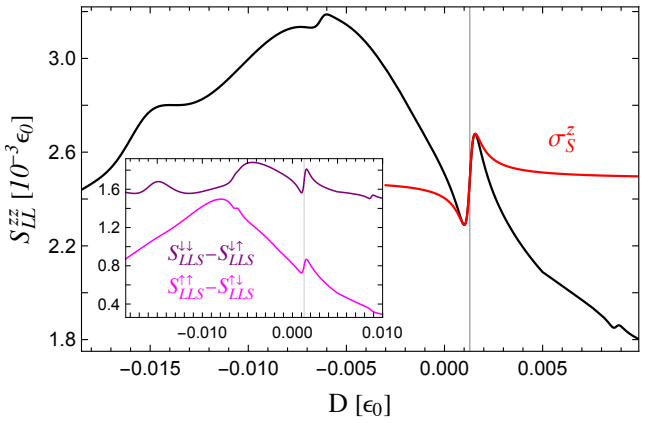

FIG. 3: (Color online) Spin-current shot noise S^{zz}_{LL} as a function of the magnetic anisotropy parameter D at zero temperature, for $\theta = \pi/3$, $\mu_L = 0.65\,\epsilon_0$, and $\mu_R = 0$, with $\vec{B} = B\vec{e}_z$. Around the resonant anisotropy parameter $D_{\rm res} = 0.00129\,\epsilon_0$ (grid line) the spin-current noise S^{zz}_{LL} (black line) matches the Fano-like shape of the resonance profile σ^z_S (red line). The inset shows contributions of $S^{\uparrow\uparrow}_{LLS} - S^{\uparrow\downarrow}_{LLS}$ (pink line) and $S^{\downarrow\downarrow}_{LLS} - S^{\downarrow\uparrow}_{LLS}$ (purple line) to the resulting shape of the resonance profile in S^{zz}_{LL}. The other parameters are set to: $\Gamma = 0.05\,\epsilon 0$, $\Gamma_L = \Gamma_R$, $\omega_L = 0.5\,\epsilon_0$ $J = 0.01\,\epsilon_0$, and $S = 100$.

ular spin with $\theta = 0$ and $\gamma = 0$ (purple dotted lines in Fig. 2), the spin current $I_{Lz} = 0$ and $S^{zz}_{LL} = 0$. In the case of $\theta = \pi/2$ (pink dashed lines in Fig. 2), the spin current I_{Lz} and noise S^{zz}_{LL} are independent of D, since $S_z = 0$. For $\theta = \pi/3$ and $\omega_L = 0.5\,\epsilon_0$ (green lines in Fig. 2) one notices maximums in I_{Lz} and S^{zz}_{LL} around $D = -0.00431\,\epsilon_0$, corresponding to $\mu_L = \mu_R = \epsilon_3$, while a minimum in I_{Lz} and local maximum in S^{zz}_{LL} around $D = 0.00766\,\epsilon_0$ correspond to $\mu_L = \mu_R = \epsilon_4$ (grid lines). For $-0.00431\,\epsilon_0 < D < 0.00766\,\epsilon_0$ all four quasienergy levels ϵ_i, with $i \in \{1, 2, 3, 4\}$, lie above the chemical potentials μ, so that both I_{Lz} and S^{zz}_{LL} drop to zero, taking into account the level broadening Γ. The spin current I_{Lz} and noise S^{zz}_{LL} vanish at $D = \omega_L/2S_z$ when $\omega = 0$, as without molecular spin precession at zero-bias conditions, elastic and inelastic tunneling processes do not occur (see e.g., green line in Fig. 2 at $D = 0.005\,\epsilon_0$). The spin current $I_{Lz} > 0$ for $D < \omega_L/2S_z$ ($\omega > 0$) since $\downarrow$ level ϵ_3 and $\uparrow$ level ϵ_4 satisfy $\epsilon_3 < \epsilon_4$, leading to positive $\uparrow$ component of spin current $I^{\uparrow}_{Lz} = -I^{\downarrow}_{Lz} > 0$, and as μ approaches $\downarrow$ level ϵ_3 with the increase of D both I_{Lz} and S^{zz}_{LL} increase. Similarly, for $D > \omega_L/2S_z$ ($\omega < 0$), $\downarrow$ level ϵ_3 lies above $\uparrow$ level ϵ_4, $\epsilon_3 > \epsilon_4$ leading to $I^{\uparrow}_{Lz} = -I^{\downarrow}_{Lz} < 0$, and hence $I_{Lz} < 0$. In the absence of the magnetic field, $\omega_L = 0$ (orange line in Fig. 2), and the molecular spin precesses around the z-axis with frequency $\omega = -2DS_z$. Hence, $I_{Lz} \geq 0$ for $D \leq 0$, and $I_{Lz} < 0$ for $D > 0$. After reaching resonances between μ and levels ϵ_3 and ϵ_4, while $\epsilon_1 > \mu$ and $\epsilon_2 > \mu$, both I_{Lz} and S^{zz}_{LL} decrease with further increase of $|D|$, as more energy is needed to flip an electron spin which is already in lower quasienergy level, and for $|D| \gg \omega_L/2S_z$ they vanish. Besides, taking into account the tunneling rate Γ, for $|D| \gg \Gamma$, the precession frequency $|\omega| \gg \Gamma$, so that the probability of exchange of spin angular momentum between molecular and a tunneling electron spin is low.

In Fig. 3, the spin-current shot noise S^{zz}_{LL} is presented as a function of the magnetic anisotropy parameter D, for $\theta = \pi/3$, with chemical potentials $\mu_L = 0.65\,\epsilon_0$ and $\mu_R = 0$, at zero temperature. As in the Fano effect,[136,137] a dip-peak feature can be observed at the resonance $\mu_L = \epsilon_4$. It is a manifestation of the quantum interference between the $\uparrow$ state with energy ϵ_4 and $\downarrow$ state with energy $\epsilon_3 \approx 0.279\,\epsilon_0$. An electron spin from the left lead can perform elastic tunneling through the $\uparrow$ state with energy ϵ_4, or it can tunnel via a spin flip from $\downarrow$ state with energy ϵ_3 to $\uparrow$ state with energy ϵ_4, involving absorption of an energy $\omega \approx 0.371\,\epsilon_0$. Similarly, the elastic tunneling can occur via the $\downarrow$ state with energy ϵ_3, or via a spin flip from $\uparrow$ state with energy ϵ_4 to $\downarrow$ state with energy ϵ_3, involving emission of an energy ω. The two tunneling pathways, one elastic and the other involving a spin flip, ending up in the same final $\uparrow$ state with energy ϵ_4, or $\downarrow$ state with energy ϵ_3, destructively (dip) or constructively (peak) interfere. The asymmetric line shape in S^{zz}_{LL} (black line in Fig. 3) mimics the asymmetric Fano resonance profile.[136,137] For $\mu_L = \epsilon_4$, the corresponding resonant anisotropy parameter equals $D_{\rm res} \approx 0.00129\,\epsilon_0$ (see grid line in Fig. 3). The destructive quantum interference corresponds to the dip (interference minimum) at $D_{\rm min} \approx 0.00101\,\epsilon_0$, while the constructive interference corresponds to the peak (interference maximum) at $D_{\rm max} \approx 0.00157\,\epsilon_0$. Around $D_{\rm res}$, the spin-current noise S^{zz}_{LL} matches the Fano-like shape $\sigma^z_S(D)$ (red line in Fig. 3) expressed as

$$\sigma^z_S(D) = C + A\frac{(D - D_{\rm res} + q\Gamma_{\rm res}/2)^2}{(D - D_{\rm res})^2 + (\Gamma_{\rm res}/2)^2}, \qquad (33)$$

where $\Gamma_{\rm res} = |D_{\rm max} - D_{\rm min}| \approx 0.00056\,\epsilon_0$ is the width of the resonance. The asymmetry parameter $q = 1$ shows that elastic and spin-flip processes occur with equal probability, so that $D_{\rm res} = (D_{\rm min} + D_{\rm max})/2$. Half of the amplitude of the Fano-like shape is given by $A = [S^{zz}_{LL}(D_{\rm max}) - S^{zz}_{LL}(D_{\rm min})]/2 \approx 0.000194\,\epsilon_0$, while $C = S^{zz}_{LL}(D_{\rm min}) \approx 0.00229\,\epsilon_0$. The inset in Fig. 3 depicts individual contributions of two interference profiles around $D_{\rm res}$ to the Fano-like shape in S^{zz}_{LL}. One profile that includes interference of elastic and spin-flip pathways ending in $\uparrow$ state with energy ϵ_4 is presented in $S^{\uparrow\uparrow}_{LLS} - S^{\uparrow\downarrow}_{LLS}$ (pink line, inset in Fig. 3). The other profile with interfering elastic and spin-flip pathways ending in $\downarrow$ state with energy ϵ_3 is given by the contribution $S^{\downarrow\downarrow}_{LLS} - S^{\downarrow\uparrow}_{LLS}$ (purple line, inset in Fig. 3). The asymmetry parameter $q = 1$ in both interference profiles, showing equal probabilities of elastic and spin-flip processes involving energy absorption (pink line) or emission (purple line).

The spin current I_{Lz} and shot noise S^{zz}_{LL} as functions of the chemical potential $\mu = \mu_L = \mu_R$ at zero temperature are presented in Figs. 4(a) and 4(b), for several values of

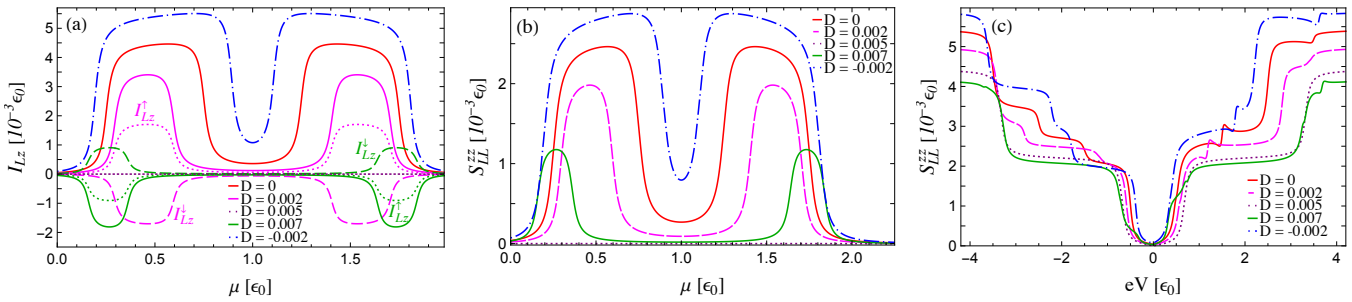

FIG. 4: (Color online) (a) Spin current I_{Lz}, (b) auto-correlation spin-current shot noise S^{zz}_{LL}, as functions of the chemical potential of the leads $\mu = \mu_L = \mu_R$, and (c) auto-correlation spin-current shot noise S^{zz}_{LL} as a function of the applied bias voltage $eV = \mu_L - \mu_R$ with $\mu_{L,R} = \pm eV/2$, for different uniaxial magnetic anisotropy parameters D, with $\vec{B} = B\vec{e}_z$, at zero temperature. The other parameters are set to: $\Gamma = 0.05\,\epsilon 0$, $\Gamma_L = \Gamma_R = \Gamma/2$, $\omega_L = 0.5\,\epsilon_0$, $J = 0.01\,\epsilon_0$, $S = 100$, and $\theta = \pi/3$. All energies are given in the units of ϵ_0. For $\mu_L = \mu_R$ and $D = \omega_L/2S_z = 0.005\,\epsilon_0$, $I_{Lz} = 0$ and $S^{zz}_{LL} = 0$ (purple dotted lines).

the magnetic anisotropy parameter D. Since $I^{\uparrow}_{Lz}$=$-I^{\downarrow}_{Lz}$ at zero-bias conditions, the corresponding charge current equals zero, with positive charge-current noise in the regions between levels connected with spin-flip events.[131] In the same regions, the shot noise of spin-current S^{zz}_{LL} is positive, while the spin current I_{Lz} takes positive (negative) values for $D < \omega_L/2S_z$ ($D > \omega_L/2S_z$). With the decrease of $|\omega|$, the magnitudes of I_{Lz} and S^{zz}_{LL} decrease. In Fig. 4(c) the dependence of spin-current shot noise S^{zz}_{LL} on the bias voltage $eV = \mu_L - \mu_R$, with $\mu_{L,R} = \pm eV/2$, is plotted for different values of the anisotropy parameter D at zero temperature. The positions of steps and dip-peak features in S^{zz}_{LL} at values of eV such that $\pm eV/2 = \mu_\xi = \epsilon_i$ denote Floquet quasienergy levels ϵ_i available for spin transport and, thus, depend on the anosotropy parameter D. For large values of $|eV|$ spin-current noise S^{zz}_{LL} is saturated.

The Gilbert damping coefficient α, the coefficient β, the magnitude of the in-plane torque component $T_\perp$ and the torque along z direction, T_z, are shown as functions of the magnetic anisotropy parameter D in Fig. 5, for five different tilt angles θ, at zero temperature. Starting with $\theta = 0$, when $S = S_z$ (purple dotted lines in Fig. 5), one notices that α has two local maximums and two local minimums around values of D that correspond to resonances $\mu_\xi = \epsilon_i$. The coefficient β has four minimums at the same values of D. Taking into account that the spin of the molecule is static for $\theta = 0$, with $\dot{\vec{S}}(t) = 0$, and $\gamma = 0$, according to Eqs. (23) and (32), the torque components $T_z = 0$ and $T_\perp = 0$. Note the presence of the elastic spin currents here, $I_{Lz} = -I_{Rz}$ [see Eq. (A3) in the Appendix]. On the other hand, for $\theta = \pi/2$, the molecular spin is perpendicular to z-axis, $S_z = 0$, and α, β, $T_\perp$ and T_z are independent of D (pink dashed lines in Fig. 5). Grid lines in Fig. 5 are related to $\theta = \pi/3$, $\omega_L = 0.5\,\epsilon_0$ (green lines) and the values of parameter D, such that $\mu_\xi = \epsilon_i$. Around $D = -0.01312\,\epsilon_0$ corresponding to $\mu_L = \epsilon_2$ (grid line), one notices a local maximum in α and $T_\perp$, a local minimum in β, while T_z has a minimum negative value. For this set of parameters, $\downarrow$ level ϵ_1 and $\uparrow$ levels ϵ_2 and ϵ_4 lie within the bias-voltage window, while $\downarrow$ level $\epsilon_3 < \mu_R$. This means that there are more inelastic tunneling pathways, involving electron spin-flip, available for $\downarrow$ electrons than for $\uparrow$ electrons. Namely, a tunneling electron in the $\downarrow$ level ϵ_3 can flip its spin and enter the $\uparrow$ level ϵ_4 within the bias voltage window, before it tunnels off the orbital, but the $\uparrow$ electron from the level ϵ_4 cannot flip its spin and enter $\downarrow$ level ϵ_3, since ϵ_3 lies below the bias voltage window. As a consequence, more $\downarrow$ electrons participate in inelastic spin transport, resulting in the negative torque component T_z. With further increase of D, for $\theta = \pi/3$ and $\omega_L = 0.5\,\epsilon_0$, the torque $T_z < 0$ until around $D = -0.00625\,\epsilon_0$, corresponding to $\mu_R = \epsilon_3$ (grid line), taking into account the level broadening Γ. Now all levels ϵ_i lie within the bias-voltage window, and T_z has another local negative minimum and a step-like increase towards zero, while α has a local maximum and a step-like decrease towards zero. On the other hand, $T_\perp$ has a maximum value at $D = -0.00625$, while β has another local minimum. As the increase of the anisotropy parameter D continues, the Gilbert damping coefficient α and T_z remain zero until around $D = 0.00875\epsilon_0$, corresponding to $\mu_R = \epsilon_4$ (grid line). Here, $\vec{T}_z$ changes its direction with T_z increasing towards a local maximum, while α reaches its maximum, β has its minimum value, and $T_\perp$ has a local maximum. With further increase of D, levels ϵ_1, ϵ_2 and ϵ_3 lie within the bias-voltage window, while $\uparrow$ level $\epsilon_4 < \mu_R$, and $\epsilon_3 > \epsilon_4$ since $\omega < 0$. Hence, there are more inelastic tunneling pathways available for $\uparrow$ particles, and the resulting $T_z > 0$. Around $D = 0.01406\,\epsilon_0$, corresponding to $\mu_L = \epsilon_1$ (grid line), the coefficient α, the magnitude $T_\perp$, and T_z have a local maximum, while β has a local minimum for $\theta = \pi/3$ and $\omega_L = 0.5\,\epsilon_0$ (green line in Fig. 5). Note that $T_\perp$ decreases from its maximum value to zero in the region $-0.00625\,\epsilon_0 < D < 0.005\,\epsilon_0$, ($\omega > 0$), and increases for $0.005\,\epsilon_0 < D < 0.00875\,\epsilon_0$ ($\omega < 0$). At $D = 0.005\,\epsilon_0$, the total frequency $\omega = \omega_L - 2DS_z = 0$ for $\theta = \pi/3$ and $\omega_L = 0.5\,\epsilon_0$, and the direction of the precession changes, while $T_\perp = 0$. Similarly, for $\theta = \pi/9$

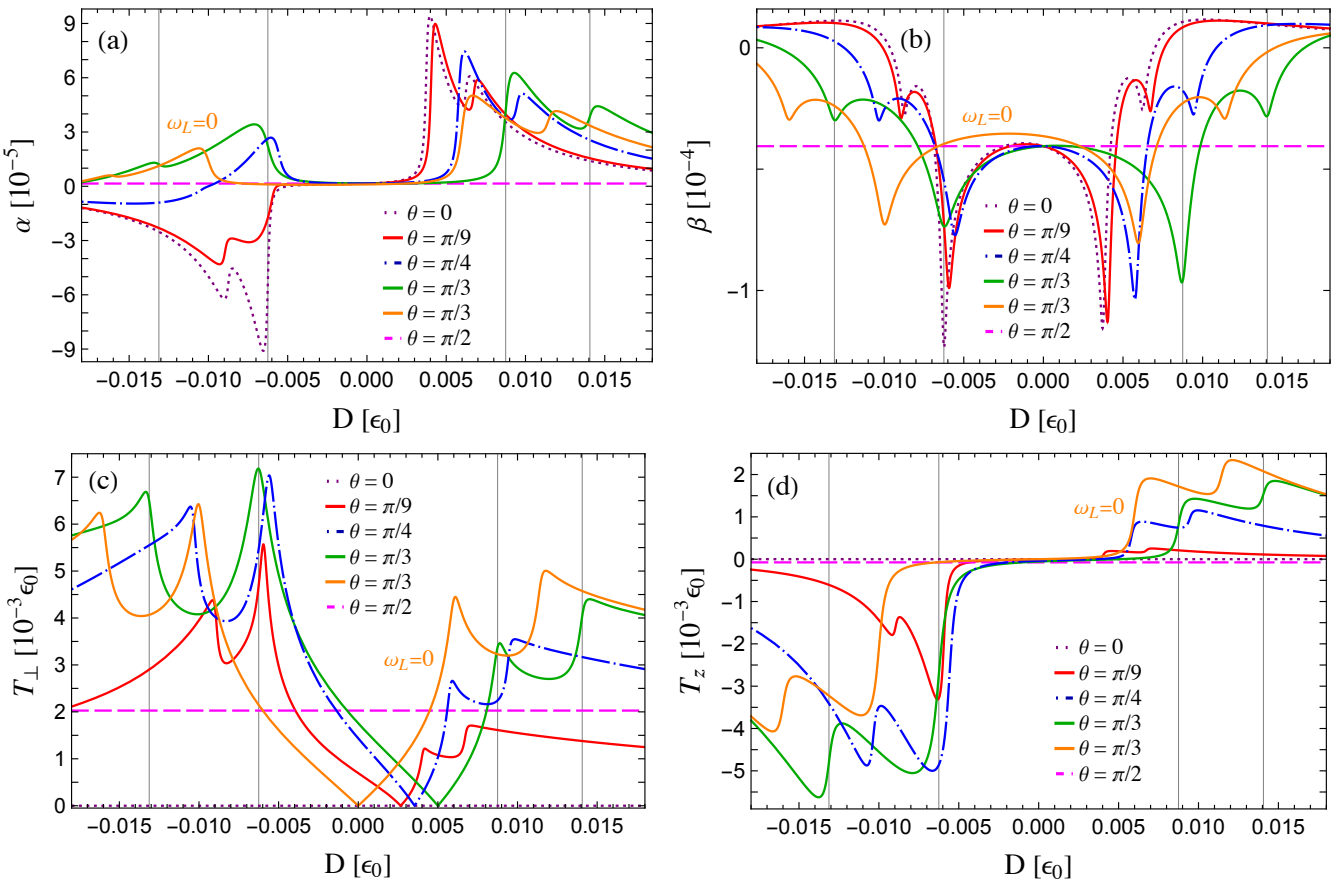

FIG. 5: (Color online) (a) Gilbert damping coefficient α, (b) coefficient β, (c) magnitude of the in-plane component of the STT, $T_\perp$ and (d) spatial component of the torque along z-direction T_z, as functions of the uniaxial magnetic anisotropy parameter D for different tilt angles θ, at zero temperature. The magnetic field $\vec{B} = B\vec{e}_z$ and Larmor frequency $\omega_L = 0.5\,\epsilon_0$, except for a zero magnetic field where $\omega_L = 0$ (orange line). The chemical potentials of the leads are equal to: $\mu_L = 2.5\,\epsilon_0$ and $\mu_R = 0$. The other parameters are set to: $\Gamma = 0.05\,\epsilon 0$, $\Gamma_L = \Gamma_R = \Gamma/2$, $\omega_L = 0.5\,\epsilon_0$, $J = 0.01\,\epsilon_0$, $S = 100$. Grid lines for $\theta = \pi/3$ (green line), are positioned at $D = -0.01312\,\epsilon_0$ ($\mu_L = \epsilon_2$), $D = -0.00625\,\epsilon_0$ ($\mu_R = \epsilon_3$), $D = 0.00875\,\epsilon_0$ ($\mu_R = \epsilon_4$), and $D = 0.01406\,\epsilon_0$ ($\mu_L = \epsilon_1$).

and $\theta = \pi/4$, the torque $T_\perp = 0$ at $D = \omega_L/2S_z$, while α and T_z vanish for the values of D such that each ϵ_i satisfies $\mu_R \leq \epsilon_i \leq \mu_L$, with respect to level broadening Γ [red and blue dot-dashed lines in Fig. 5]. In the absence of the magnetic field ($\omega_L = 0$), for $\theta = \pi/3$, the magnitude $T_\perp = 0$ at $D = 0$ [orange line in Fig. 5(c)]. At a high anisotropy, $|D| \gg \omega_L/2S_z$, the elastic tunneling processes are dominant and consequently α, β, $T_\perp$ and T_z approach zero.

The torque coefficients α and β, the magnitude $T_\perp$, and T_z, are presented as functions of the applied bias-voltage eV in Fig. 6, for several different magnetic anisotropy parameters D at zero temperature. The bias voltage is varied according to $\mu_{L,R} = \pm eV/2$. For $D = \omega_L/2S_z = 0.005\,\epsilon_0$, the molecular spin is static ($\omega = 0$), and only elastic spin transport occurs through two available transport channels, so that α, β and $\vec{T}$ vanish (purple dotted lines in Fig. 6). For $D \neq 0.005\,\epsilon_0$, one notices that α and T_z approach constant values for chemical potentials μ_ξ positioned between quasienergy levels ϵ_i connected with spin-flip events. With the decrease of D, for $D < \omega_L/2S_z$, these values of α and T_z decrease [pink dashed, red, blue dot-dashed lines in Figs. 6(a) and 6(d)], vanish for $\omega = 0$, and arise again for $D > \omega_L/2S_z$ [green lines in Figs. 6(a) and 6(d)]. Note that $T_z > 0$ for $D < \omega_L/2S_z$, and $T_z < 0$ for $D > \omega_L/2S_z$. Moreover, the width of the bias-voltage regions where the inelastic tunneling events occur depends on D as $w = 2\omega = 2\omega_L - 4DS_z$, taking into account the level broadening Γ. Within these regions, the coefficient β increases(decreases) from a local minimum(maximum) to a local maximum(minimum), so that the torque $\beta\dot{\vec{S}}$ tends to oppose(enhance) the rotational motion of the molecular spin $\vec{S}$, for negative(positive) β. All peaks in $T_\perp$ correspond to $\mu_\xi = \epsilon_i$. Their values decrease with the increase of D for $\omega > 0$, drop to zero for $\omega = 0$, and arise again for $\omega < 0$ [see Fig. 6(c)]. For the values of eV such that $\beta = 0$, while α and $|T_z|$ approach their maximums, the magnitude $T_\perp$ has local minimums.

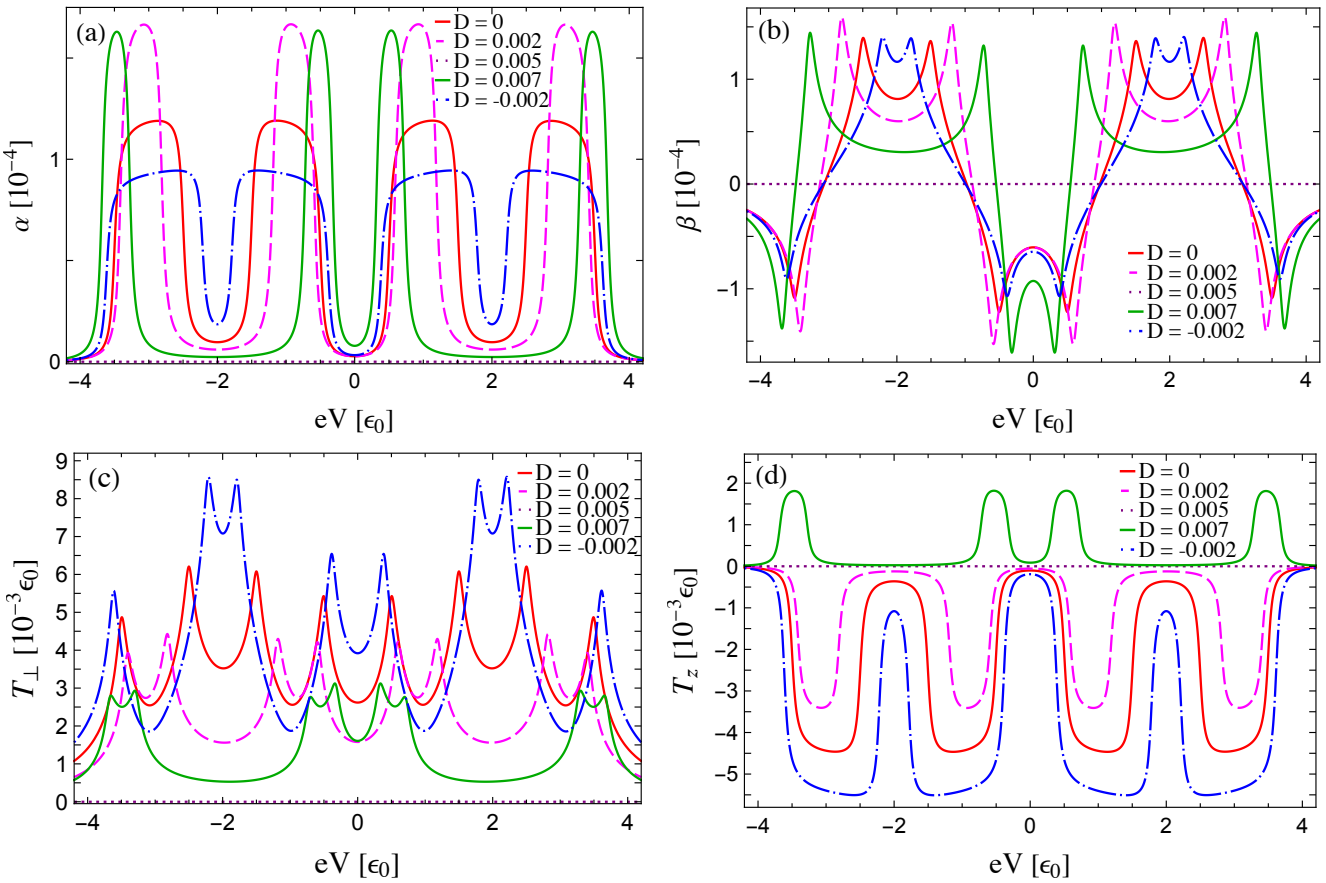

FIG. 6: (Color online) (a) Gilbert damping coefficient α, (b) coefficient β, (c) magnitude of the in-plane component of the STT, $T_\perp$ and (d) spatial component of the torque along z-direction T_z, as functions of the applied bias voltage $eV = \mu_L - \mu_R$ with $\mu_{L,R} = \pm eV/2$ and $\vec{B} = B\vec{e}_z$, for different uniaxial magnetic anisotropy parameters D at zero temperature. The other parameters are set to: $\Gamma = 0.05\,\epsilon 0$, $\Gamma_L = \Gamma_R = \Gamma/2$, $\omega_L = 0.5\,\epsilon_0$, $J = 0.01\,\epsilon_0$, $S = 100$, and $\theta = \pi/3$. All energies are given in the units of ϵ_0. For $D = \omega_L/2S_z = 0.005\,\epsilon_0$, $\alpha = 0$, $\beta = 0$, and $\vec{T} = 0$ (purple dotted lines).

In Fig. 7 the coefficients α and β, the magnitude of the in-plane torque component, $T_\perp$, and T_z, are plotted as functions of the Larmor frequency ω_L at zero temperature, for four different values of the magnetic anisotropy parameter D. The bias voltage is varied as $eV = \mu_L - \mu_R$, with $\mu_L = 2.5\,\epsilon_0$ and $\mu_R = 0$. The positions and values of all local maximums in α, steps in T_z, peaks and dips in β, and peaks in $T_\perp$ depend on the parameter D. They correspond to resonances $\mu_\xi = \epsilon_i$. For the anisotropic molecular spin, α, β and $T_\perp$ are even functions, while T_z is an odd function of ω (ω_L for $D = 0$)[88]. Around $\omega_L = 0.5\,\epsilon_0$ (grid lines), a maximum value for $D = 0.00875\,\epsilon_0$ and a local maximum for $D = -0.00625\,\epsilon_0$ can be observed in α due to resonances $\mu_R = \epsilon_4$ and $\mu_R = \epsilon_3$, while β shows negative minimums, $T_\perp$ local maximums, and T_z step-like decreases [blue dot-dashed and green lines in Fig. 7]. Looking at $\omega_L > 0$ for $D = -0.00625\,\epsilon_0$ (green lines in Fig. 7), one notices that for $\omega_L < 0.5\,\epsilon_0$ all quasienergy levels ϵ_i lie within the bias-voltage window. With the increase of ω_L they leave the bias-voltage window after reaching a resonance with μ_R or μ_L: $\epsilon_3 = \mu_R$ at $\omega_L = 0.5\,\epsilon_0$, $\epsilon_2 = \mu_L$ at $\omega_L = 1.5\,\epsilon_0$, $\epsilon_1 = \mu_R$ at $\omega_L = 2.25\,\epsilon_0$, and $\epsilon_4 = \mu_L$ at $\omega_L = 3.25\,\epsilon_0$. If we take into account the level broadening Γ, all quasienergy levels ϵ_i leave the bias-voltage window around $\omega_L = 3.25\,\epsilon_0$, with $\epsilon_{2(4)} > \mu_L$, and $\epsilon_{1(3)} < \mu_R$. With further increase of ω_L, α and β vanish, while $T_\perp$ and T_z become saturated due to spin-flip processes, involving electron spins from the leads, entering $\downarrow$ levels ϵ_1 or ϵ_3, and absorbing energy ω during the interaction with the molecular spin (note that saturated $T_z < 0$ for $\omega_L > 0$). At $\omega_L = 2DS_z$, the STT vanishes. E.g., at $\omega_L = 0.5\,\epsilon_0$ for $D = 0.005\,\epsilon_0$, $T_\perp = 0$ and $T_z = 0$ [intersection between grid line and pink-dashed line in Figs. 7(c) and 7(d)].

V. CONCLUSIONS

In this paper, the properties of spin transport through a junction consisting of a single orbital of a magnetic molecule with precessing anisotropic spin in a constant magnetic field was theoretically studied. The orbital is

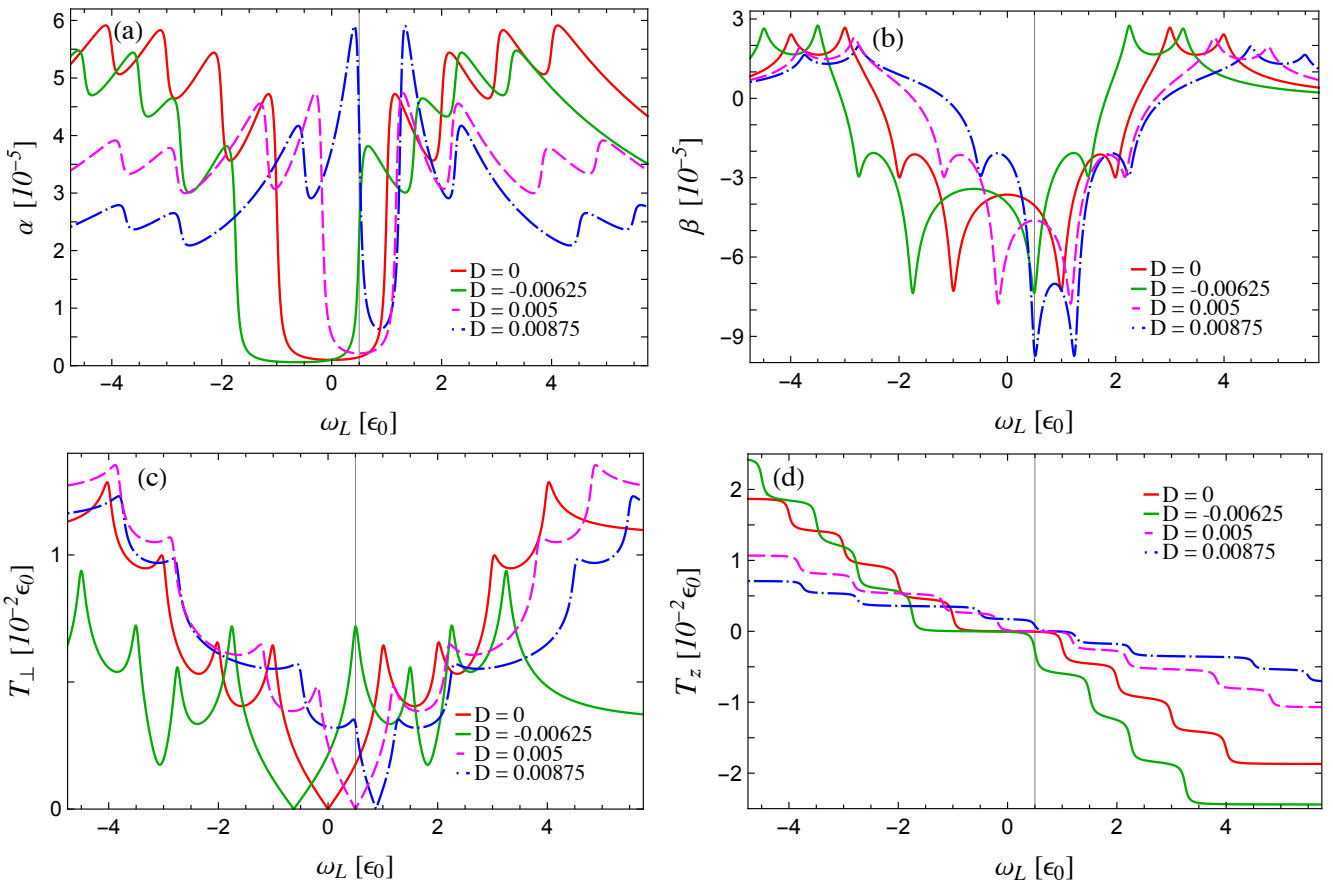

FIG. 7: (Color online) (a) Gilbert damping coefficient α, (b) coefficient β, (c) magnitude of the in-plane component of the STT, $T_\perp$ and (d) spatial component of the torque along z-direction T_z, as functions of the Larmor frequency ω_L for different uniaxial magnetic anisotropy parameters D. All plots are obtained at zero temperature with $\vec{B} = B\vec{e}_z$. The chemical potentials of the leads are equal to: $\mu_R = 0$ and $\mu_L = 2.5\,\epsilon_0$. The other parameters are set to: $\Gamma = 0.05\,\epsilon 0$, $\Gamma_L = \Gamma_R = \Gamma/2$, $J = 0.01\,\epsilon_0$, $S = 100$, and $\theta = \pi/3$. All energies are given in the units of ϵ_0. For a suppressed precession, with $\omega = 0$, $\omega_L = 2DS_z$, the STT vanishes, $T_\perp = 0$ and $T_z = 0$ (intersection between grid line and pink dashed line).

connected to two Fermi leads. The precession is kept undamped by external means and the precession frequency involves two contributions, one is Larmor frequency and the other is a term involving the uniaxial magnetic anisotropy parameter. Using the Keldysh NEGF technique, the spin currents, noise of z-polarized spin current, STT with the Gilbert damping coefficient and other torque coefficients were derived.

The results were discussed and analysed at zero temperature. The observed spin-transport characteristics such as steps, peaks and dips are related to resonances between chemical potentials of the leads and molecular quasienergy levels which depend on the uniaxial magnetic anisotropy parameter of the molecular spin. The inelastic tunneling of an electron spin that involves a spin-flip and absorption(emission) of an energy that depends on the magnetic anisotropy occurs due to exchange interaction with the precessing anisotropic molecular spin. During that process, the STT is exerted on the spin of the molecule and compensated by external means. The opposite torque is exerted by the molecular spin onto the spin currents, thus affecting the spin-transport properties of the junction. Both torque coeficients α and β, as well as the magnitude of the in-plane torque $T_\perp$ are even functions, while T_z is an odd function of the total precession frequency, taking into consideration the contribution of the magnetic anisotropy to the precession.

By adjusting the uniaxial magnetic anisotropy parameter with respect to the Larmor precession frequency and the tilt angle between the magnetic field and the molecular spin, one can control the spin current and noise, the STT, the Gilbert damping and the other torque coefficients. The quantum interference effects between the states connected with spin-flip processes are manifested in the spin-current noise as peaks and dips, resembling the Fano-like resonance profiles, controlled by the anisotropy parameter and Larmor frequency. Furthermore, it might be possible to perform a measurement of the dc-spin current and STT components, since they reveal the quasienergy level structure in the molecular

orbital. All spatial components of the STT vanish for the anisotropy contribution to the precession frequency that matches the Larmor frequency, when the precession is suppressed, thus allowing to determine the anisotropy and other parameters. Also, large magnetic anisotropy parameter leads to vanishing of the spin current, spin-current noise, and STT.

Taking into account that the spin currents and noise, and magnitude, direction and sign of the STT can be manipulated by the uniaxial magnetic anisotropy and other parameters, even if the magnetic field is turned off, the obtained results might be useful in spintronic applications using molecular magnets. Since magnetic anisotropy parameter is important for applications of molecular magnets in magnetic storage, it might be suitable to study noise of STT to obtain additional characteristics of spin-transport, and use quantum-mechanical description of the anisotropic molecular spin in tunnel junctions with normal or ferromagnetic leads.

Acknowledgments

The author acknowledges funding provided by the Institute of Physics Belgrade, through the grant No: 451-03-68/2022-14/200024 of the Ministry of Education, Science, and Technological Development of the Republic of Serbia.

Appendix: Expressions for the spin-current spatial components and zero frequency limit of the torque coefficients

The expressions for complex functions $I_{\xi x}(D)$ and $I_{\xi y}(D)$ introduced by Eqs. (7) and (8), and spin-current component $I_{\xi z}$, are presented here in terms of the Green's functions $\hat{G}^{0r}(\epsilon)$ and $\hat{G}^{0a}(\epsilon) = [\hat{G}^{0r}(\epsilon)]^\dagger$. They can be written as

$$\begin{aligned} I_{\xi x}(D) =& -i\int\frac{d\epsilon}{4\pi}\Bigg\{\frac{\Gamma_\xi\Gamma_\eta}{\Gamma}[f_\xi(\epsilon)-f_\eta(\epsilon)]\Bigg[\frac{\gamma G_{11}^{0r}(\epsilon+\omega_L-2DS_z)G_{22}^{0r}(\epsilon)}{|1-\gamma^2 G_{11}^{0r}(\epsilon+\omega_L-2DS_z)G_{22}^{0r}(\epsilon)|^2} \\ &+\frac{2i\gamma\mathrm{Im}\{G_{11}^{0r}(\epsilon)\}G_{22}^{0a}(\epsilon-\omega_L+2DS_z)+\gamma^3|G_{11}^{0r}(\epsilon)G_{22}^{0r}(\epsilon-\omega_L+2DS_z)|^2}{|1-\gamma^2 G_{11}^{0r}(\epsilon)G_{22}^{0r}(\epsilon-\omega_L+2DS_z)|^2}\Bigg] \\ &+\sum_{\lambda,\zeta=L,R}\frac{\Gamma_\lambda\Gamma_\zeta}{\Gamma}[f_\lambda(\epsilon-\omega_L+2DS_z)-f_\zeta(\epsilon)] \\ &\times\Big[\delta_{\zeta\xi}-\delta_{\lambda\xi}\gamma^2 G_{11}^{0a}(\epsilon)G_{22}^{0r}(\epsilon-\omega_L+2DS_z)\Big]\frac{\gamma G_{11}^{0r}(\epsilon)G_{22}^{0a}(\epsilon-\omega_L+2DS_z)}{|1-\gamma^2 G_{11}^{0r}(\epsilon)G_{22}^{0r}(\epsilon-\omega_L+2DS_z)|^2}\Bigg\},\ \eta\neq\xi, \end{aligned} \tag{A1}$$

$$I_{\xi y}(D) = iI_{\xi x}(D), \tag{A2}$$

$$\begin{aligned} \text{and }\ I_{\xi z} =& \int\frac{d\epsilon}{4\pi}\Bigg\{\frac{\Gamma_\xi\Gamma_\eta}{\Gamma}[f_\xi(\epsilon)-f_\eta(\epsilon)]\Bigg[\frac{2\mathrm{Im}\{G_{11}^{0r}(\epsilon)\}}{|1-\gamma^2 G_{11}^{0r}(\epsilon)G_{22}^{0r}(\epsilon-\omega_L+2DS_z)|^2}-\frac{2\mathrm{Im}\{G_{22}^{0r}(\epsilon)\}}{|1-\gamma^2 G_{11}^{0r}(\epsilon+\omega_L-2DS_z)G_{22}^{0r}(\epsilon)|^2}\Bigg] \\ &+\sum_{\lambda,\zeta=L,R}\Gamma_\lambda\Gamma_\zeta[f_\lambda(\epsilon-\omega_L+2DS_z)-f_\zeta(\epsilon)](\delta_{\lambda\xi}+\delta_{\zeta\xi})\frac{\gamma^2|G_{11}^{0r}(\epsilon)G_{22}^{0r}(\epsilon-\omega_L+2DS_z)|^2}{|1-\gamma^2 G_{11}^{0r}(\epsilon)G_{22}^{0r}(\epsilon-\omega_L+2DS_z)|^2}\Bigg\},\ \eta\neq\xi. \end{aligned} \tag{A3}$$

In the limit $\omega\to 0$, i.e., $D\to\omega_L/2S_z$, considering that $f_\xi(\epsilon-\omega)-f_\xi(\epsilon)\to-\omega\partial_\epsilon f_\xi(\epsilon)$, the expressions for the spin-torque coefficients α and β given by Eqs. (29) and (30) result in

$$\lim_{\omega\to0}\alpha = \frac{\Gamma}{S}\int\frac{d\epsilon}{2\pi}\sum_\xi\Gamma_\xi[\partial_\epsilon f_\xi(\epsilon)]\frac{(JS_z/2\Gamma)\mathrm{Im}\{G_{11}^{0r}(\epsilon)G_{22}^{0a}(\epsilon)\}-\gamma^2|G_{11}^{0r}(\epsilon)G_{22}^{0r}(\epsilon)|^2}{|1-\gamma^2 G_{11}^{0r}(\epsilon)G_{22}^{0r}(\epsilon)|^2}, \tag{A4}$$

$$\lim_{\omega\to0}\beta = J\int\frac{d\epsilon}{4\pi}\sum_\xi\Gamma_\xi[\partial_\epsilon f_\xi(\epsilon)]\frac{\mathrm{Re}\{G_{11}^{0r}(\epsilon)G_{22}^{0a}(\epsilon)\}-\gamma^2|G_{11}^{0r}(\epsilon)G_{22}^{0r}(\epsilon)|^2}{|1-\gamma^2 G_{11}^{0r}(\epsilon)G_{22}^{0r}(\epsilon)|^2}. \tag{A5}$$

[1] L. Thomas, F. Lionti, R. Ballou, D. Gatteschi, R. Sessoli, and B. Barbara, Macroscopic quantum tunnelling of magnetization in a single crystal of nanomagnets, Nature (London) **383**, 145-147 (1996).

[2] D. Gatteschi, R. Sessoli, and J. Villain, *Molecular Nanomagnets*, Oxford University Press, New York (2006).

[3] L. Bogani and W. Wernsdorfer, Molecular spintronics using single-molecule magnets, Nature Mater. **7**, 179-186 (2008).

[4] C. Timm and M. Di Ventra, Memristive properties of single-molecule magnets, Phys. Rev B **86**, 104427 (2012).

[5] M. N. Leuenberger and D. Loss, Quantum computing in molecular magnets, Nature (London) **410**, 789-793 (2001).

[6] R. E. P. Winpenny, Quantum information processing using molecular nanomagnets as qubits, Angew. Chem. Int. Ed., **47**, 7992-7994 (2008).

[7] M. -H. Jo, J. E. Grose, K Baheti, M. M. Deshumukh, J. J. Sokol, E. M. Rumberger, D. N. Hendrickson, J. R. Long, H. Park, and D. C. Ralph, Signatures of molecular magnetism in single-molecule transport spectroscopy, Nano Lett. **6**, 2014 (2006).

[8] A. S. Zyazin, J. W. G. van den Berg, E. A. Osorio, H. S. J. van der Zant, N. P. Konstantinidis, M. Leijnse, M. R. Wegewijs, F. May, W. Hofstetter, C. Danieli, and A Cornia, Electric field controlled magnetic anisotropy in a single molecule, Nano Lett. **10**, 3307 (2010).

[9] E. Burzurí, A. S. Zyazin, A. Cornia, and H. S. J. van der Zant, Direct Observation of Magnetic Anisotropy in an Individual Fe_4 Single-Molecule Magnet, Phys. Rev. Lett. **109**, 147203 (2012).

[10] M. Misiorny, M. Hell, and M. R. Wegewijs, Spintronic magnetic anisotropy, Nature Physics **9**, 801-805 (2013).

[11] H. B. Heersche, Z. de Groot, J. A. Folk, H. S. J. van der Zant, C. Romeike, M.R. Wegewijs, L. Zobbi, D. Barreca, E. Tondello, and A. Cornia, Electron transport through single Mn_{12} molecular magnets, Phys. Rev. Lett. **96**, 206801 (2006).

[12] R. Sessoli, Magnetic molecules back in the race, Nature **548**, 400-401 (2017).

[13] F. Delgado and J. Fernández-Rossier, Storage of Classical Information in Quantum Spins, Phys. Rev. Lett. **108**, 196602 (2012).

[14] S. Kahle, Z. Deng, N. Malinowski, C. Tonnoir, A. Forment-Aliaga, N. Thontasen, G. Rinke, D. Le, V. Turkowski, T. S. Rahman, S. Rauschenbach, M. Ternes, and K. Kern, The Quantum Magnetism of Individual Manganese-12-Acetate Molecular Magnets Anchored at Surfaces, Nano Lett. **12**, 518-521 (2012).

[15] F. -S. Guo, B. M. Day, Y. -C. Chen, M. -L. Tong, A. Mansikkamäki, and R. A. Layfield, Magnetic hysteresis up to 80 kelvin in a dysprosium metallocene single-molecule magnet, Science **362**, 1400-1403 (2018).

[16] R. Sessoli, D. Gatteschi, A. Caneschi, and M. A. Novak, Magnetic bistability in a metal-ion cluster, Nature (London) **365** 141-143 (1993).

[17] M. Misiorny and J. Barnaś, Effects of intrinsic spin-relaxation in molecular magnets on current-induced magnetic switching, Phys. Rev. B **77**, 172414 (2008).

[18] Y. Shiota, T. Nozaki, F. Bonell, S. Murakami, T. Shinjo, and Y. Suzuki, Induction of coherent magnetization switching in a few atomic layers of FeCo using voltage pulses, Nature Mater. **11**, 39-43 (2012).

[19] B. W. Heinrich, L. Braun, J. I. Pascual, K. J. Franke, Tuning the magnetic anisotropy of single molecules, Nano Lett. **15**, 4024-4028 (2015).

[20] J. D. V. Jaramillo, H. Hammar, and J. Fransson, Electronically mediated magnetic anisotropy in vibrating magnetic molecules, ACS Omega **3**, 6546-6553 (2018).

[21] B. Rana and Y. Otani, Towards magnonic devices based on voltage-controlled magnetic anisotropy, Commun. Phys. **2**, 90 (2019).

[22] R. E. George, J. P. Edwards, and A. Ardavan, Coherent spin control by electrical manipulation of the magnetic anisotropy, Phys. Rev. Lett. **110**, 027601 (2013).

[23] A. Sarkar and G. Rajaraman, Modulating magnetic anisotropy in Ln(III) single-ion magnets using an external electric field, Chem. Sci. **11**, 10324-10330 (2020).

[24] Y. Lu, Y. Wang, L. Zhu, L. Yang, and L. Wang, Electric field tuning of magnetic states in single magnetic molecules, Phys. Rev. B **106**, 064405 (2022).

[25] M. Pletyukhov, D. Schuricht, and H. Schoeller, Relaxation versus Decoherence: Spin and Current Dynamics in the Anisotropic Kondo Model at Finite Bias and Magnetic Field, Phys. Rev. Lett. **104**, 106801 (2010).

[26] R. Wieser, Comparison of Quantum and Classical Relaxation in Spin Dynamics, Phys. Rev. Lett. **110**, 147201 (2013).

[27] R. Mondal, M. Berritta, and P. M. Oppeneer, Relativistic theory of spin relaxation mechanisms in the Landau-Lifshitz-Gilbert equation of spin dynamics, Phys. Rev. B **94**, 144419 (2016).

[28] M. Sayad, R. Rausch, and M. Potthoff, Relaxation of a Classical Spin Coupled to a Strongly Correlated Electron System, Phys. Rev. Lett. **117**, 127201 (2016).

[29] A. Barman, S. Mandal, S. Sahoo, and A. De, Magnetization dynamics of nanoscale magnetic materials: A perspective, J. Appl. Phys. **128**, 170901 (2020).

[30] L. Yang, P. Glasenapp, A. Greilich, D. Reuter, A. D. Wieck, D. R. Yakovlev, M. Bayer, and S. A. Crooker, Two-colour spin noise spectroscopy and fluctuation correlations reveal homogeneous linewidths within quantum-dot ensembles, Nat. Commun. **5**, 4949 (2014).

[31] W. D. Rice, W. Liu, T. A. Baker, N. A. Sinitsyn, V. I. Klimov, and S. A. Crooker, Revealing giant internal magnetic fields due to spin fluctuations in magnetically doped colloidal nanocrystals, Nat. Nanotechnol. **11**, 137-142 (2016).

[32] M. Swar, D. Roy, S. Bhar, S. Roy, and S. Chaudhuri, Detection of spin coherence in cold atoms via Faraday rotation fluctuations, Phys. Rev. Res. **3**, 043171 (2021).

[33] C. Stahl and M. Potthoff, Anomalous Spin Precession under a Geometrical Torque, Phys. Rev. Lett **119**, 227203 (2017).

[34] U. Bajpai and B. K. Nikolić, Spintronics Meets Nonadiabatic Molecular Dynamics: Geometric Spin Torque and Damping on Dynamical Classical Magnetic Texture due to an Electronic Open Quantum System, Phys. Rev. Lett. **125**, 187202 (2020).

[35] P. M. Gunnink, T. Ludwig, and R. A. Duine, Charge conservation in spin-torque oscillators leads to a self-induced torque, Phys. Rev. B **109**, 024408 (2024).

[36] D. C. Ralph and M. D. Stiles, Spin transfer torques, J. Magn. Magn. Mater. **320**, 1190-1216 (2008).

[37] J.-X. Zhu, Z. Nussinov, A. Shnirman, and A. V. Balatsky, Novel Spin Dynamics in a Josephson Junction, Phys. Rev. Lett. **92**, 107001 (2004).

[38] Z. Nussinov, A. Shnirman, D. P. Arovas, A. V. Blaltsky, and J.-X. Zhu, Spin and spin-wave dynamics in Josephson junctions, Phys. Rev. B **71**, 214520 (2005).

[39] J.-X. Zhu and J. Fransson, Electric field control of spin dynamics in a magnetically active tunnel junction, J. Phys.: Condens. Matter **18**, 9929-9936 (2006).

[40] J. Fransson and J.-X. Zhu, Spin dynamics in a tunnel junction between ferromagnets, New J. Phys. **10**, 013017 (2008).

[41] J. Fransson, Subnanosecond switching of local spin-exchange coupled to ferromagnets, Phys. Rev. B **77**, 205316 (2008).

[42] J. Fransson. J. Ren, and J.-X. Zhu, Electrical and thermal control of magnetic exchange interactions, Phys. Rev. Lett. **113**, 257201 (2014).

[43] H. Hammar and J. Fransson, Time-dependent spin and transport properties of a single-molecule magnet in a tunnel junction, Phys. Rev. B **94**, 054311 (2016).

[44] H. Hammar and J. Fransson, Transient spin dynamics in a single-molecule magnet, Phys. Rev. B **96**, 214401 (2017).

[45] H. Hammar and J. Fransson, Dynamical exchange and phase induced switching of a localized molecular spin, Phys. Rev. B **98**, 174438 (2018).

[46] H. Hammar, J. D. V. Jaramillo, and J. Fransson, Spin-dependent heat signatures of single-molecule spin dynamics, Phys. Rev. B **99**, 115416 (2019).

[47] I. Makhfudz, E. Olive, and S. Nicolis, Nutation wave as a platform for ultrafast spin dynamics in ferromagnets, Appl. Phys. Lett. **117**, 132403 (2020).

[48] R. Rahman and S. Bandyopadhyay, An observable effect of spin inertia in slow magneto-dynamics: increase of the switching error rates in nanoscale ferromagnets, J. Phys.: Condens. Matter **33**, 355801 (2021).

[49] J. C. Slonczewski, Current-driven excitation of magnetic multilayers, J. Magn. Magn. Mater. **159**, L1-L7 (1996).

[50] L. Berger, Emission of spin waves by a magnetic multilayer traversed by a current, Phys. Rev. B **54**, 9353-9358 (1996).

[51] M. Tsoi, A. G. M. Jansen, J. Bass, W. -C. Chiang, M. Seck, V. Tsoi and P. Wyder, Excitation of a Magnetic Multilayer by an Electric Current, Phys. Rev. Lett. **80**, 4281 (1998).

[52] J. Z. Sun, Current-driven magnetic switching in manganite trilayer junctions, J. Magn. Magn. Mater. **202**, 157-162 (1999).

[53] Y. Tserkovnyak, A. Brataas, and G. E. W. Bauer, Spin pumping and magnetization dynamics in metallic multilayers, Phys. Rev. B **66**, 224403 (2002).

[54] G. E. W. Bauer, E. Saitoh, and B. J. van Wees, Spin caloritronics, Nature Mater. **11**, 391 (2012).

[55] E. B. Myers, D. C. Ralph, J. A. Katine, R. N. Louie, and R. A. Buhrman, Current-Induced Switching of Domains in Magnetic Multilayer Devices, Science **285**, 867-870 (1999).

[56] F. J. Albert, N. C. Emley, E. B. Myers, D. C. Ralph, and R. A. Buhrman, Quantitative Study of Magnetization Reversal by Spin-Polarized Current in Magnetic Multilayer Nanopillars, Phys. Rev. Lett. **89**, 226802 (2002).

[57] S. I. Kiselev, J. C.Sankey, I. N. Krivorotov, N. C. Emley, R. J. Schoelkopf, R. A. Buhrman, and D. C. Ralph, Microwave oscillations of a nanomagnet driven by a spin-polarized current, Nature **425**, 380-383 (2003).

[58] L. Liu, C. -F. Pai, Y. Li, H. W. Tseng, D. C. Ralph, and R. A. Buhrman, Spin-Torque Switching with the Giant Spin Hall Effect of Tantalum, Science **336**, 555-558 (2012).

[59] A. Chudnovskiy, Ch. Hübner, B. Baxevanis, and D. Pfannkuche, Spin switching: From quantum to quasiclassical approach, Phys. Status Solidi B, **251**, 1764 (2014).

[60] T. Ludwig, I. S. Burmistrov, Y. Gefen, and A. Shnirman, Strong nonequilibrium effects in spin-torque systems, Phys. Rev. B **95**, 075425 (2017).

[61] M. Misiorny and J. Barnaś, Magnetic switching of a single molecular magnet due to spin-polarized current, Phys. Rev. B **75**, 134425 (2007).

[62] M. Misiorny and J. Barnaś, Effects of Transverse Magnetic Anisotropy on Current-Induced Spin Switching, Phys. Rev. Lett. **111**, 046603 (2013).

[63] K. Wrześniewski and I. Weymann, Time-dependent spintronic anisotropy in magnetic molecules, Phys. Rev B **101**, 245434 (2020).

[64] H.-B. Xue, J.-Q. Liang and W.-M. Liu, Manipulation and readout of spin states of a single-molecule magnet by a spin-polarized current, Physica E **138**, 115086 (2022).

[65] C. Timm and F. Elste, Spin amplification, reading, and writing in transport through anisotropic magnetic molecules, Phys. Rev. B **73**, 235304 (2006).

[66] K. Xia, P. J. Kelly, G. E. W. Bauer, A. Brataas, and I. Turek, Spin torques in ferromagnetic/normal-metal structures, Phys. Rev B **65**, 220401(R) (2002).

[67] Y. Tserkovnyak, A. Brataas, G. E. E. Bauer, and B. I. Halperin, Nonlocal magnetization dynamics in ferromagnetic heterostructures, Rev. Mod. Phys. **77**, 1375 (2005).

[68] E. M. Hankiewicz, G. Vignale, and Y. Tserkovnyak, Gilbert damping and spin Coulomb drag in a magnetized electron liquid with spin-orbit interaction, Phys. Rev. B **75**, 174434 (2007).

[69] E. M. Hankiewicz, G. Vignale, and Y. Tserkovnyak, Inhomogeneous Gilbert damping from impurities and electron-electron interactions, Phys. Rev. B **78**, 020404(R) (2008).

[70] Y. Tserkovnyak, E. M. Hankiewicz, and G. Vignale, Transverse spin diffusion in ferromagnets, Phys. Rev. B **79**, 094415 (2009).

[71] G. Tatara, H. Kohno, and J. Shibata, Microscopic approach to current-driven domain wall dynamics, Phys. Rep. **468**, 213 (2008).

[72] G. Tatara, Effective gauge field theory of spintronics, Physica E **106**, 208 (2019).

[73] C. Bell, S. Milikisyants, M. Huber, and J. Aarts, Spin Dynamics in a Superconductor-Ferromagnet Proximity System, Phys. Rev. Lett. **100**, 047002 (2008).

[74] M. Houzet, Ferromagnetic Josephson Junction with Precessing Magnetization, Phys. Rev. Lett. **101**, 057009 (2008).

[75] J. P. Morten, A. Brataas, G. E. W. Bauer, W. Belzig, and Y. Tserkovnyak, Proximity-effect-assisted decay of spin currents in superconductors, EPL **84**, 57008 (2008).

[76] S. Teber, C. Holmqvist, and M. Fogelström, Transport and magnetization dynamics in a superconductor/single-molecule magnet/superconductor junction, Phys. Rev. B **81**, 174503 (2010).

[77] C. Holmqvist, M. Fogelström, and W. Belzig, Spin-polarized Shapiro steps and spin-precession-assisted multiple Andreev reflection, Phys. Rev. B **90**, 014516 (2014).

[78] Y. Yao, Q. Song, Y. Takarnura, J. P. Cascales, W. Yuan, Y. Ma, Y. Yun, X. C. Xie, J. S. Moodera, and W. Han, Probe of spin dynamics in superconducting NbN thin films via spin pumping, Phys. Rev. B **97**, 224414 (2018).

[79] T. Kato, Y. Ohnuma, M. Matsuo, J. Rech, T. Jonckheere, and T. Martin, Microscopic theory of spin transport at the interface between a superconductor and a ferromagnetic insulator, Phys. Rev. B **99**, 144411 (2019).

[80] N. S. Wingreen, A.-P. Jauho, and Y. Meir, Time-dependent transport through a mesoscopic structure, Phys. Rev. B **48**, 8487 (1993).

[81] A.-P. Jauho, N. S. Wingreen, and Y. Meir, Time-dependent transport in interacting and noninteracting resonant-tunneling systems, Phys. Rev. B **50**, 5528 (1994).

[82] A.-P. Jauho and H. Haug, *Quantum Kinetics in Transport and Optics of Semiconductors* (Springer, Berlin, 2008).

[83] Q.-f. Sun, H. Guo, and J. Wang, A Spin Cell for Spin Current, Phys. Rev. Lett. **90**, 258301 (2003).

[84] J. Fransson and M. Galperin, Inelastic scattering and heating in a molecular spin pump, Phys. Rev. B **81**, 075311 (2010).

[85] A. Saraiva-Souza, M. Smeu, L. Zhang, A. G. Souza Filho, H. Guo, and M. A. Ratner, Molecular Spintronics: Destructive Quantum Interference Controlled by a Gate, J. Am. Chem. Soc. **136**, 42, 15065-15071 (2014).

[86] J. Fransson, O. Eriksson, and A. V. Balatsky, Theory of spin-polarized scanning tunneling microscopy applied to local spins, Phys. Rev. B **81**, 115454 (2010).

[87] D. Rai and M. Galperin, Spin inelastic currents in molecular ring junctions, Phys. Rev. B **86**, 045420 (2012).

[88] M. Filipović, C. Holmqvist, F. Haupt, and W. Belzig, Spin transport and tunable Gilbert damping in a single-molecule magnet junction, Phys. Rev. B **87**, 045426 (2013); **88**, 119901 (2013).

[89] M. Filipović and W. Belzig, Photon-assisted electronic and spin transport in a junction containing precessing molecular spin, Phys. Rev. B **93**, 075402 (2016).

[90] S. Lounis, A. Bringer, and S. Blügel, Magnetic Adatom Induced Skyrmion-Like Spin Texture in Surface Electron Waves, Phys. Rev. Lett **108**, 207202 (2012).

[91] D. Yudin, D. R. Gulevich, and M. Titov, Light-Induced Anisotropic Skyrmion and Stripe Phases in a Rashba Ferromagnet, Phys. Rev. Lett. **119**,147202 (2017).

[92] F. Xu, G. Li, J. Chen, Z. Yu, L. Zhang, B. Wang, and J. Wang, Unified framework of the microscopic Landau-Lifshitz-Gilbert equation and its application to skyrmion dynamics, Phys. Rev. B **108**, 144409 (2023).

[93] B. Wang, J. Wang, and H. Guo, Shot noise of spin current, Phys. Rev. B **69**, 153301 (2004).

[94] F. M. Souza, A.-P. Jauho, and J. C. Egues, Spin-polarized current and shot noise in the presence of spin flip in a quantum dot via nonequilibrium Green's functions, Phys. Rev. B **78**, 155303 (2008).

[95] M. Filipović and W. Belzig, Shot noise of charge and spin transport in a junction with a precessing molecular spin, Phys. Rev. B **97**, 115441 (2018).

[96] C. Romeike, M. R. Wegewijs, W. Hofstetter, and H. Schoeller, Quantum-tunneling-induced Kondo effect in single molecular magnets, Phys. Rev. Lett **96**, 196601 (2006).

[97] J. J. Parks, A. R. Champagne, T. A. Costi, W. W. Shum, A. N. Pasupathy, E. Neuscamman, S. Flores-Torres, P. S. Cornaglia, A. A. Aligia, C. A. Balseiro, G. K.-L. Chan, H. D. Abruña, and D. C. Ralph, Mechanical control of spin states in spin-1 molecules and the underscreened Kondo effect, Science **328**, 1370-1373 (2010).

[98] F. Elste and C. Timm, Resonant and Kondo tunneling through molecular magnets, Phys Rev. B **81**, 024421 (2010).

[99] M. Misiorny, I. Weymann, and J. Barnaś, Temperature dependence of electronic transport through molecular magnets in the Kondo regime, Phys. Rev. B **86**, 035417 (2012).

[100] Y. Li, H. Kan, Y. Miao, S. Qiu, G. Zhang, J. Ren, C. Wang, and G. Hu, Magnetic manipulation of orbital hybridization and magnetoresistance in organic ferromagnetic co-oligomers, Physica E **124**, 114327 (2020).

[101] R.-Q. Wang, L. Sheng, R. Shen, B. Wang, and D. Y. Xing, Thermoelectric effect in single-molecule-magnet junctions, Phys. Rev. Lett. **105**, 057202 (2010).

[102] M. Misiorny and J. Barnaś, Spin-dependent thermoelectric effects in transport through a nanoscopic junction involving a spin impurity, Phys. Rev. B **89**, 235438 (2014).

[103] M. Misiorny and J. Barnaś, Effect of magnetic anisotropy on spin-dependent thermoelectric effects in nanoscopic systems, Phys. Rev. B **91**, 155426 (2015).

[104] M. Misiorny and J. Barnaś, Spin polarized transport through a single-molecule magnet: Current-induced magnetic switching, Phys. Rev. B **76**, 054448 (2007).

[105] Z. Zhang and L. Jiang, Bias voltage induced resistance switching effect in single-molecule magnets' tunneling junction, Nanotechnology **25**, 365201 (2014).

[106] A. Płomińska and I. Weymann, Pauli spin blockade in double molecular magnets, Phys. Rev. B **94**, 035422 (2016).

[107] A. Płomińska and I. Weymann, Magnetoresistive properties of a double magnetic molecule spin valve in different geometrical arrangements, J. Magn. Magn. Mater. **480**, 11-21 (2019).

[108] J. R. Petta, S. K. Slater, and D. C. Ralph, Spin-Dependent Transport in Molecular Tunnel Junctions, Phys. Rev. Lett. **93**, 136601 (2004).

[109] U. Ham and W. Ho, Spin Splitting Unconstrained by Electron Pairing: The Spin-Vibronic States, Phys. Rev. Lett. **108**, 106803 (2012).

[110] G. Czap, P. J. Wagner, F. Xue, L. Gu, J. Li, J. Yao, R. Wu, and W. Ho, Probing and imaging spin interactions with a magnetic single-molecule sensor, Science **364**, 670 (2019).

[111] A. Landig, J. Koski, P. Scarlino, C. Reichl, W. Wegscheider, A. Wallraff, K. Ensslin, and T. Ihn, Microwave-Cavity-Detected Spin Blockade in a Few-Electron Double Quantum Dot, Phys. Rev. Lett. **122**, 213601 (2019).

[112] M. Urdampilleta, S. Klyatskaya, J. -P. Cleuziou, M. Ruben, and W. Wernsdorfer, Supramolecular spin valves, Nature Mater. **10**, 502 (2011).

[113] U. Ham and W. Ho, Imaging single electron spin in a molecule trapped within a nanocavity of tunable dimension, J. Chem. Phys. **138**, 074703 (2013).

[114] L. Landau and E. M. Lifshitz, On the Theory of the Dispersion of Magnetic Permeability in Ferromagnetic Bodies, Phys. Z. Sowjetunion **8**, 153 (1935).

[115] T. L. Gilbert, A Lagrangian formulation of the gyromagnetic equation of the magnetic field, Phys. Rev. **100**, 1243 (1955).

[116] T. L. Gilbert, A phenomenological theory of damping in ferromagnetic materials, IEEE Trans. Magn. **40**, 3443

(2004).
[117] J. Xiao, G. E. W. Bauer, K. C. Uchida, E. Saitoh, and S. Maekawa, Theory of magnon-driven spin Seebeck effect, Phys. Rev. B **81**, 214418 (2010).
[118] S. K. Kim and Y. Tserkovnyak, Landau-Lifshitz theory of thermomagnonic torque, Phys. Rev. B **92**, 020410(R) (2015).
[119] L. Arrachea and F. von Open, Nanomagnet coupled to quantum spin Hall edge: An adiabatic quantum motor, Physica E **74**, 596-602 (2015).
[120] J. Fransson, Detection of spin reversal and nutations through current measurements, Nanotechnology **19**, 285714 (2008).
[121] N. Bode, L. Arrachea, G. S. Lozano, T. S. Nunner, and F. von Oppen, Current-induced switching in transport through anisotropic magnetic molecules, Phys. Rev. B **85**, 115440 (2012).
[122] L. Berger, Low-field magnetoresistance and domain drag in ferromagnets, J. Appl. Phys. **49**, 2156-2161 (1978).
[123] S. Zhang and Z. Li, Roles of Nonequilibrium Conduction Electrons on the Magnetization Dynamics of Ferromagnets, Phys. Rev. Lett. **93**, 127204 (2004).
[124] K. M. D. Hals and A. Brataas, Spin-orbit torques and anisotropic magnetization damping in skyrmion crystals, Phys. Rev. B **89**, 064426 (2014).
[125] M. Sayad, R. Rausch, and M. Potthoff, Relaxation of a Classical Spin Coupled to a Strongly Correlated Electron System, Phys. Rev. Lett. **117**, 127201 (2016).
[126] M. O. A. Ellis, M. Stamenova, and S. Sanvito, Multiscale modeling of current-induced switching in magnetic tunnel junctions using *ab initio* spin-transfer torques, Phys. Rev. B **96**, 224410 (2017).
[127] U. Bajpai and B. Nikolić, Time-retarded damping and magnetic inertia in the Landau-Lifshitz-Gilbert equation self-consistently coupled to electronic time-dependent nonequilibrium Green functions, Phys. Rev. B **99**, 134409 (2019).
[128] A. Suresh, U. Bajpai, and B. K. Nikolić, Magnon-driven chiral charge and spin pumping and electron-magnon scattering from time-dependent quantum transport combined with classical atomistic spin dynamics, Phys. Rev. B **101**, 214412 (2020).
[129] M. Elbracht and M. Potthoff, Accessing long timescales in the relaxation dynamics of spins coupled to a conduction-electron system using absorbing boundary conditions, Phys. Rev. B **102**, 115434 (2020).
[130] R. Smorka, M. Thoss, and M. Žonda, Dynamics of spin relaxation in nonequilibrium magnetic nanojunctions, New. J. Phys. **26**, 013056 (2024).
[131] M. Filipović, Effect of uniaxial magnetic anisotropy on charge transport in a junction with a precessing anisotropic molecular spin, Phys. Rev. B **111**, 165415 (2025).
[132] G. Floquet, Sur les équations différentielles linéaires à coefficients périodiques, Ann. Sci. École Normale Supérieure **12**, 47 (1883).
[133] J. H. Shirley, Interaction of a Quantum System with a Strong Oscillating Field, PhD Thesis, California Institute of Technology (1963).
[134] M. Grifoni and P. Hänggi, Driven quantum tunneling, Phys. Rep. **304**, 229 (1998).
[135] B. H. Wu and C. Timm, Noise spectra of ac-driven quantum dots: Floquet master-equation approach, Phys. Rev. B **81**, 075309 (2010).
[136] U. Fano, Effects of Configuration Interaction on Intensities and Phase Shifts, Phys. Rev. **124**, 1866 (1961).
[137] A. E. Miroshnichenko, S. Flach, and Y. S. Kivshar, Fano resonances in nanoscale structures, Rev. Mod. Phys. **82**, 2257 (2010).
[138] C. Kittel, On the theory of ferromagnetic resonance absorpton, Phys. Rev. **73**, 155 (1948).
[139] C. Godfrin, S. Thiele, A. Ferhat, S. Klyatskaya, M. Ruben, W. Wernsdorfer, and F. Balestro, Electrical Read-Out of a Single Spin Using an Exchange-Coupled Quantum Dot, ASC Nano **11**, 3984 (2017).
[140] B. Wang, J. Wang, and H. Guo, Quantum spin field effect transistor, Phys. Rev. B **67**, 092408 (2003).
[141] H. Bruus and K. Flensberg, *Many-Body Quantum Theory in Condensed Matter Physics* (Oxford University Press, Oxford, UK, 2004).
[142] O. Sauret and D. Feinberg, Spin-Current Shot Noise as a Probe of Interactions in Mesoscopic Systems, Phys. Rev. Lett. **92**, 106601 (2004).
[143] A. Fetter and J. D. Walecka, *Quantum Theory of Many-Particle Systems* (Dover, Mineola, NY, 2003).
[144] D. C. Langreth, in *Linear and Nonlinear Electron Transport in Solids*, edited by J. T. Devreese and E. Van Doren (Plenum, New York, 1976).